



**Politecnico
di Torino**

Politecnico di Torino

Master Degree Course in Biomedical Engineering
A.Y. 2021/2022
December 2022

**Running analysis on treadmill and on track based on
magneto-inertial sensing technology**

Supervisors:

Prof. Ing. Andrea CEREATTI
Ing. Rachele ROSSANIGO

Candidate:

Elena DIPALMA

*To mom and dad,
who always supported me to take on the craziest adventures.
And to my brother,
for always being able to bring foolishness in the darkest days.*

Acknowledgments

I would like to express my gratitude to my professor and supervisor Andrea Cereatti, who guided me throughout this work, for bringing me to this project and for his invaluable knowledge and feedback.

I also could not have undertaken this journey without my co-supervisor Rachele Rossanigo, who supported me throughout the whole process and provided a fundamental help. Thank you to all the members of the office in which I have been spending most of my days since the beginning of this project, for providing help and knowledge when needed, and occasionally a good laugh.

I would also like to thank my family who never failed to support me, both emotionally and economically, and my truest friends (you know who you are) for always being by my side, in spite of distance and difficulties.

Abstract

Running temporal parameters, i.e. running cycle, stance and swing durations, are an effective way to evaluate running performances. Running characterization can be useful to predict the advent of injuries, enabling to reduce their entity or prevent them. [1] During the last decades, magneto inertial measurements units (MIMUs) have become the most widespread wearable solution to investigate running in outdoor conditions, evaluating the runner's actual performances [2]. In the literature there is an extensive number of different methods for the detection of temporal events; however, each method is usually targeted to a restrict range of running speeds due to the high variability of the morphology of the inertial signals varying running paces.

The aim of the present work is to perform a comparative evaluation of different state of the art methods [61-64, 66-70] for the estimation of running temporal events (i.e. instants of initial, IC, and final contacts, FC, with the ground) across different running paces. Nine methods selected from the literature were implemented and adapted to the collected data based on the different sampling frequencies and sensor locations.

In addition, an original template-based method, using Wavelet Transformations [26] and Dynamic Time Warping [22] suitable for accurately defining and segmenting the running cycle on a wide speed range (8-32 km/h) was implemented.

For the aim of this thesis, three datasets were analysed. All the recruited subjects were equipped with a MIMU fixed to the shoelaces of each shoe. The first dataset included 11 subjects that ran at two different constant speeds (8 km/h and 10 km/h) in outdoor and indoor conditions, equipped with MIMUs and sensorised pressure insoles, considered as a portable gold standard [55], both sampled at 100 Hz. The second dataset included data of 10 amateur runners who were asked to run at 14 km/h on a treadmill, instrumented with MIMUs sampled at 200 Hz and retro-reflective markers, since the stereophotogrammetric system was taken as the gold standard. Lastly, the third dataset included 9 elite runners, whose speeds ranged from 20 to 32 km/h and was on an outdoor running track, adopting sensorised pressure insoles as gold standard, acquired at 100 Hz.

Comparing the performances on the three datasets in terms of root mean square errors (RMSE) of running events and mean absolute percentage errors (MAPE) of running phases against the available gold standard, Blauburger et al. (2021) [61] was selected as the best tradeoff for the temporal parameters estimation, resulting in a RMSE lower than 0.04 s on IC, and lower than 0.06 s on FC for all the speeds analysed.

Furthermore, the results obtained via the novel method were compared to the performance obtained with the one proposed by Blauburger et al. The proposed method reported a RMSE lower than 0.033 s on the detection of ICs, and an RMSE lower than 0.049 s on the detection of FCs for all the different running paces. These results were deemed comparable to the ones achieved with the most suitable method from the literature for different paces, thus the proposed method is promising for the detection of temporal parameters on a wide speed range and in out-of-lab applications.

. Results coming from the first and the last datasets were compared to the ones obtained with sensorised pressure insoles, considered as a portable gold standard.

Comparing the performances on the three datasets in terms of root mean square errors (RMSE) of running events and mean absolute percentage errors (MAPE) of running phases against the available gold standard, Blauburger et al. was selected as the best trade-off for the temporal parameters estimation, resulting in a RMSE lower than 0.04 s on IC, and lower than 0.06 s on FC for all the speeds analysed.

Furthermore, the results obtained via the novel method were compared to the performance obtained with the one proposed by Blauburger et al. The proposed method reported a RMSE lower than 0.033 s on the detection of ICs, and a RMSE lower than 0.049 s on the detection of FCs for all the different running paces. These results were deemed comparable to the ones achieved with the most suitable method from the literature for different paces, thus the proposed method is promising for the detection of temporal parameters on a wide speed range and in out-of-lab applications.

Contents

1. Contents.....	V
2. Introduction	15
3. Background	17
1.1 The biomechanics of running.....	17
1.1.1 Gait and running cycle.....	17
1.1.2 Gait and running spatio-temporal parameters	19
1.2 Running Analysis	20
1.2.1 State of the art for the identification of running events.....	20
1.3.1 Instrumentation.....	23
1.3.1.1 Magneto Inertial Measurement Units (MIMU).....	23
1.3.1.1 Accelerometer	23
1.3.1.2 Gyroscope.....	25
1.3.1.3 Magnetometer.....	27
1.3.2 Validation systems	29
1.3.2.1 Optoelectronic systems	29
1.3.2.2 Force plates	30
1.3.2.3 Foot switches.....	31
1.3.2.4 Pressure insoles	32
1.3.3 Algorithms for the identification of gait and running temporal parameters.....	33
1.3.3.1 Traditional techniques based on peak detection.....	33
1.3.3.2 Wavelet transformations	34
1.3.4 Dynamic Time Warping.....	35
4. Materials and methods	37
2.1 Experimental setup.....	37
2.1.1 Amateurs protocol – 8 and 10 km/h.....	37
2.1.2 Amateurs protocol – 14 km/h.....	38

2.1.3 Sprinters protocol	38
2.2 Literature methods for the detection of temporal parameters	39
2.2.1 Methods proposed for high speeds.....	41
2.2.1.1 Blauberger et al.	41
2.2.1.2 Schmidt et al.....	42
2.2.1.3 Falbiard et al.....	43
2.2.2 Methods proposed for recreational runners.....	44
2.2.2.1 Bailey et Harle.....	44
2.2.2.2 Reenalda et al	46
2.2.2.3 Mo and Chow	46
2.2.2.4 Chew et al.....	47
2.2.2.5 Benson et al.	48
2.2.2.6 Yang et al.	48
2.3 Newly proposed method.....	50
5. Results	57
3.1 Results of methods from the literature	58
3.1.1 Comparison of methods performances at 8 km/h.....	58
3.1.2 Comparison over 10 km/h.....	60
3.1.3 Comparison over 14 km/h.....	62
3.1.4 Comparison over sprinters	64
3.1.5 Choice of the best trade-off method.....	66
3.2 Novel method results.....	67
3.2.1 Sensibility analysis.....	70
3.3 Comparison of the novel method with the best trade-off from the literature.....	73
6. Discussion and conclusions.....	77
4.1 Discussion	77
4.1 Conclusion.....	83
7. References	85
8. Appendix 1	93
Cover Insole analysis	93
1. Analysis of pressure insoles data quality without any cover insoles.....	94
2. Analysis of pressure insoles data quality with leather cover insoles.....	94

3.	Analysis of pressure insoles data quality with Chlorophyll cover insoles.....	95
4.	Analysis of pressure insoles data quality with cotton cover insoles.....	96
5.	Analysis of pressure insoles data quality with Noene Insoles	96
6.	Analysis of pressure insoles data quality with Podovis Insoles.....	97
7.	Comparison Table.....	98
8.	References.....	98
9.	Appendix 2.....	99
	Sampling frequency enhancement	99
	1. Analysis protocol	99
	2. Selected pressure sensors.....	103
	3. References.....	103

List of Figures

Figure 1-1 - The phases of the running gait cycle [8] 18

Figure 1-2 - The phases of the gait cycle. (A) Walking, (B) Running 19

Figure 0-3 – Visualization of the different positioning of the IMUs on a running shoe. [7]
..... 22

Figure 0-4 – Accelerometer spring-mass-damper system [41]..... 24

Figure 0-5 – sprint trial acceleration. In blue, the vertical acceleration, in orange the mediolateral acceleration and in yellow the anteroposterioir acceleration during a sprinting trial. The hatched lined indicates a change in motion: in the first part, the subject was standing, in the central part the subject was sprinting and, lastly, the subject began to walk. 25

Figure 0-6 – visual representation of the three different angular rate measurements: Roll, Pitch and Yaw [42]..... 26

Figure 0-7 – Gyroscope signals acquired along three ortogonal axis during a sprinting trial. In blue, the vertical axis, in orange the mediolateral axis, in yellow the anteroposterioir axis. The hased lines indicates a change in motion: in the first part, the subject was standing, in the middle part running, and finally walking. 27

Figure 0-8 – Visual representation of the Hall effect. The red signs (- and +) represent the charge buildup on the sides of the conductive surface, which result in an electric field. Based on the charge of the aprticle traveling on the surface, it will tend to accumulate on one side or the other. Source: <http://hyperphysics.phy-astr.gsu.edu/hbase/magnetic/Hall.html> 28

Figure 0-9 – Magnetometer signal acquired during a running trial along three orthogonal axes: in blue the vertical axis, in orange the mediolateral axis, in yellow the anteroposterior axis. The hashed line indicates a change in motion. In the first part the subject was standing, then running and in the end the subject began to walk. 29

Figure 0-10 – Optoelectronic setup for the motion capture. Source: <https://assistiverobotcenter.github.io/images/toolbox/sensors/qualysis.jpg>..... 30

Figure 0-11 – Example of force plate. Source: <https://www.technogym.com/wpress/wp-content/uploads/2019/04/Force-plate.jpg> 31

Figure 0-12 – example of foot switch and their positioning. Source: https://www.motion-labs.com/prod_access_footswitches.html 32

Figure 0-13 – Pressure Insole developed by Salis et al. [48] 33

Figure 0-14 - representation of the discrete wavelet transformations. In the picture, $g[n]$ represents low pass filters, while $h[n]$ represents high pass filters. The signals are down sampled after each filtering step..... 35

Figure 0-15 – On the left, example of a comparison between two signals when using the euclidean distance, on the right by using the dynamic time warping. Source: https://rtavenar.github.io/blog/fig/dtw_vs_euc.svg	36
Figure 2-1 – Subject wearing the INDIP multisensory sistem and sensorised insoles.....	38
Figure 2-2 – Subject wearing the Opal system and retro-reflective markers.	38
Figure 2-3 – Subject equipped with MIMUs affixed to the shoelaces of each show and with sensorised insoles.	39
Figure 2-4 – In this figure, taken from [55] , the position of the MIMU on one of the athletes’ shoes is shown.	42
Figure 2-5 In the figure, taken from [62] , the IMU device used in this paper and its positioning on one of the athletes is shown.....	43
Figure 2-6 – The figure, taken from [63] shows both the technical frame of the foot-worn IMU (XT, YT, ZT) and the functional frame of the foot (XF, YF, ZF) and the positioning and the attachment of the IMU to the foot.	44
Figure 2-7- In the figure, taken from [64] , the IMU and its placement on the shoe is shown.	45
Figure 2-8- Figure taken from [67] that shows the positioning of four of the IMUs used in their study.....	47
Figure 2-9- In the figure, taken from [68] , the positioning of the IMU is shown.	47
Figure 2-10- Figure taken from [70] showing the placement of the IMU on the ankle	49
Figure 2-11 – Flowchart highlighting the steps of the template-based method	50
Figure 2-12 – DWT decomposition of a portion of the anteroposterior acceleration at level 1 using s ‘db6’ mother wavelet. In red, the original signal, in blue the approximation coefficients (which are equal to the denoised signal in the tecnique used in this work) and in greed the detail coefficients.....	51
Figure 2-13 - DWT decomposition of a portion of the anteroposterior acceleration at level 2 using s ‘db6’ mother wavelet. In red, the original signal, in blue the approximation coefficients (which are equal to the denoised signal in the tecnique used in this work) and in greed the detail coefficients.....	51
Figure 2-14 - DWT decomposition of a portion of the anteroposterior acceleration at level 3 using a ‘db6’ mother wavelet. In red, the original signal, in blue the approximation coefficients (which are equal to the denoised signal in the tecnique used in this work) and in greed the detail coefficients.....	52
Figure 2-15 – Description of the method for the identification of the events. The way the two signals are deformed is shown graphically at the top of the image, while at the bottom a sample-wise representation is shown. To deform the signal, some sample will be repeated, as defined by the deformation vector, indicated by the figure as ‘Original Sample’, so the positioning of the events will not match exactly what is in the template sample-wise, but the	

value of the signal in that instance will still be the same. When the two signals are both warped, they are ‘equal’, which means that finding the event on the template signal when is warped is the same of finding the event on the new signal, as it will happen on the same sample..... 54

Figure 2-16 – First step, non warped signals. The signal is matched with the template with the highest similarity. 55

Figure 2-17 – Second step, signals warping. The signals are deformed to obtain the highest similarity. The IC is traslated by the deformation. The algorithm takes note of the new IC sample, and translates the information on the analysed signal. 55

Figure 2-18 – Step three, the information is reported on the orininal non-warped signals. The event is detected. 56

Figure 3-1 – Example image of a mid-swing to mid-swing cycle with the events detected via each of the different methods over the medio-lateral projection of the angular velocity at 8 km/h. The two different colors of the points differentiate ICs, in blue, and FCs, in red. Each method is associated to a different symbol, as stated in the legend. The two black filled points are the actual events, detected via the gold standard. The black lines show the signal acquired via the pressure insoles..... 60

Figure 3-2 - Example image of a mid-swing to mid-swing period with the events detected via each of the different methods over the medio-lateral projection of the angular velocity at 10 km/h. The two different colors of the points differentiate ICs, in blue, and FCs, in red. Each method is associated to a different symbol, as stated in the legend. The two black filled points are the actual events, detected via the gold standard. The black lines show the signal acquired via the pressure insoles..... 62

Figure 3-3- Example image of a mid-swing to mid-swing period with the events detected via each of the different methods over the medio-lateral projection of the angular velocity at 14 km/h. The two different colors of the points differentiate ICs, in blue, and FCs, in red. Each method is associated to a different symbol, as stated in the legend. The two black filled points are the actual events, detected via the gold standard. The black line shows the vertical displacement of the foot. The vertical displacement presents a offset equal to ~10 cm due to the treadmill height..... 64

Figure 3-4 –Example image of a mid-swing to mid-swing segment with the events detected via each of the different methods over the medio-lateral projection of the angular velocity of a sprinter. The two different colors of the points differentiate ICs, in blue, and FCs, in red. Each method is associated to a different symbol, as stated in the legend. The two black filled points are the actual events, detected via the gold standard. The black lines show the signal acquired via the pressure insoles. 66

Figure 4-1 – Example of inertial signals acquired during an 8 km/h run. In the picture, the acceleration norm (in red) and the gyroscope norm (in blue) are shown since they are the signals considered by Blauberger et al. for the detection of the events. The black lines represent the pressure insoles signal. The black vertical lines highlight the points in which the

events were identified by the method, while the blue and red filled circled indicate the events detected via the gold standard (pressure insoles). 79

Figure 4-2 – Vector magnitude unit (VMU) of x, y, and z acceleration (A) and angular velocity (B) throughout one single sprint step, that is the norms of the signals, from dataset used in [14]. The blue dashed line marks the initial contact event; the red dashed line the terminal contact. The solid red line indicates the resulting ground contact period for the inertial measurement unit (IMU). The photo-electric-measured (Optogait) ground contact time is represented by the solid blue line. 79

Figure 4-3 – Mid-swing to mid-swing cycle from the 10 km/h trials. In the picture, the vertical acceleration, in pink, and the medio-alteral angular velocity, in light blue, are shown, since these are the signals used in Schmidt et al. [62] for the events identification. The shape of the inertial signals closely resembles the one described in the paper. 80

Figure 4-4 – Mid-swing to mid-swing cycle from a sprinter running at 32 km/h . The mediolateral angular velocity has been pictured as it is the inertial signal used in Falbiard et al. [63] for the identification of the events. As shown by the results, the performances in the identification of the FC seem to be worse than the ones on the IC..... 81

Figure 4-5 – Mid-swing to mid-swing cycles for all the four speeds analysed. The events identified by Blauburger et al. are shown as well as the events detected via the GS. It can be noted that the performance for the method for all four dataset seem to be acceptable based on the distance between the GS and the method-detected event..... 82

List of Tables

Table 1.1 – In the table, different systems for the running evaluation and their usages are listed. [14].....	21
Table 2.1 – Summary of the implemented methods. MAD = Mean Absolute Difference, MAE = Mean Absolute Error, ME = Mean Error, IQR = Interquartile Range.....	41
Table 3.1 – Summary of the number of total running cycles analysed for each speed	58
Table 3.2 - RMSE and missed events for IC and FC, MAPE for stride, swing and stance duration obtained via each of the tested method over the 8 km/h dataset.....	59
Table 3.3 - RMSE and missed events for IC and FC, MAPE for stride, swing and stance duration obtained via each of the tested method over the 10 km/h dataset.....	61
Table 3.4 - RMSE and missed events for IC and FC, MAPE for stride, swing and stance duration obtained via each of the tested method over the 14 km/h dataset.....	63
Table 3.5 – RMSE and missed events for IC and FC, MAPE for stride, swing and stance duration obtained via each of the tested method over the sprinters dataset (20-32 km/h).....	65
Table 3.6 – Summary of the results obtained by the best method identified for all the four speed ranges. The results are shown in terms of RMSE and missed events for IC and FC, and in terms of MAPE for the durations (stride, stance and swing).....	67
Table 3.7 – Table showing the results of the template-based method while using the accelerometer norm for the detection of both IC and FC.....	68
Table 3.8 – Table showing the results of the template-based method while using the accelerometer norm for the detection of the IC and the gyroscope norm for the detection of the FC.....	68
Table 3.9 – Table showing the results of the template-based method when using the vertical acceleration for the detection of the IC, and the mediolateral gyroscope for the detection of the FC.....	69
Table 3.10 - Summary of the results obtained by the template method for all the four speed ranges. The results are shown in terms of RMSE and missed events for IC and FC, and in terms of MAPE for the durations (stride, stance and swing).	70
Table 3.11 – Specification used for the computation of the specificity. In the table, the total number of strides analysed and the total number of missed events is shown for each speed, together with the specificity derived from these data.	70
Table 3.12 – Results obtained via the template-based method bereft of any filtering	71
Table 3.13 - Results obtained via the template-based method by using Deubachies 6 and decomposing to the first level	71

Table 3.14- Results obtained via the template-based method by using Deubachies 6 and decomposing to the third level 72

Table 3.15- Results obtained via the template-based method by using Symlets 5 and decomposing to the first level 72

Table 3.16 - Results obtained via the template-based method by using Symlets 5 and decomposing to the third level 73

Table 3.17 – statistical test results over the three speeds on the stride duration. The values indicated with a * are the ones lower than the reference p-value, leading to a statistical difference. The differences reported are referred to the means of the parameters for the speeds where a t-test was employed, and for their medians otherwise..... 75

Table 3.18 – statistical tests results over the four speeds on the swing duration. The values indicated with a * are the ones lower than the reference p-value, leading to a statistical difference. The differences reported are referred to the means of the parameters for the speeds where a t-test was employed, and for their medians otherwise..... 75

Table 3.19 – statistical tests results over the four speeds on the swing duration. The values indicated with a * are the ones lower than the reference p-value, leading to a statistical difference. The differences reported are referred to the means of the parameters for the speeds where a t-test was employed, and for their medians otherwise..... 76

Introduction

Running is an activity for which people have been increasingly showing more and more interest. The need to study the movement in detail is ever growing, and advances in technology have made the devices needed to analyse the movement accessible to anyone and easy to use. In particular, temporal parameters have been studied over the years to have a better understanding of the movements made by the athletes, in order to intervene if necessary to fix any erroneous movements, or to assess the performances of athletes in general.

Over the years, lots of studies have been conducted over this subject, usually constrained to a specific speed, or using very high sampling frequencies, which may not be available to anyone. The aim of this thesis is that of testing the performances of nine state of the art methods over a wide running speed range (8-32 km/h) and that of providing a new method that could be suitable for the detection of temporal events through the very different running speeds, even at lower sampling frequencies. The structure of the present work is further described in the following paragraphs.

In Chapter 1 a brief introduction to the theory behind this study is provided. In particular, in the first section, a summary on gait analysis, with focus on running, is presented, followed by a review of the state of the art regarding running analysis and an explanation of the different validation methods that have been employed over the years.

In Chapter 2 the description of the protocols for the data acquisitions brought on to build the wide range datasets is presented, followed by brief descriptions of the nine methods implemented from the literature that have been put to the test. At the end of this chapter, a description of the newly template-based method is provided.

In Chapter 3 the results obtained from the nine literature methods over the three datasets are provided. In particular, a method for each dataset is highlighted as better performing, and one among all is selected as best performing on the whole speed range. After that, a comparison between the results obtained via the newly proposed method and the best trade-off is provided, together with a t-test to check whether the two methods yielded a statistical difference.

Finally, in Chapter 4, the results are further discussed, then conclusions are drawn, ending with some examples of possible future developments and insights on the subject analysed in this work.

Chapter 1

Background

1.1 The biomechanics of running

Worldwide, one of the most practiced sport activities has always been running, the popularity of which has been increasing in the last decade. As a matter of fact, even though the world has been plagued with a pandemic and its subsequent lockdowns in the last few years, more and more people chose running as the perfect way to escape their routine and remain in shape. Recent statistics, based on data aggregated from various fitness tracker apps and devices, show that lockdowns resulted in a raise in the activity level of people worldwide, as stated by the Strava 2020 report. [3]

The interest for this kind of activity has not emerged recently, but it dates way back, as proven by paintings and studies from Ancient Greece. During the years, people have been trying to study and analyse running as a movement, in order to understand it better and be able to improve the performances of athletes that compete in sprinting, for instance, avoiding at the same time despicable injuries. As technology develops further, so have the appliances used to study the movements, which have become more and more precise and complex. Injuries provoked by running are not, as one may think, due to physical abnormalities or different skeletal features one may have, but they are a consequence of repetitive wrong applications of significant loads, even for a very short amount of time, which, if brought on for a long time, will inevitably lead to said injuries. [4]

Although different people will run in different ways based on their anatomical differences, there are some main features that will be found in each period of running.

1.1.1 Gait and running cycle

A gait cycle is the basic unit of measurement in gait analysis [5], and it is composed by the ensemble of movements that intercur between the contact of one foot to the ground and

the subsequent contact of the ipsilateral foot. It can always be divided into two different phases:

- Stance phase: the period in which the foot remains in contact with the ground. It begins with the foot strike, called initial contact (IC) and it ends with the toe off, terminal contact, called final contact (FC).
- Swing phase: in this phase, the lower limb swings forward in advancement from a final contact, which marks the beginning of the phase, to the subsequent initial contact of the other foot, which marks its ending. [6]

These two phases can be found in both running and walking, although differences in timings occur. In walking, there is a phase of double support, when moving from a foot to another, in which both lower limbs are in contact with the ground; on the other hand, in running there is no double support phase, which is replaced by a *double float* phase, happening two times per cycle, in which both lower limbs are not in contact with the ground, thus increasing the time spent in swing phase at the expense of the stance phase. As speed increases, runners tend to have shorter stance phases, since the propulsion the runner needs to move forward is given by the constant swinging of both upper and lower limbs, in opposite to walking, in which the forward momentum is given by the stance leg. [7] In Figure 1-1, the different phases of the running gait cycle are shown, while in Figure 1-2 the differences in the running and walking gait cycle are presented.

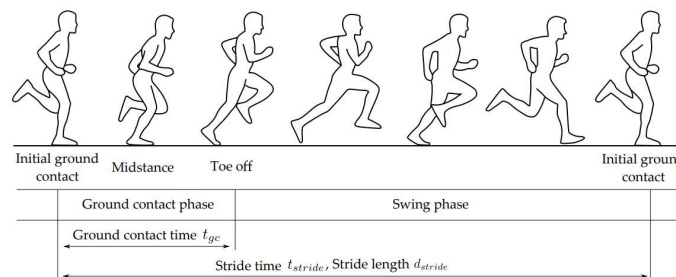


Figure 1-1 - The phases of the running gait cycle [8]

Generally, as speed increases moving from running to sprinting, the types of initial contact changes from *rearfoot* contact to *forefoot* contact. Competitive runners are usual to hit the ground with the forefoot only, without ever touching the ground with the rearfoot, with the main purpose of covering as much distance as possible in the least amount of time; in running at lower speeds the whole foot gets in contact with the ground: as shown by statistics, the vast majority of runners are rear-foot strikers (80%), the remaining are mid-foot strikers. [8]

On the other hand, the swing phase is made out of initial swing, at the beginning of which the first float phase occurs, and terminal swing, at the end of which the second float phase takes place. [7]

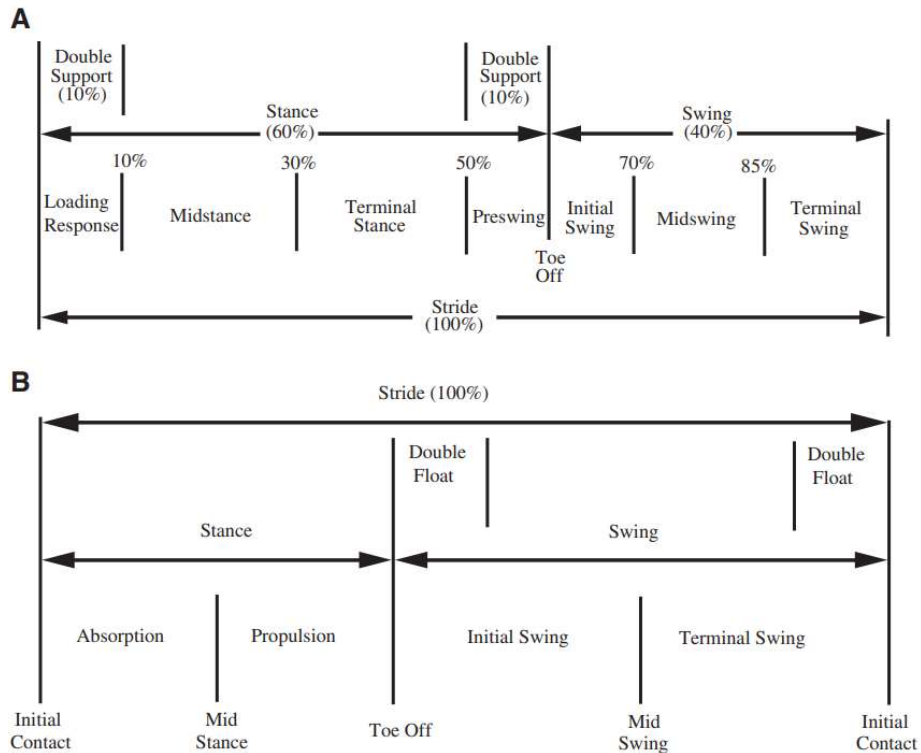


Figure 1-2 - The phases of the gait cycle. (A) Walking, (B) Running

Running at any speed is an alternation of accelerations and decelerations. The first half of the stance phase is absorption (pronation), the second half propulsion (supination). [7] The two phases are divided by the mid-swing event. [8]

1.1.2 Gait and running spatio-temporal parameters

Spatio-temporal parameters over the years have shown a very strong connection to the performance of the athletes, which makes them perfect indicators of one's activity, allowing coaches and athletes to better understand their movements. [10]

In gait analysis, a stride is defined as the ensemble of events that take place between a contact of the foot with the ground and the subsequent contact of the same foot, the *stride duration*, or *running cycle*, is defined as the time that intercurrs between said contacts. Accordingly, a step is defined as the ensemble of events that take place between the contact of the foot to the ground and the contact of the other foot. It follows that a stride is made up of two steps.

Gait parameters can be divided into spatial and temporal parameters. Spatial parameters, or distance parameters, can be described as [11] :

- Stride length: the distance between two consecutive contacts with the ground of the same foot. Its direction defines the direction of the gait;
- Step length: the distance between the contact of one foot to the ground and the consecutive contact of the other foot;
- Stride width: the distance, computed perpendicularly to the direction of the gait, between the contact of one foot to the ground and the consecutive contact of the other foot.

Temporal parameters can be further divided into [12] :

- Stride Rate, the number of strides per unit of time;
- Stride Duration, the duration of the stride;
- Speed, the distance covered by the subject per unit of time;
- Step Duration, the duration of the step;
- Stance Duration, the duration of the stance phase;
- Swing Duration, the duration of the swing phase.

1.2 Running Analysis

In this section, a brief summary of the papers utilised to redact this master thesis is presented. The aim of the subsequent paragraphs is that of outlining the present state of the art regarding the analysis of the running motion via inertial measurement units (IMU) or magneto inertial measurements units (MIMU).

The references utilised to redact this section are reported in the dedicated section at the end of the present work, in order of appearance in the text.

1.2.1 State of the art for the identification of running events

The analysis of the human movement has been a topic of interest for many years. In particular, the gait analysis in the last decades has shifted from being merely an academic discipline, to gaining a certain clinical relevance, as from it some observations about a subject health could be made. [13]

As of running, the increasing interest that people have shown toward this activity has led to the necessity to evaluate the motion in detail, with the aim of evaluating performances to improve them, prevent injuries or even monitor the rehabilitation process after an injury. The proliferation of technology has made the devices needed for said evaluation accessible to a wider range of people, and this allowed for the running analysis to be feasible even outside clinical gait analysis centres. [14] Through the years, motion analysis systems, force platforms, inertial measurements units, in-sole pressure sensors and electrogoniometers have been used, with different aims, a summary of which has been presented in Table 1.1.

Sensor/System	Measured Parameters
Motion analysis systems	Segment position and orientation, linear and angular velocity, and acceleration
Force platforms	Ground reaction force, loading rates, center of pressure, joint moment, and power (when used with segment position and orientation data)
Pressure sensors	Pressure distribution, vertical force, center of pressure, spatiotemporal gait parameters
Electromyography	Muscle activation and timing patterns, muscle fatigue
Accelerometers	Segment acceleration and orientation, spatiotemporal gait parameters
Electrogoniometers	Relative joint angles
Gyroscopes	Segment orientation, angular velocity, and acceleration

Table 1.1 – In the table, different systems for the running evaluation and their usages are listed. [14]

However, as running tends to be a more fast-paced movement compared to walking, various studies has been conducted on the appropriate way to analyse it in terms of correct sampling frequency, sensor positioning, gold standard utilised, and so on. In terms of temporal parameters estimation, as stated in Table 1.1, IMUs and MIMUs, that include accelerometers, gyroscopes, and magnetometers, are broadly used. Sensors have been positioned on the tibia, on the lumbar spine and on the foot for the evaluation of the running events. A systematic review made by Horsley et al. [15] suggested that the positioning of the sensor is not the most critical factor for the accurate detection of the events, that depends more on the mathematical approach followed. Moreover, Zrenner er al. [8] conducted a comparative study with focus on the positioning of the IMU on the foot for the estimation of running gait parameters, with the result that the best positioning would be under the arch of the feet, in a cavity created in the sole of the shoe. In Figure 1-3 a depiction of the different positioning evaluated is presented. Anwary et al. [16] investigated the same issue but on bare feet as they believed that the wear and tear of the shoes could affect the accuracy of the detection of the events. Their findings suggest that the best positioning for the sensor on bare feet is the metatarsal region.

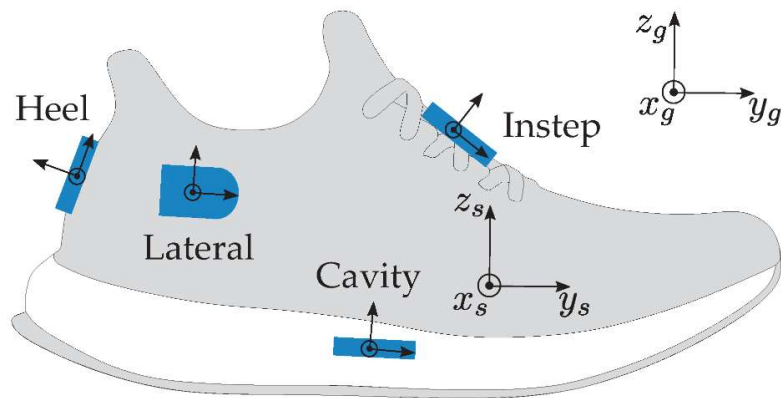


Figure 1-3 – Visualization of the different positioning of the IMUs on a running shoe. [7]

When speaking of sampling frequencies, many studies have attested that for a movement as fast paced as running can be, a higher sampling frequency than the ones normally employed for walking should be adopted. Diaz et al. [17] stated that the most appropriate sampling frequency for the accurate acquisition of running movements should be between 200 Hz and 300 Hz, because of the very high peaks the accelerometer can present when put under very high velocities, Blauberger et al. [55] also supported their findings by attesting that the most suitable sampling rate for sprinting motions should be of around 200 Hz. Macadam et al. [18] attested that for sprinting the minimum sampling frequency of 200 Hz should be adopted, even though even at 100 Hz reliable data could be acquired. In the following chapters of the present study, an attempt to detect temporal events during running at 100 Hz has been made, to reduce computational requirements and allow the running analysis even though IMUs with a sampling frequency constraint are employed.

Concerning the actual detection of the temporal events, different approaches have been adopted. The most common one is based on peaks detection coming from the inertial signals acquired by the IMUs. Blauberger et al. [55], Reenalda et al. [66] and Yang et al. [70] used the norm of the accelerometer and the gyroscope, Benson et al. [69] used solely the norm of the accelerometer, Schmidt et al. [62] used the vertical acceleration and the mediolateral gyroscope, Falbiard et al. [63] used different combinations of signals to conclude that the mediolateral angular velocity resulted in the best performances, similarly to Mo et al. [67] that, among all, chose the norm of the accelerometer and the vertical acceleration to be the best performing. Moreover, Bailey et al. [64] used the vertical acceleration and the mediolateral gyroscope, Chew et al. [68] opted for the anteroposterior acceleration.

Other different detection techniques have also been used for walking, but not in running. Dynamic Time Warping is a technique that has been used for the detection of temporal events in walking or slow running. Dot et al. [19] developed a greedy template-based step detection algorithm by exploiting the mediolateral angular velocity and a singular step as template for the detection of temporal events during walking. Oudre et al. [20] and Vienne-Jumeau et al. [21] developed a database of templates for the walking gait detection, with the help of a gold standard to annotate the templates. Chakraborty et al. [22] exploited dynamic time warping for the identification of temporal events during running at 8 km/h. To this date, no method exploiting dynamic time warping or templates has been developed for the detection of the temporal events during running on a wide speed range.

Furthermore, the use of wavelet transformations in terms of detection and denoising is becoming increasingly popular. Aung et al. [23] and Gouwanda et al. [24] used discrete

wavelet transformations for the identification of the gait events, Aminian et al. [25] and Soangra et al. [26] used it as a form of peak enhancement and Dautov et al. [27] analysed its potential as a denoising technique. The potential of this technique in the detection of running temporal events is yet to be investigated.

All the different methods available for the detection of running temporal parameters were targeted toward a specific running speed, or a narrow range of speeds.

Finally, for validation purposes, a different range of systems have been adopted. Some papers used a high-speed video acquisition system for reference [28] others opted for a optoelectronics systems, for example stereophotogrammetric systems, [30] [31] [55] [62] force plates [29] [67] [69] instrumented treadmills [32] [63] foot switches [6] and pressure insoles [55] [48]

1.3.1 Instrumentation

In this section, a brief explanation of the different instrumentations usually exploited for the running analysis is presented.

1.3.1.1 Magneto Inertial Measurement Units (MIMU)

Human movement has been increasingly monitored by using wireless sensors, either to assess the performances of athletes [36] [37] [38] or to prevent injuries. [39] [40] The main reasons for which one may opt for a wireless sensor are the low cost, ease of use which makes the presence of a technician useless and the fact that they can be used in out-of-lab assessments, making them suitable for the analysis of the actual performances of the athletes. Among the different types of wireless sensors, two of the most used ones are IMU (inertial measurements units), that measure acceleration and angular velocity via exploiting the concept of inertia (mass and acceleration), and MIMUs (magneto inertial measurements units), that in addition to that measure the magnetic field as well. These are the only type of instrumentation that allow the extraction of both temporal and spatial parameters. They are composed of tri-axial sensors such as: accelerometer, gyroscope and magnetometer.

Being a low-cost equipment, a MIMU is affected by a variety of issues, mainly caused by the limitation of the sensors when looked at singularly. Specifically, the accelerometer is affected by gravity and other types of accelerations that may be present in the environment, the gyroscope is affected by different biases depending on the axis and finally the magnetometer is sensible to ferro-magnetic disturbances and is also the most difficult to calibrate. In this section, a detailed explanation of the components of a MIMU is presented.

1.3.1.1 Accelerometer

The accelerometer is a sensor that measures the linear acceleration a along one of its sensible axes, from which the proper acceleration can be computed, that is the difference between the acceleration the sensor senses a_s and the gravity acceleration g , as in (1.1). It underwent a wave of popularity due to its miniaturization following the advent of microelectromechanical systems (MEMS) technology. They can either be single or multi axial, but, with focus on the MIMU, miniaturized multi-axial accelerometers are mainly used.

$$a = a_s - g \quad (1.1)$$

The physical principle exploited by these sensors is the linear velocity change of the mass affected by the acceleration. There is a frame, to which a mass m is connected through a spring with elastic constant k . In parallel to this system, linked to the mass, there is a damper with damping coefficient b , as shown in Figure 1-4. When an acceleration a is applied to the mass, the force applied can be computed following the inertia principle, as in (1.2):

$$\sum_{i=1}^N F_i = ma \quad (1.2)$$

where the first term indicates all the forces applied on the mass, which are the applied force $F_{applied}$, the spring force $F_{spring} = kx$, where x indicates the displacement of the mass, and the damper force $F_{damper} = bv$, where v indicates the speed at which the mass moves. From (1.2):

$$F_{applied} + F_{spring} + F_{damper} = ma \quad (1.3)$$

Given that the speed of the mass can be computed by deriving its displacement, and the acceleration can be obtained by deriving the speed, the equation in (1.3) becomes as in (1.4):

$$F_{applied} = m\ddot{x} - b\dot{x} - kx \quad (1.4)$$

From which it can be stated that, in order to obtain the acceleration of the mass, the displacement of the same has to be known, which is exactly the principle on which accelerometers are built. [41]

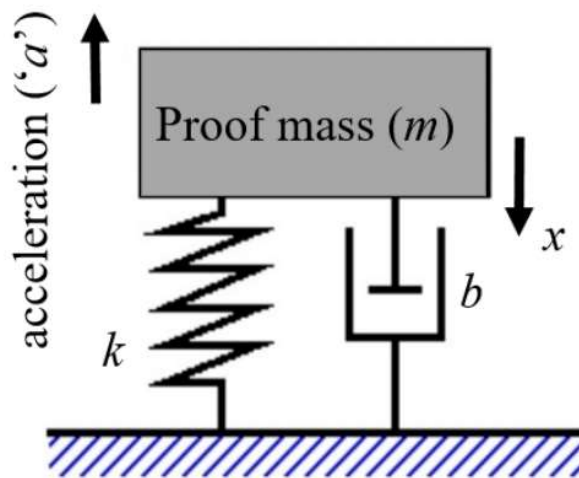


Figure 1-4 – Accelerometer spring-mass-damper system [41]

The accelerometers, even if they all rely on the same physical principle, can be built in different ways, in particular different transducers can be adopted such as: piezoelectric crystals, servo force balance transducers, electronic piezoelectric sensors, piezoresistive sensors and variable capacitance sensors. The last two are the mostly used in gait analysis. [8]

In capacitive accelerometers the displacement of the mass is converted into a capacitance change which gets converted and amplified into a voltage signal. In piezoelectric accelerometers, the mass travels on the surface of a piezoelectric crystal that, if subjected to the movement of the mass, will be deformed, and thus generate a proportional electric current.

An accelerometer has different parameters such as:

- Bandwidth (Hz) which indicates the frequency range to which the accelerometer is sensible. A bandwidth of 40-60 Hz is usually adequate for the analysis of the human movement.
- Sensitivity which measures the minimum change in the output corresponding to a mechanical change.
- Voltage noise density that is the noise associated to the measurement.
- Dynamic range (g) that is the range of measurements feasible with the sensor.

The output of the accelerometer varies based on the way it is mounted on the subject and the motion. In Figure 1-5 an example of a tri-axial accelerometer output acquired via a foot-mounted MIMU during a running trial is shown.

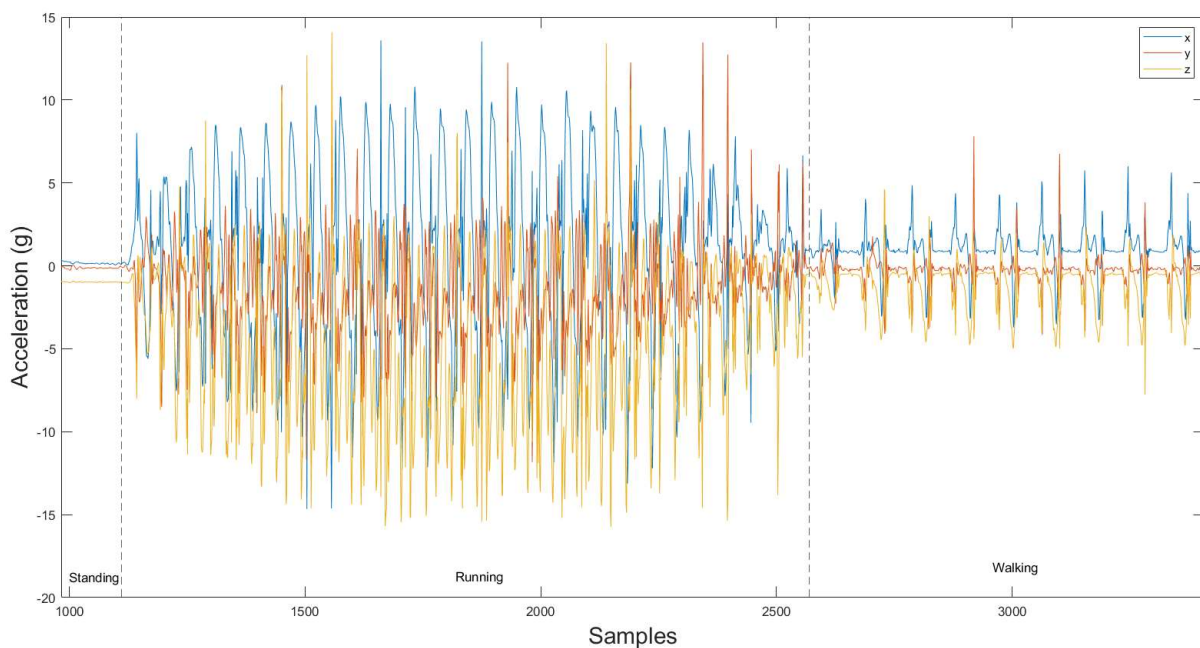


Figure 1-5 – sprint trial acceleration. In blue, the vertical acceleration, in orange the mediolateral acceleration and in yellow the anteroposterior acceleration during a sprinting trial. The hatched lined indicates a change in motion: in the first part, the subject was standing, in the central part the subject was sprinting and, lastly, the subject began to walk.

1.3.1.2 Gyroscope

Gyroscopes are sensors that measure and maintain the orientation and the angular velocity of an object in motion. They usually are composed by three orthogonal axes on which the measurements are performed. They can be very useful when one needs to compute the rate of turn of an object without a fixed point of reference.

There are three different types of angular rate measurements that can be achieved via the gyroscope, illustrated in Figure 1-6:

- Yaw, that is the horizontal rotation of an object seen from above
- Pitch, the vertical rotation of an object
- Roll, the horizontal rotation of an object seen from the front.

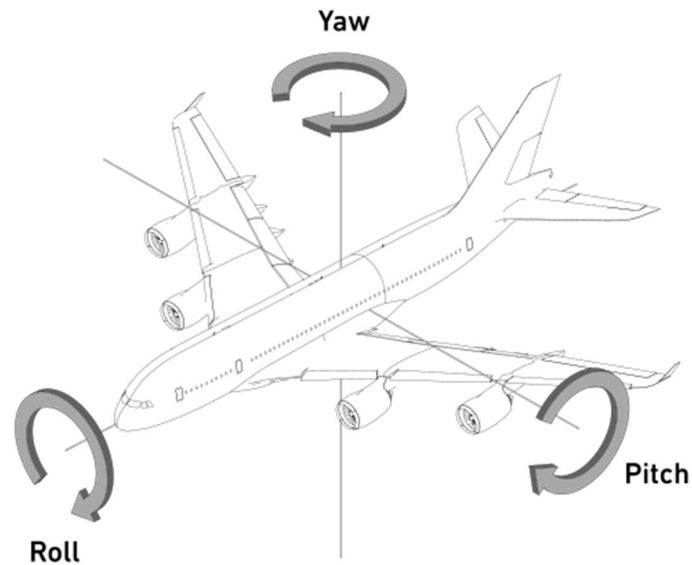


Figure 1-6 – visual representation of the three different angular rate measurements: Roll, Pitch and Yaw [42]

There are different commercially available classes of gyroscopes, but the more commonly used are mechanical and optical gyroscopes, which differ on the operating physical principle they use to measure the angular velocity. [43]

A mechanical gyroscope is made out of a spinning mass that rotates around one of its axes. This movement the mass is subjected to, i.e. the rotation, makes it so that the mass tends to oppose to any changes in its orientation, it tends to remain parallel to itself, and this happens even if the mass changes its rotation direction.

Most gyroscopes rely on Coriolis' force, that is an apparent force: when an object travels on a rotating surface, from an external point of view the object trajectory will seem straight, while from a point of view belonging to the rotating surface, that rotates with it, the trajectory will seem curved, as if some kind of force has been applied to it – that is the Coriolis' force. This force is dependent on the angular velocity ω as stated in (1.5), and the displacement of the object is proportional to the Coriolis' force. By measuring the displacement, the angular rate can be obtained, which is then converted into an electric signal.

$$F_c = -2m \cdot (v \times \omega) \quad (1.5)$$

The working principle is strictly linked to the inertia principle, as the accelerometer. Since the working principle is based on the detection of the displacement of the mass, the transducers used in them must be sensible to it, by relying on different sensing technologies: electrostatic, which exploits the capacitance changes to detect the motion; piezoelectric that is based on direct piezoelectric effect; and piezoresistive, which detects the change of the resistance in response to a mechanical deformation.

One of the most important parameters for gyroscopes is the drift rate, that is the phenomena for which the gyroscope returns a value different than zero when the expected value should be null. It is mainly composed by:

- Bias, that indicates the measurement the sensor returns when it is still. It indicates the initial rotation of the sensor.

- Environmentally sensitive drift rate, that are the components sensitive to the environment conditions, such as temperature, acceleration, vibration, etc.

Gyroscopes are usually divided into three groups: navigation, that are usually exploited in mobile phones and cars; tactical-grade, that are used for military applications, and rate-grade devices, typically used in rockets, with a crescent precision degree. [44] Just like the accelerometers, the output of the gyroscopes depends on the way they are mounted and on the motion they are subjected to, as shown in Figure 1-7.

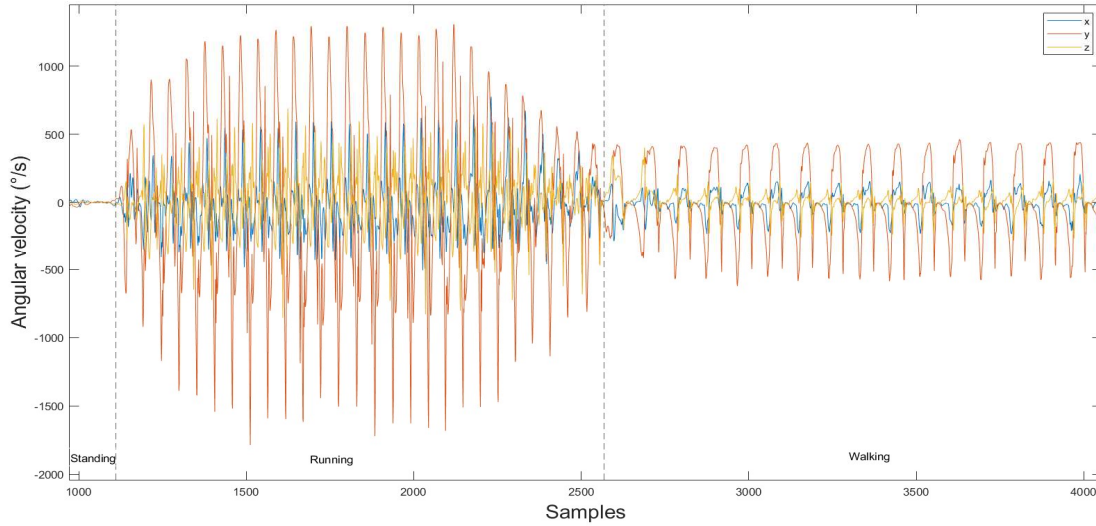


Figure 1-7 – Gyroscope signals acquired along three orthogonal axis during a sprinting trial. In blue, the vertical axis, in orange the mediolateral axis, in yellow the anteroposterior axis. The hased lines indicates a change in motion: in the first part, the subject was standing, in the middle part running, and finally walking.

1.3.1.3 Magnetometer

The magnetometer was firstly invented by Friederich Gauss to measure the magnetic field. The measure of the magnetic field components along its three axes allows for a univocal definition of the magnetic field vector in the point in which the measure is held. It relies on the Lorentz force.

Let's consider a charge q moving with a certain speed v on a conductive surface on which a constant magnetic field B is applied. The charge will be subjected to a force, known as Lorents force, described by the equation in (1.6).

$$F_L = q(v \times B) \quad (1.6)$$

Because of this force, the charge starts moving transversally, causing an electric field E_{hall} to form on the sides of the conductive surface, which leads to the production of an electric force. The total amount of forces to which the charge is subjected can be described as in (1.7).

$$F = q(v \times B) + qE_{hall} \quad (1.7)$$

which leads to (1.8) in equilibrium conditions:

$$(v \times B) = -E_{hall} \quad (1.8)$$

This is called the Hall Effect which creates a voltage V_H on the conductive surface that is proportional to the magnetic field applied. A visual representation is provided in Figure 1-8.

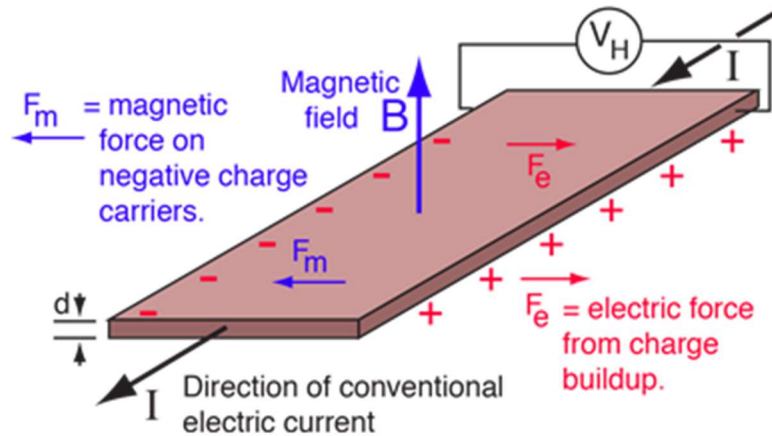


Figure 1-8 – Visual representation of the Hall effect. The red signs (- and +) represent the charge buildup on the sides of the conductive surface, which result in an electric field. Based on the charge of the particle traveling on the surface, it will tend to accumulate on one side or the other. Source: <http://hyperphysics.phy-astr.gsu.edu/hbase/magnetic/Hall.html>

However, not all the magnetometers rely on the Hall effect. Some of them use magneto induction methods, that calculate how magnetized a material becomes when exposed to a magnetic field; or magnetoresistance methods that consider the capacity of the object to change its resistance when exposed to a magnetic field.

Magnetometers are, as one may think, very sensible to ferro-magnetic disturbances, making them useful for outside evaluations, but less for indoors, since in those conditions more disturbances are present. Due to its problems, in gait analysis the magnetometer is often neglected, but there are a few examples of how it could be useful in the events detection, such as for stride segmentation, [34] or gait phase detection. [35] Usually they are used in combination with gyroscopes and accelerometers in MIMUs.

The output coming from a magnetometer changes based on where it is mounted and the motion of the subject, a visual representation of this is provided in Figure 1-9.

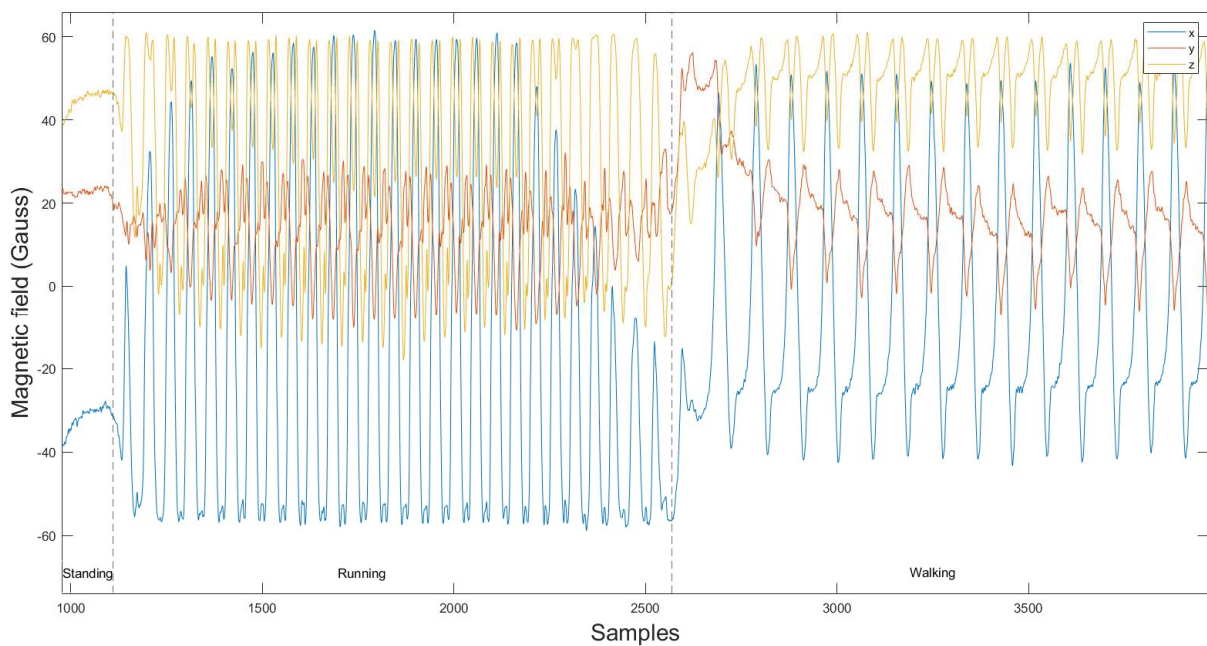


Figure 1-9 – Magnetometer signal acquired during a running trial along three orthogonal axes: in blue the vertical axis, in orange the mediolateral axis, in yellow the anteroposterior axis. The hashed line indicates a change in motion. In the first part the subject was standing, then running and in the end the subject began to walk.

1.3.2 Validation systems

As stated before, in literature different validation systems have been employed. In this section, a brief explanation of each system is provided.

1.3.2.1 Optoelectronic systems

The optoelectronic systems are very accurate motion-capture tools. They are often utilized as gold standard, indeed. Usually, the aim of the movement analysis is to obtain information about the movement of the body parts during the motion, such as the movement of the centre of mass, the movement of adjacent bones or joint kinematics, which is feasible through stereophotogrammetric systems. [45]

Optoelectronic stereophotogrammetry is based on the steps here defined:

- the acquisition of 2D images through cameras, the number of which can vary from a minimum of two (for the 3D reconstruction) to about fifty, that are used to capture the positioning of markers on the subject, which will be labelled to identify the body segment in the planes of the image.
- a transaction to 3D models in order to obtain the position of each marker in a global reference system.
- The definition of a local reference system for each body segment, that will allow the identification of their positioning thanks to the definition of a human body mathematical model.

A visual representation of the system is provided in Figure 1-10.

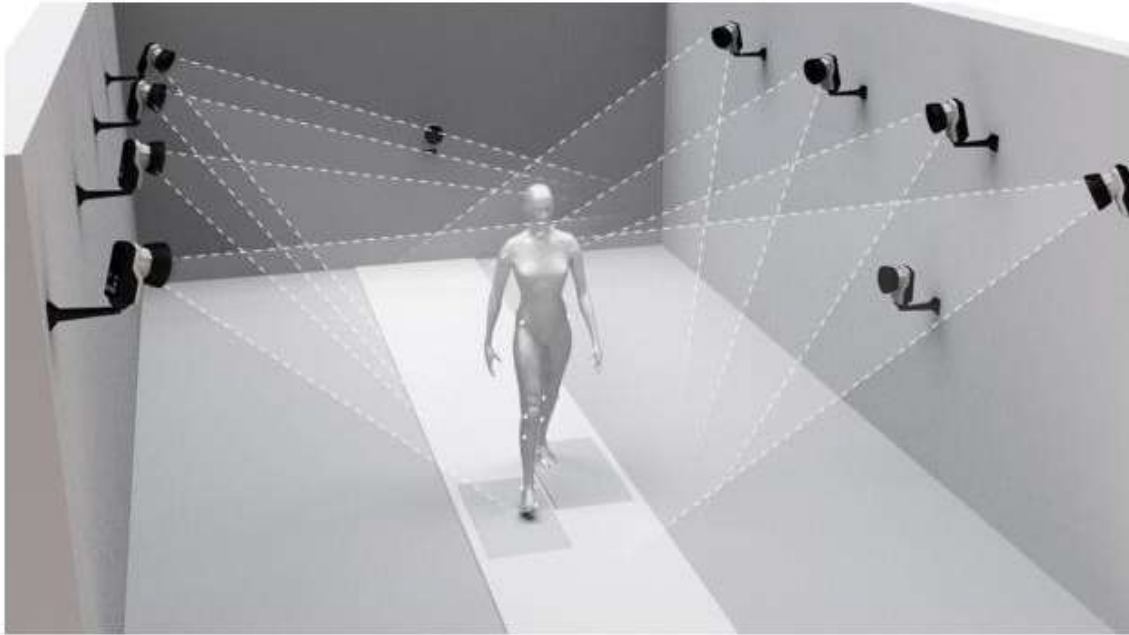


Figure 1-10 – Optoelectronic setup for the motion capture. Source: <https://assistiverobotcenter.github.io/images/toolbox/sensors/qualysis.jpg>

Optoelectronic system can either be active or passive. Passive markers are covered in a reflective material that will reflect the IR light coming from the cameras, while active markers are a direct source of light, as they are usually IR LEDs. This type of marker implies that the light has to travel the distance between the camera and the marker only once, which results in an enlarged volume of acquisition in respect to the ones achievable through passive markers. The main drawback of this type of marker is that it requires an active power supply for each marker to allow the emission of the light.

The main issue related to optoelectronic systems is that they are relegated to a laboratory environment, which limits not only the movement in exam, that is confined to a constricted acquisition area, but also the utility of the device, since it will not be able to monitor motions happening during daily activities. Nonetheless, it still is a very accurate motion-capture system, which makes it a go-to gold standard when it comes to gait analysis.

1.3.2.2 Force plates

Force plates are a tool that has been broadly adopted for motion analysis and allow the measurement of the different components of the ground reaction force vector, while also allowing the establishment of the point of application of the same. [46]

By knowing the frequency of the force data acquired, additional measures can be computed, such as:

- Speed
- Power
- Displacement
- Temporal parameters
- Left/Right Asymmetry

They can be either single axial, that allows the measurement of only one component of the ground reaction force, or multi-axial, which enable the detection of all the components of said vector. Over the years, they have gained popularity when it comes to the evaluation of athletes, to monitor training effectiveness. [47] A force plate visual representation is provided in Figure 1-11.

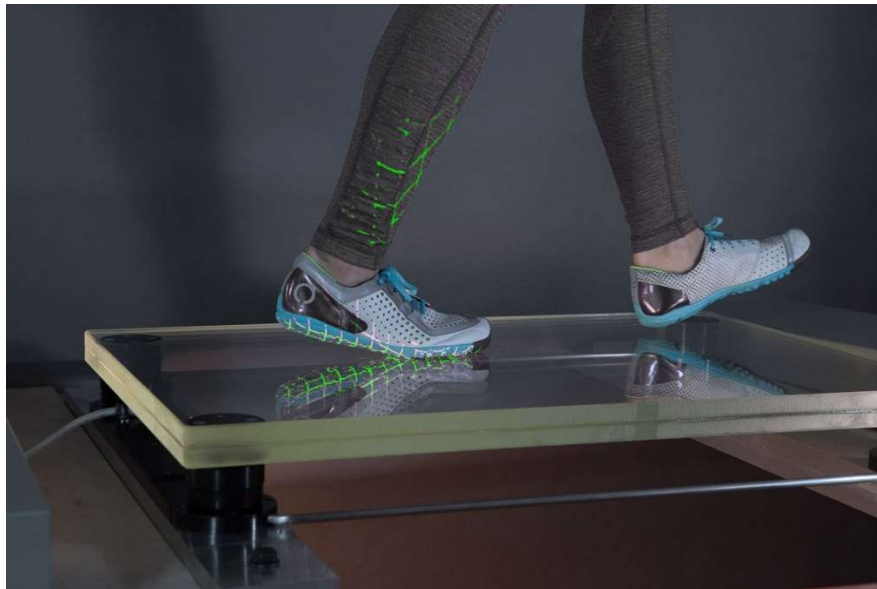


Figure 1-11 – Example of force plate. Source: <https://www.technogym.com/wp-content/uploads/2019/04/Force-plate.jpg>

Force plates usually rely on load cells containing piezoelectric elements, strain gauges, capacitance gauges, piezoresistive elements or rely on the Hall effect. All of these technologies make it so that when a force is applied a proportional voltage is generated. To obtain a reliable measurement, the force plates should be installed below the floor level, so that they could not be sensed by the subject when walking. Other applications involve the use of instrumented treadmills, with force plates embedded. Because of their ease of use, they have been broadly considered as gold standard in gait analysis. The use of instrumented treadmills, however, calls for a laboratory environment and, furthermore, it is not adequate for the evaluation of a subject's speed, as it has a set speed which gets imposed on the subject.

Apart from being limited to controlled environments, these devices are not portable and can be expensive, which limits the analysis to a few strides and straight walking.

1.3.2.3 Foot switches

Foot switches are very popular devices implied as gold standard in gait analysis. They are a very inexpensive tool to obtain gait events. There are two different types of foot switches:

- Compression closing switches: they are made of thin pieces of brass separated by a compressible layer of rubber. When pressure is applied, the rubber gets in contact with the two brass layers, which leads to the closing of an electrical circuit.
- Force sensitive resistors: they are made out of thin layers of plastic on which circuits are engraved. When pressure is applied, a resistive electrical circuit is created. [48]

Foot switches are a great way to estimate gait events, and they have been previously adopted in different studies [6] , however they are usually limited to two to three sensing elements, that have to be singularly placed on the foot, thus limiting their repeatability and spatial resolution. In Figure 1-12, an example of foot switch is provided.



Figure 1-12 – example of foot switch and their positioning. Source: https://www.motion-labs.com/prod_access_footswitches.html

1.3.2.4 Pressure insoles

In-shoe instrumented devices are becoming more and more popular in the domain of gait analysis, mainly due to their low cost and portability. They usually tend to be based on different technologies and configurations, similar to the foot-switches ones, with the aim of providing a high-resolution pressure map, which needs a very dense grid of sensors, whose number varies from 99 to 960, making them more expensive and computationally complex as the number of sensors goes up. Such a high number of sensing elements is not needed for the gait events estimation.

However, recently, Salis et al. [55] developed a new type of pressure insole especially thought for the gait events estimation, which includes only sixteen sensing elements. These sensing elements are based on force sensing resistor, which exhibit a resistance which is inversely proportional to the force that is applied to them. The resistance is then converted to voltage. This new type of pressure insoles is what has been used in this study for two of the three datasets analysed. In Figure 1-13, a visual representation of the pressure insole is provided. For the way they are thought, pressure insoles compensate the drawbacks of foot switches, since they have a better spatial resolution, and the placement is way more repeatable.

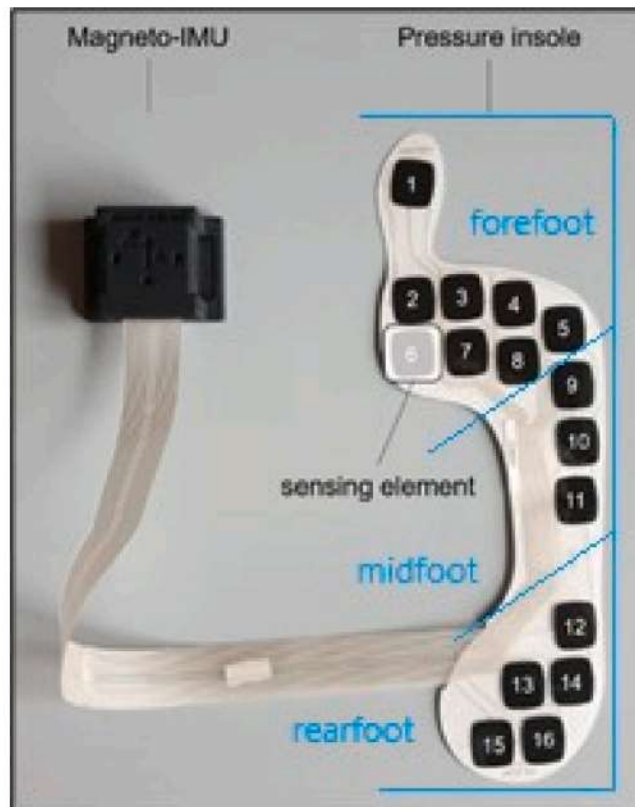


Figure 1-13 – Pressure Insole developed by Salis et al. [48]

1.3.3 Algorithms for the identification of gait and running temporal parameters

The detection of running temporal parameters has been of great interest in the latest years. In this section, a short explanation of the techniques cited above is provided.

1.3.3.1 Traditional techniques based on peak detection

Traditional algorithms rely on peaks detection. These techniques exploit the morphology of the different signals acquired via the inertial sensors to detect the events. This is made possible because the movement of the athlete causes abrupt changes in both the accelerometer and gyroscope signals, which result in peaks. Because of the nature of the movement itself, the easier event to detect is the initial contact, since it usually results in very prominent peaks, especially in the accelerometer signals; on the other hand, since the final contact is not linked to strong changes in the movement, its detection can be more complex.

During the years, all sorts of different peak detection algorithm have been developed, changing the signals exploited and the detection strategy employed. Detection strategies include:

- Stride segmentation to ease the detection:
- The use of thresholds to discriminate between the peaks of the signals. The thresholds could be numeric or parametric;
- The identification of global minimums and maximums between certain search windows.

- Exploitation of the signals zero crossings, either to detect the events or to define some search windows, to allow a better identification.

1.3.3.2 Wavelet transformations

Wavelets can be used in many ways. In the gait analysis field, wavelet transformations have been mainly adopted for the events detection [23] [24] and for the denoising of the signals [25]. Wavelet transformations are mathematical tools used to divide the original signals in different component based on frequency. To perform a wavelet transformation, many different waves can be used, called mother wavelets ψ , that are portions of signals that will travel forward in time. Each mother wavelet must meet the condition indicated in (1.9).

$$\int \psi(t) dt = 0 \quad (1.9)$$

Different types of mother wavelets can be used based on the application in exam. [49] In gait detection, it has been proved that the most suitable are the mother wavelets belonging to the Daubechies family. [26] [71]

The core of the wavelet transformations is the decomposition of the signals in different frequency levels of coefficients, allowing the analysis of the signals for different frequency bands. There are two types of wavelet transforms:

- Continuous Wavelet Transform (CWT): it can be defined as in (1.10). It returns a complete representation of a signal by letting the scale and translational parameters, called coefficients, vary continuously. The daughter wavelets will be a translated and scaled versions of the mother wavelet.

$$X_w(a, b) = \frac{1}{a^{\frac{1}{2}}} \int_{-\infty}^{+\infty} x(t) \bar{\psi}\left(\frac{t-b}{a}\right) dt \quad (1.10)$$

Where $\psi(t)$ is the mother wavelet, a is the scale factor and b the translational value. It uses every possible wavelet, so there can be an infinite number of scales and locations.

- Discrete Wavelet Transform (DWT): it is any wavelet transform that uses discretely sampled wavelets. It decomposes the signal into a set of orthogonal wavelet functions. They are, as the CWT, translated and scaled versions of the mother wavelet, but the variations are discretized to integers power of 2.[50] It is invertible, which makes it possible to recover the original signal from its transform. It can only use a definite set of wavelets. It can be defined as in (1.11).

$$X_w(a, b) = \frac{1}{a^{\frac{1}{2}}} \int_{-\infty}^{+\infty} x(t) (a_0^{-m} t - nb_0) dt \quad (1.11)$$

Where $\psi(t)$ is defined as in (1.12), $x(t)$ is the series analysed.

$$\psi_{a,b}(t) = a_0^{-\frac{1}{2}} \psi\left(\frac{t-b}{a}\right) \quad (1.12)$$

where $\psi(t)$ is the mother wavelet, t indicates time, a represents the scale factor, which is usually an integer power of 2 and indicates how the signal will be distorted. Each wavelet works on different frequency spans, which are dictated by the scale factor: high scale factors correspond to low frequencies, while low ones correspond to high frequencies. The parameter b allows the signal to move in time, which is strictly linked to a :

$$a = 2^j, \quad \text{with } j \in \mathbb{Z}$$

$$b = 2^j m, \quad \text{with } m \in \mathbb{Z}$$

The scale and time factors transform the mother wavelets in daughter wavelets. Wavelet transform basically is the convolution of the signal with the mother wavelet, hence it can be seen as linear filtering and successfully implemented via an analogue filter bank. The signal is put through two filters: a high pass filter, which returns detail coefficients, and a lowpass filter, which return approximation coefficients. After the filtering, the signal is down sampled with base 2. The process can be repeated a number of times, defined by the parameter ‘levels’, which indicates how many time the signal will be filtered, as indicated in Figure 1-1. This is how the discrete wavelet transformation is computed in MATLAB, where an orthogonal filter is built based on the mother wavelet chosen. The parameters needed for this type of computation are the mother wavelet to be used and the level to which the decomposition must go down to.

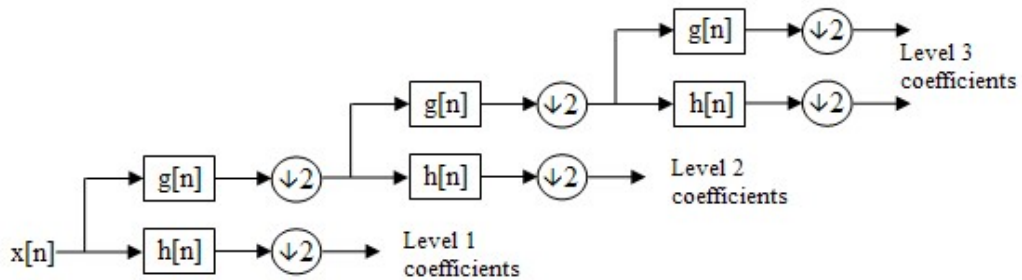


Figure 1-14 - representation of the discrete wavelet transformations. In the picture, $g[n]$ represents low pass filters, while $h[n]$ represents high pass filters. The signals are down sampled after each filtering step.

In order to apply some denoising to the signals, a DWT based wavelet decomposition has to be brought forward for which one of the most important parameters to choose is the level of decomposition. A common approach to the denoising involves the decomposition of the signals to a certain level and the choice of a threshold to apply to the coefficients: all the coefficients larger than the threshold would be discarded. From the thus obtained coefficients, the denoised signals will be reconstructed. There are many already existing threshold techniques that are commonly used to define the threshold value.

1.3.4 Dynamic Time Warping

Dynamic Time Warping (DTW) is a technique commonly employed to measure the similarity between two signals, firstly thought for speech analysis. It has been broadly used in gait analysis for validation purposes, or to identify the phases of the gait based on the shape of the signals acquired. It consists in measuring the similarity of two signals through a distance metric, which could be of different types (Euclidean, squared, etc.), and it does not require the signals involved to be of the same length. Any linear sequence of data can undergo dynamic time warping.

When measuring the distance between two signals by using the Euclidean distance, for example, the two analysed series must have the same length, as there will be a one-to-one relationship between each of the samples. However, DTW does not maintain this constraint, as the one-to-one relationship is demolished, as shown in Figure 1-15. That happens because the DTW searches for the combination of the two signals that minimises the Euclidean distance, or in general the distance used to compute it.

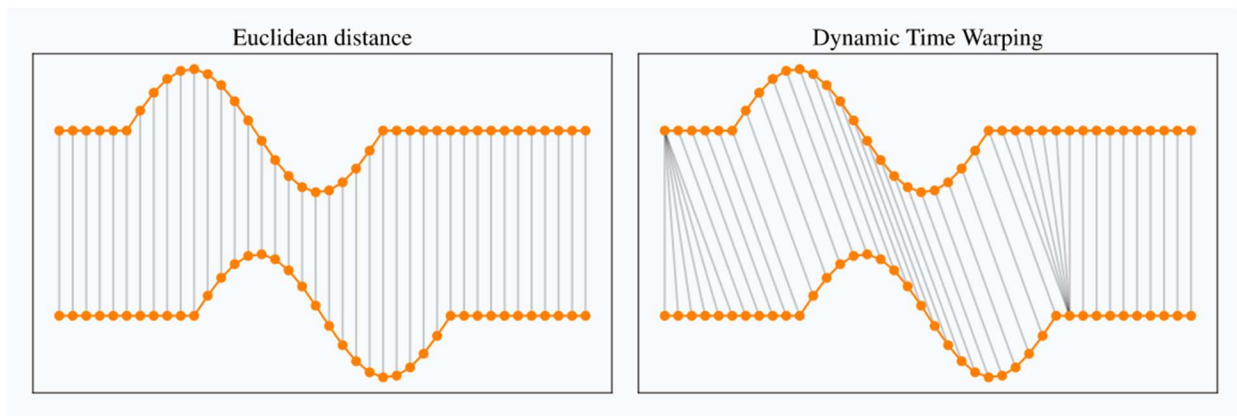


Figure 1-15 – On the left, example of a comparison between two signals when using the euclidean distance, on the right by using the dynamic time warping. Source: https://rtavenar.github.io/blog/fig/dtw_vs_euc.svg

Since it is capable of identifying similarities in the signals and since running, just like walking, tends to be a very repetitive movement, DTW can be a useful tool for the detection of phases and parameters through different subjects and speeds, as it will be analysed in the following chapters of the present work. DTW works on the following rules:

- Each sample of each signal must be matched with at least one sample from the other signal.
- The first samples in both signals must be matched with each other.
- The last samples in both signals must be matched with each other.
- The indices which indicate the mapping of the first signal must be monotonically increasing.

The two signals, to minimise the distance, are non-linearly warped, that is they get deformed so that the differences between them get minimised.

Chapter 2

Materials and methods

2.1 Experimental setup

In this section the experimental sessions involving running trials at different speeds and conditions are described.

2.1.1 Amateurs protocol – 8 and 10 km/h

Eleven recreational runners (6 M, 5F, age: 21 ± 1.3 years, height: 167 ± 7.1 cm, weight: 63 ± 8.6 kg) with familiarity with the treadmill system volunteered to run at 8 km/h and 10 km/h on treadmill and running track on different days. After an initial 3 minutes warming up session, each subject was asked to run at 8 km/h for 400 m, and then, after a period of rest, at 10 km/h again for 400 m [55]. All subjects were equipped with an INDIP multisensory system [54] sampling at 100 Hz, attached to the shoelaces of each shoe, and sensorised insoles (mod. YETI, 22le Srl, Padua, Italy, sixteen pressure sensors; element area = 310 mm; force threshold = 5 N [55]), considered as a portable gold standard for temporal events. Some of the subjects were further equipped with a protective leather insole. In Figure 2-1 an example of equipment is shown.



Figure 2-1 – Subject wearing the INDIP multisensory sistem and sensorised insoles.

2.1.2 Amateurs protocol – 14 km/h

Ten subjects (M, age: 32.3 ± 9.9 years, height: 172.5 ± 4.3 cm, weight: 69.4 ± 4.9 kg) were recruited following these inclusion criteria; i) all subjects had to be aged between 18-50 years, ii) be recreational rearfoot striker runners, iii) be familiar to treadmill running, iv) wear 38 or 42 shoe size (EU), v) be injury-free for at least three months preceding the acquisition, and vi) be able to run effortlessly for 55 minutes straight. All the subjects were asked to perform different 6 minutes running trials on a treadmill, at 14 km/h, in eight different running conditions, simulated through the usage of a different shoe model, with varying midsole thickness [31]. Each subject was equipped with a foot-mounted MIMU (mod: Opal v2, APDM, Portland, USA), sampling at 200 Hz affixed to the arch of the feet over the shoes with a strap, and retro-reflective markers of stereophotogrammetric system, which was the adopted gold standard. In Figure 2-2 a visual representation of the equipment is provided.



Figure 2-2 – Subject wearing the Opal system and retro-reflective markers.

2.1.3 Sprinters protocol

The data acquisition for the sprinters took place on outdoors official running tracks. Nine elite runners (M, age: 23.4 ± 3.5 years, height: 182.4 ± 8.5 cm, weight: 72.8 ± 6.9 kg) with a score of over 700 points in the tables of World Athletics were recruited, that is covering 100 meters in less than 11.66 s [57]. In addition, no musculoskeletal injuries were reported for each runner at least in the preceding six months.

After an initial 40 minutes warming-up period to avoid any injury, each subject was asked to perform six 80 m sprint trials along the lane of an official 400 m track at three different speeds: 70%, 85% and 100% of their maximal speed. The timing was measured via a hand chronometer (Sasso Marconi (Bo), Italia, Motus chronometry millennium MTS50, sensitivity 1/1000) [58] . Reached speeds ranged from 20 km/h to 32 km/h.

Each subject wore their own running shoe model and was equipped with a MIMU, in particular an INDIP multisensory system [54] , sampling at 100 Hz, attached to the shoelaces of each shoe. In addition, subjects were equipped with sensorised insoles (mod. YETI, 22le Srl, Padua, Italy, sixteen pressure sensors; element area = 310 mm; force threshold = 5 N [55]), considered as the gold standard. An ad-hoc study was conducted to identify the best cover insole to shield the sensorised ones and a very thin insole (thickness ~1 mm) was selected and fixed with tape to avoid any unwanted movement of the insole. An extensive analysis regarding the procedure of evaluation of different types of protection for the insoles is provided in Appendix 1. In Figure 2-3 a visual representation of the equipment is shown.



Figure 2-3 – Subject equipped with MIMUs affixed to the shoelaces of each show and with sensorised insoles.

2.2 Literature methods for the detection of temporal parameters

After a literature review, nine methods were selected, as they provided the best results in the estimation of running temporal parameters using foot or ankle mounted MIMUs, a summary of which is presented in Table 2.1. All the methods were implemented using MATLAB.

Method	Description	Location	# of subjects	Sampling frequency (Hz)	MIMU position	Speeds	Declared errors
Blauberger et al. (2021)	IC identified as local minimum in the acceleration norm, FC al local minimum in the angular rate norm.	Running track	5	512	Ankle	~ 32.724 km/h	ME: 3.55 ± 6.16ms

Schmidt et al. (2016)	IC as local maximum while the mediolateral gyroscope yields a constant slope and FC as local minimum in the vertical acceleration	Running track	12	1000	In line with the ankle, on the side of the shoe	30 km/h	MAD (on stance duration): 4.3ms
Falbiard et al. (2018)	IC and FC as minimums in the mediolateral angular rate	Treadmill and running track	41	500	Shoelaces	8-20 km/h	Inter-trial median (bias) ± IQR on stance duration: 15 ± 12ms
Mo and Chow (2018)	IC as maximum in the acceleration norm, FC as minimum in the vertical acceleration	Running track	11	200	Shoelaces	Up to 14.76 km/h	MAD: IC= 0.006±0.005s; FC= 0.020 ± 0.008s
Benson et al. (2019)	IC and FC as maximum in the acceleration norm	Treadmill and running track	54	200	Shoelaces	Up to 12.96 km/h	MAD: IC=0.06±0.2s; FC=0.01±0.06s
Bailey and Harle (2015)	IC as the point in the mediolateral gyroscope that surpasses a certain threshold before a local minimum, FC as local maximum in the vertical acceleration	Treadmill	5	1000	In line with the ankle, on the heel	Up to 12.24 km/h	ME: IC= 9.89±3.37 ms FC= 0.47±3.84 ms;
Reenaldae	IC and FC as local	Marathon	3	1800	Shoelaces	~ 13	Not

t al. (2016)	maximums in the acceleration norm	track				km/h	declared
Chew et al. (2018)	IC and FC as zerocrossings in the anteroposterior acceleration	Treadmill	10	128	Shoelaces	Up to 11.2 km/h	MAE of -0.3±14.7ms on the detection of ICs and 4.45±18.04 ms on the detection of FCs.
Yang et al. (2022)	IC as local maximum in the acceleration norm, FC as local maximum in the angular rate norm	Running track	38	500	Ankle	Self selected maximum speed	MAE between 5 and 37 ms on both IC and FC

Table 2.1 – Summary of the implemented methods. MAD = Mean Absolute Difference, MAE = Mean Absolute Error, ME = Mean Error, IQR = Interquartile Range

2.2.1 Methods proposed for high speeds

There are a very few studies that investigate sprinting running speeds with inertial sensors. [59-62] It has to be noted that, to the knowledge of the author, as of December 2022, hitherto no other method for higher speeds at 100 Hz has been developed.

2.2.1.1 Blauberger et al.

The method proposed by Blauberger et al. [61] was developed for the extraction of ground contact time (GCT) from inertial sensor signals in sprinting, by studying the performances of five elite athletes.

They analysed a total of 1140 steps obtained from two IMUs, positioned above the ankle of each athlete. The IMUs used in this study included an accelerometer with $\pm 16g$ operating range and a gyroscope with a $\pm 2000^\circ/s$ operating range, both sampling at 512 Hz. Through the method here described, they achieved a mean error of $3.55 \pm 6.16ms$.



Figure 2-4 – In this figure, taken from [55], the position of the MIMU on one of the athletes' shoes is shown.

After being instrumented with the MIMUs, the athletes were asked to perform 34 sprints at maximum speed for 50 and 100 m each. The data thus obtained was then analysed to estimate the ground contact time (GCT) of each step based on the features of the recorded IMU signals. For the purposes of this study, only the analysis of the temporal parameters is taken into consideration.

Both the accelerometer and the gyroscope outputs were summarized as one vector by obtaining the norm of the signals as in (2.1):

$$A_{norm} = \sqrt{A_x^2 + A_y^2 + A_z^2} \quad (2.1)$$

The resulting vectors were then filtered using a 2nd order Butterworth low pass filter with a cut-off frequency of 70 Hz, which for our data has been brought down to 6Hz, given that the data obtained at 100 Hz did not have any component over 70 Hz, to obtain signals similar to the ones shown in the article. Since the running cycle segmentation was not described in detail, we purposefully applied an autocorrelation approach to the division of the running portion into the single different strides described by Falbiard et al. [63]

The running events detection algorithm takes into consideration the cyclical nature of the running movement. The authors had observed that the contact of the foot with the ground, that is the initial contact caused a rapid change of the acceleration, which is the reason why they identified the IC as a local minimum in the acceleration. After the detection of the IC, the final contact was then found by looking for two peaks in the combined angular velocity: the FC is identified as the minimum that lies between these two peaks.

2.2.1.2 Schmidt et al.

In the paper published in 2016, Schmidt et al. presented an IMU-based wearable measurement system for performance analysis in-the-field and online monitoring [62] Each of the twelve athletes recruited in the study was asked to perform maximal sprints while wearing the IMU device attached to their ankles. Their aim was to compute the stance duration of the athletes, on which they achieved a mean absolute difference of 4.3 ms.



Figure 2-5 In the figure, taken from [62] , the IMU device used in this paper and its positioning on one of the athletes is shown.

For the development of their algorithm, they analysed the data acquired from the accelerometer, with a range of $\pm 16g$, and the gyroscope, with an operative range of ± 1000 $^{\circ}/s$, both sampling at 1000 Hz. The signals were processed without applying any further filtering.

The detection algorithm was based on peak detection, and it exploited the vertical component of the acceleration to find both the temporal parameters. The autocorrelation method described in Falbiard et al. [63] was applied to this method. The IC was searched in the area in which the vertical acceleration surpassed a certain threshold (usually 5 g, but it has been modified in certain subjects) and, at the meantime, the mediolateral angular velocity had a continuous slope. When the condition was met, the IC was set as the minimum that preceded the peak in the vertical acceleration. After a certain amount of time from the IC, which is a scalable deadtime set to 0.25 s for 8 km/h and 10 km/h, 0.16s for 14 km/h and 0.10 s for sprints based on previous observations, a global minimum in the vertical acceleration within a time window that went from half the mid-swing to mid-swing cycle to its end was set as FC.

2.2.1.3 Falbiard et al.

In 2018 Falbiard et al. published a paper with the aim of assessing the performance of different kinematic features measured by wearable inertial sensors, in order to estimate the inner-stride phases duration (e.g. contact time, flight time, swing time, step time). [63]

They asked forty-one healthy amateur runners to run multiple trials on an instrumented treadmill while wearing a MIMU on the shoelaces of each shoe. In the paper, different algorithms were proposed, evaluated, and compared. For the sake of the present work, the one that has been deemed the best has been replicated. The IMUs with which the runners were equipped consisted of both a 3D accelerometer (range $\pm 16g$) and a 3D gyroscope (range ± 2000 $^{\circ}/s$), sampling at 500 Hz. The performances of their method were tested via the computation of the inter-trial median (bias) \pm Interquartile range on the stride duration, which amounted to $15 \pm 12ms$.

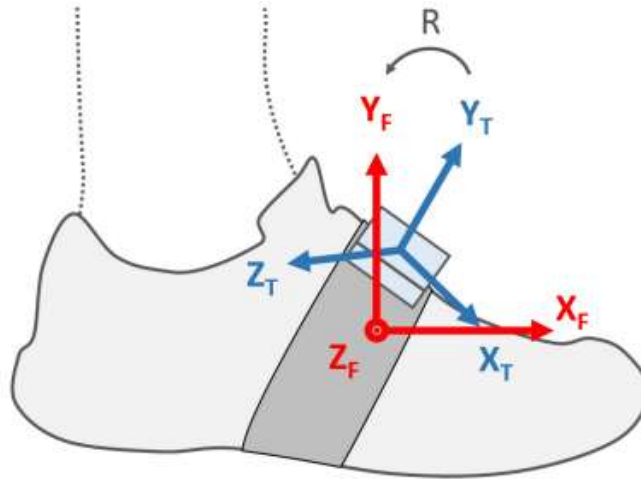


Figure 2-6 – The figure, taken from [63] shows both the technical frame of the foot-worn IMU (X_T , Y_T , Z_T) and the functional frame of the foot (X_F , Y_F , Z_F) and the positioning and the attachment of the IMU to the foot.

They implemented a mid-swing to mid-swing segmentation. A 2nd order lowpass Butterworth filter was designed with an adaptive cut-off frequency based on the stride frequency, estimated using autocorrelation over a 5 s sliding window. The adaptive filter thus developed was proposed to be suitable for different speeds. Once the gait had been segmented into the singular mid-swing to mid-swing periods, a further segmentation on filtered signals was done to identify the research windows for both the IC and the FC by exploiting zero-crossings.

The IC was searched for between the first zero-crossing of the anteroposterior angular velocity and the mid stance, while the FC between the mid stance and the last zero crossing. The minimum of anteroposterior angular velocity in the proper research window was selected as IC and FC, respectively.

2.2.2 Methods proposed for recreational runners

Running at lower to moderate speeds has been more thoroughly studied, which leads to a definitely higher number of records that met the research criteria. The methods that have been studied were all tested over datasets at low/medium speeds (4-15 km/h).

2.2.2.1 Bailey et Harle

With the aim of developing a threshold free algorithm to assess temporal running parameters, Bailey et Harle in 2015 provided a new method exploiting IMUs, especially thought to provide the opportunity to monitor changes in sporting techniques to prevent injuries [64]

Each participant to the study was equipped with an IMU composed by a 3D accelerometer ($\pm 16g$) and a gyroscope (± 2000 °/s). All the IMU signals were sampled at 1kHz, the device was attached to the lateral side of the shoe, in line with the ankle, as seen in Figure 2-7. The events detected via their method had a mean error of 9.89 ± 3.37 ms on the detection of the ICs and 0.47 ± 3.84 ms on the detection of FCs.



Figure 2-7- In the figure, taken from [64], the IMU and its placement on the shoe is shown.

Five participants were asked to run for 90 seconds at 4 different self-selected speeds. For each participant and each speed, 90 steps were extracted for further analysis, which lead to the detection of 1800 steps in total. In the method described, first a modified version of the Normalised Autocorrelation based Step Counting (NASC) algorithm [65] was used to detect the running period and to roughly segment the signals into individual steps. Based on the intrinsic nature of gait signals, which are periodic, the base assumption is that their autocorrelation value should be the highest in correspondence of the period of the gait cycle. The anteroposterior angular rate g_z^{ion} was used, based on the high repeatability and the low amount of noise present on this axis, to compute the normalised autocorrelation χ for lag τ at the m^{th} sample, as in (2.2):

$$\chi(m, \tau) = \frac{\sum_{k=0}^{k=\tau-1} [\alpha(m, \tau, k)\alpha(m + \tau, \tau, k)]}{\tau\sigma(m, \tau)\sigma(m + \tau, \tau)} \quad (2.2)$$

$$\alpha(i, \tau, k) = g_z^{ion}(i + k) - \mu(i, \tau) \quad (2.3)$$

Where $\mu(k, \tau)$ and $\sigma(k, \tau)$ are the mean and standard deviation of the samples. Since τ is unknown, the algorithm tries many values of τ between two selected values to find the lag for which the autocorrelation is maximum. Once the highest value of the autocorrelation is found, two pieces of information can be gathered:

- a high value for the autocorrelation, closer to one, represents a walking or running movement;
- the value of τ for which the autocorrelation is at its maximum is the exact periodicity of the subject's gait.

A further moving average filter with a 5 second window is used; the period of running is detected by means of a threshold of 0.8 on the autocorrelation. Next, running cycles were segmented without the use of thresholds, so that the method could be robust to speed changes. To segment the cycle, the maximum value of the anteroposterior angular rate in the first two seconds is detected, which represents the beginning of the first stride. Subsequent cycles are found, by exploiting the periodicity computed beforehand to find research windows in which the maximum value of the anteroposterior angular rate can be found. Each segment is guaranteed to contain an IC and a FC, given that the anteroposterior angular rate is maximum during the swing phase.

The initial contacts are detected by searching for changes in the anteroposterior angular rate signal. The IC is detected by the identification of rough changes in the signals, that can be

highlighted with the computation of the first differential. A first estimation of the IC is made by identifying the minimum in the differential signal, which corresponds to the maximum rate of change that happens right after the initial contact. For this reason, the estimation of the IC is refined by looking backwards for the point where the angular rate rises above constant threshold. If heel strikes cause abrupt changes in the signals, the same cannot be said for the toe off events, which causes a small local maximum in the vertical acceleration, difficult to detect, which leads to the need for a further segmentation of the stride to allow an easier peak detection. The segmentation relies on the zero-crossing of the filtered angular rate signals. After the detection of the zero-crossings, the extremities of the FC research window were defined as in (2.4) and (2.5):

$$w_{start} = z_0 + \frac{(z_1 + z_0)}{2} \quad (2.4)$$

$$w_{end} = \frac{4(z_1 - w_{start})}{5} + w_{start} \quad (2.5)$$

Where z_0 and z_1 indicate the first and the second zero crossings found. In the window thus found, the minimum in the vertical acceleration can be more reliably found, especially at higher speeds.

2.2.2.2 Reenalda et al

In 2016 Reenalda et al. proposed a peak detection-based algorithm for the identification of running events. [66]

Three well trained marathon runners were equipped with different inertial measurements units, with two attached to the feet by means of clips attached to the shoelaces and secured with tape. Each MIMU contained a 3D accelerometer ($\pm 16g$), a 3D gyroscope (± 1200 °/s) and a 3D magnetometer (± 1.5 Gauss), all sampling at 1800 Hz. Their study was bereft of any gold standard, so no information about its performance is available. Stride detection was based on raw inertial data but, since no further explanation has been given, the stride segmentation implemented was the same as Falbiard et al. [63]

The peak-detection based algorithm exploited the accelerometer norm to detect maxima within the segmented stride identified as ICs. The peak in the gyroscope norm that comes right after the peak in the accelerometer was identified as FC.

2.2.2.3 Mo and Chow

Mo and Chow evaluated the accuracy of three different methods for temporal events during jogging and running. For the purposes of the present work, from their result, the best performing one has been selected, which was the combination of the S-method, for the detection of the ICs, and the M-method, for the FCs, defined in the reference paper. [67]

Eleven runners were recruited for the study and asked to jog (3.1 ± 0.1 m/s) and run (4.1 ± 1.2 m/s) on a 10m running track in a random order. Each of them was equipped with five IMUs, two of which attached to the dorsal surface of each foot by means of a tight strap. Each IMU comprised a triaxial accelerometer ($\pm 16g$) and sampled at 200 Hz. The thus defined

combination was deemed to be capable of detecting temporal events with a MAD of 0.006 ± 0.005 s on the detection of the ICs and 0.020 ± 0.008 s on the detection of the FCs.



Figure 2-8- Figure taken from [67] that shows the positioning of four of the IMUs used in their study.

In the S-method, the IC was defined by searching for the moment in which the norm of the acceleration exceeded a certain threshold ($2g$). The FCs were found by means of the M-method, which consists of detecting a minimum in the acceleration norm in the region of interest, which comes after the second maximum in the acceleration signal.

2.2.2.4 Chew et al.

With the final goal of detecting stride length and running speed, Chew et al [68] recruited ten healthy subjects that were instructed to run on a treadmill for two 10-minute sessions at six different walking to running speeds: 1.3, 4, 8, 9, 10 and 11 km/h. The subjects were all provided with two IMUs, attached to the shoelaces, (Figure 2-9) which were able to measure acceleration, with a range of ± 16 g, and angular velocity for a range of ± 2000 $^{\circ}/s$ with a sampling rate of 128 Hz. Their method reported a MAE of -0.3 ± 14.7 ms on the detection of ICs and 4.45 ± 18.04 ms on the detection of FCs.



Figure 2-9- In the figure, taken from [68], the positioning of the IMU is shown.

The anteroposterior acceleration was analysed for the detection of the temporal events, since it presented two prominent local minimums, the first of which represents the IC while the second the FC. To detect these events, the first derivative of the anteroposterior acceleration is computed; then, the zero crossings of the derivative are found and considered as a possible event. Subsequently, a constant threshold (-8 m/s^2) is applied: if the acceleration

in correspondence of the zero crossing is less than the threshold, then the zero crossings are to be considered running events. After all the events in the cycle have been found, the events with greater amplitude are identified as ICs, the others as FCs.

2.2.2.5 Benson et al.

Benson et al in 2019 developed an algorithm for the definition of running events based on data collected via IMUs placed on the feet. [69] Their method performed with a MAD of 0.06 ± 0.2 s on the detection of ICs and 0.01 ± 0.06 s on the detection of FCs.

Three different experiments were held, each in a different setting. All of the subjects were wearing triaxial accelerometers with a range of ± 16 g, sampling at 200 Hz:

1. Instrumented treadmill: Twelve recreational runners were recruited for the study and asked to run at slow, intermediate and fast self-selected speeds for 90 s.
2. Indoor track: Twenty recreational runners were asked to run two 60-m trials for each of the three different self-selected speeds and to perform two different types of heel strike (rearfoot or forefoot) for a total of 12 trials.
3. Outdoor: Twenty-two healthy runners were asked to run for 600m at a self-selected speed, for 16 trials (4800 m total for each subject).

The accelerometer signals were first pre-processed via a fourth order zero-lag Butterworth filter, cut-off 10 Hz, and they were trimmed by eliminating the beginning and the end of each trial, to ensure that all the signals analysed came from a steady run. The accelerometer method developed was based on different assumptions:

1. The time between ipsilateral steps would be between 0.5 s and 1s, half for the contralateral ones;
2. FC would occur not before 0.1 s after the detected IC.

The norm of the accelerometer is exploited to search major positive peaks, distant at least 0.5 s between each other, which are considered to be ICs. Once all the ICs are detected, a research window is defined by setting the lower bound at 0.1 s after the ICs, and the upper bound at the midpoint between the last and the next IC. In the thus defined research window, peaks are searched for: if a peak exists, it is set as FC, otherwise the maximum of the signal in that region is considered to be the FC.

2.2.2.6 Yang et al.

The research for more and more precise methods for the detection of temporal parameters during in-field running is currently evolving; in fact, recently, Yang et al. published a paper proposing two new methods for the detection of initial and final contacts [70] For their purpose, they collected data from thirty-six healthy players of an Australian football league team who underwent 30 m running efforts at three different speeds: 75%, 85% and 95% of their maximum speed, all while wearing the IMU device attached to their ankle, as shown in Figure 2-10. Said device was sampling with a 500 Hz sampling rate and measured both acceleration via a 3D accelerometer (± 16 g) and angular velocity via a 3D gyroscope ($\pm 2000^\circ/\text{s}$). In total, they managed to collect 53280 steps, that were used to build the algorithm. The best performing combination returned a MAE between 5 and 37ms.



Figure 2-10- Figure taken from [70] showing the placement of the IMU on the ankle

A pre-processing algorithm was first applied to the raw data, to eliminate the non-running sections from the signal. To successfully detect the running portion, first the square value of the acceleration in the three directions A_{square} is computed as in (2.7):

$$A_{square} = A_x^2 + A_y^2 + A_z^2 \quad (2.7)$$

This was done to enhance the peaks in the signal, making the difference between running and non-running phases more prominent. On the signal thus obtained, a sliding window of 0.5s was applied. In each window, the average square value A_{avg} of the sum was computed as in (2.8):

$$A_{avg} = \frac{\sum_n^{n+s*f} A_{square}}{s * f} \quad (2.8)$$

Where f is the sampling frequency, s the amplitude of the sliding window. If A_{avg} exceeds a certain threshold for more than three consecutive seconds, that point is set as the beginning of the running period, while the end of said period is marked when the A_{avg} value drops below the set threshold.

Two different algorithms were elaborated, one based on the accelerometer data and one based on the gyroscope. For the current work, only the method deemed to be the best performing was considered, which resulted to be a combination of the two: accelerometer based for the IC detection, and gyroscope based for the FC detection. In the accelerometer-based method, the vertical acceleration was exploited. First, the norm of the accelerometer was calculated, then the difference sample per sample was computed, as shown in (2.10):

$$SqDiff = A_{norm}(i + 1) - A_{norm}(i) \quad (2.10)$$

The local maximum in the square difference was then set as IC. To ease the detection, a stride segmentation algorithm was applied. Since in the paper no further segmentation method was described, the same autocorrelation-based segmentation presented in Falbiard et al. [63] was applied. The gyroscope-based algorithm exploited the norm of the gyroscope signals, filtered via a 2nd-order Butterworth low-pass filter with cut-off frequency of 10 Hz. The first local maximum in each window was then considered to be a FC.

2.3 Newly proposed method

The method hereby proposed uses a set of templates to search for and identify the running temporal events. A summary of the method is provided via flowchart in Figure 2-11.

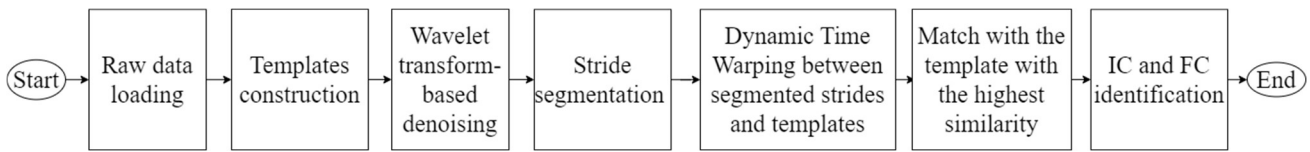


Figure 2-11 – Flowchart highlighting the steps of the template-based method

Before any kind of elaboration, the raw inertial signals have been rotated so that the vertical component would be perpendicular to the ground.

Then, instead of a traditional filtering, the re-aligned accelerations and angular velocities have been denoised by means of a wavelet transformations-based method. This method has been chosen to avoid the selection of a numerical threshold for the cut-off frequency, which could be dependent on running speed. For the sake of clearness, the implementation of the method is performed via a filtering cascade made by low-pass and high-pass filters, which all share the same cut-off frequency whose value depends on the mother wavelet chosen. After each level (i.e. a filter), a down sampling of the signals is performed, which halves the number of the samples. In particular, the mother wavelet chosen was one of the Daubechies, ‘db6’, stated to be the most suitable for gait analysis by Ji et al [71] who analysed the performances of 32 different mother wavelets in term of gait events detection through the computation of time-errors with respect to foot switches events and F1score, based on the definition of precision and recall.

Signals were decomposed to the second level, choice made empirically after a preliminary tuning of the level parameter by looking at the effects of the decomposition at different levels: level 1 was deemed to have almost no effect on the signals, which was the same as applying a low pass filter with a cut-off frequency of $0.5 * \frac{f_s}{2}$ Hz (that is 25 Hz for the signals acquired at 100 Hz and 50 Hz for the signals acquired at 200 Hz) to the signals, while level 3 erased too much valuable information from them, as if the $0.5 * \frac{f_s}{2}$ Hz lowpass filter had been applied to the signal three times in a row, halving the sampling frequency for each step (e.g. 25 Hz, then 12.5 Hz, then 6 Hz for the signals acquired at 100 Hz). For instance, in Figure 2-12, Figure 2-13 and Figure 2-14 a visual representation of the results of the decompositions cited on the anteroposterior acceleration of a sprinter is provided. Thus, to denoise inertial signals (with maximum frequency component equal to ~ 15 Hz for signals acquired at 100 Hz and ~ 30 Hz for signals acquired at 200 Hz), they were firstly decomposed into approximation and detail coefficients at second level, which correspond to low and high frequency coefficients respectively.

At this point, in the literature, a fine tuning of the denoising method is usually performed, in order to choose a threshold to apply on both the approximation and the detail coefficients: all the coefficients that surpass the set threshold would be discarded. However, to avoid the tuning of a further parameter, the implemented denoising is based on the one proposed by Soangra et al. [26], which considers only the approximation components. Thus, all the detail coefficients were discarded, and the signals were reconstructed starting from the approximation coefficients.

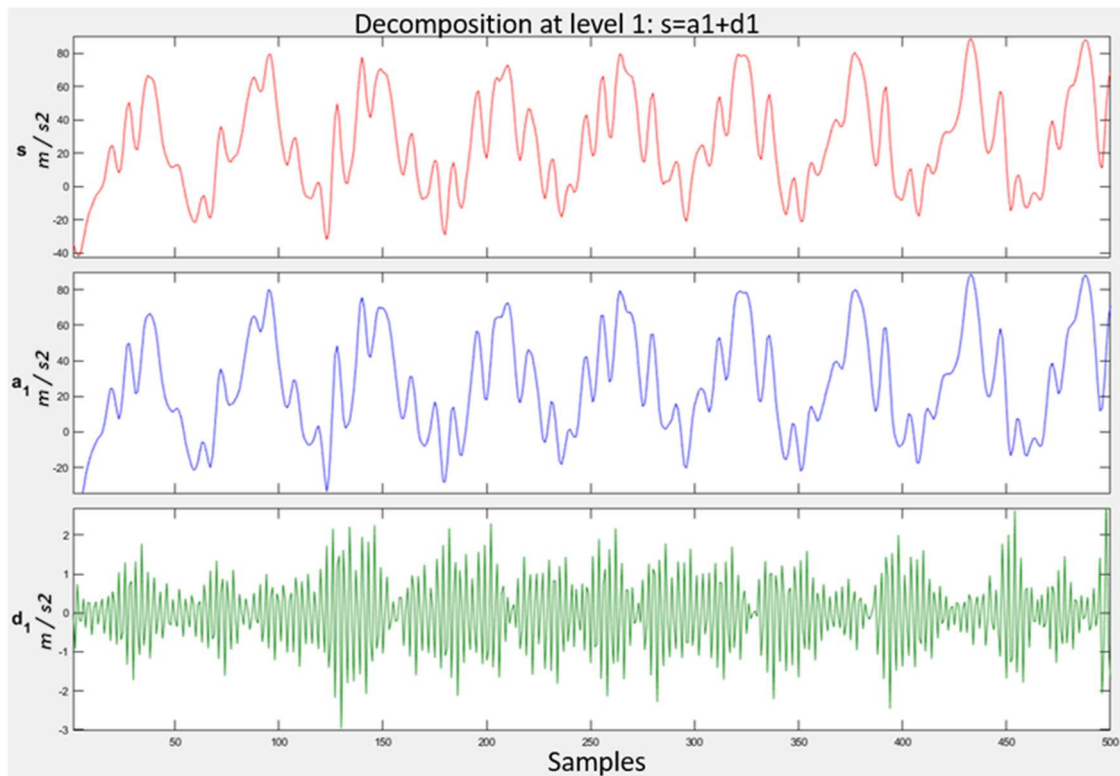


Figure 2-12 – DWT decomposition of a portion of the anteroposterior acceleration at level 1 using s ‘db6’ mother wavelet. In red, the original signal, in blue the approximation coefficients (which are equal to the denoised signal in the technique used in this work) and in green the detail coefficients.

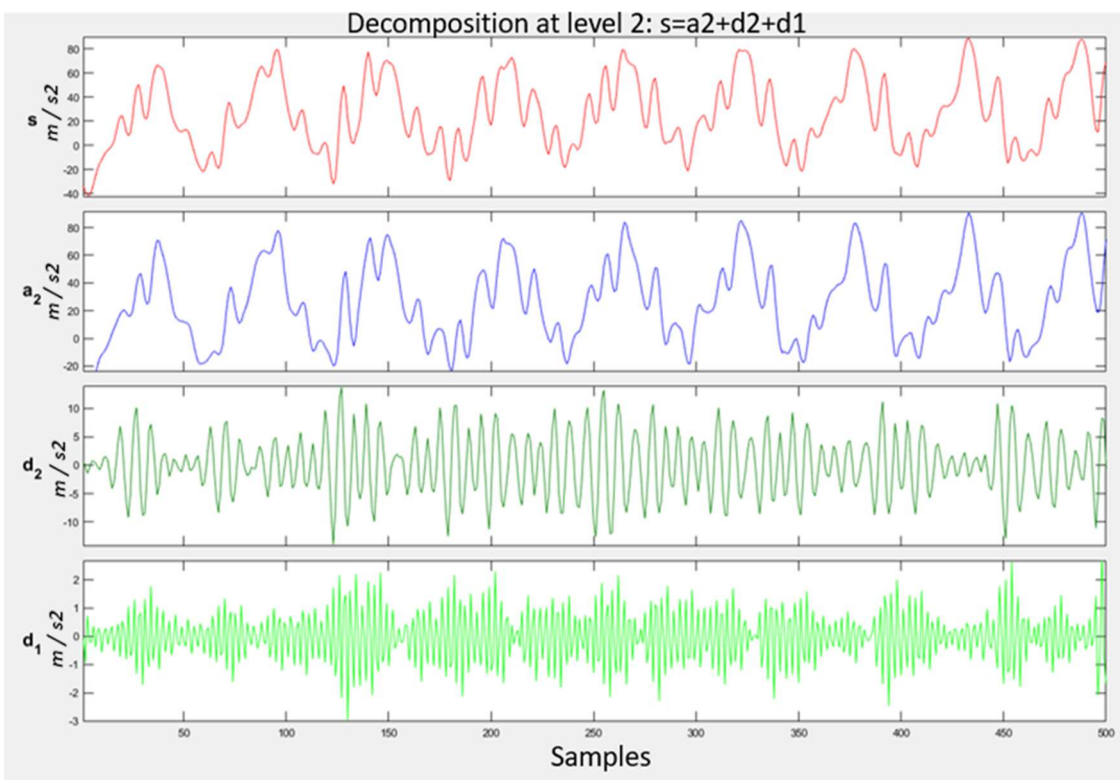


Figure 2-13 - DWT decomposition of a portion of the anteroposterior acceleration at level 2 using s ‘db6’ mother wavelet. In red, the original signal, in blue the approximation coefficients (which are equal to the denoised signal in the technique used in this work) and in green the detail coefficients.

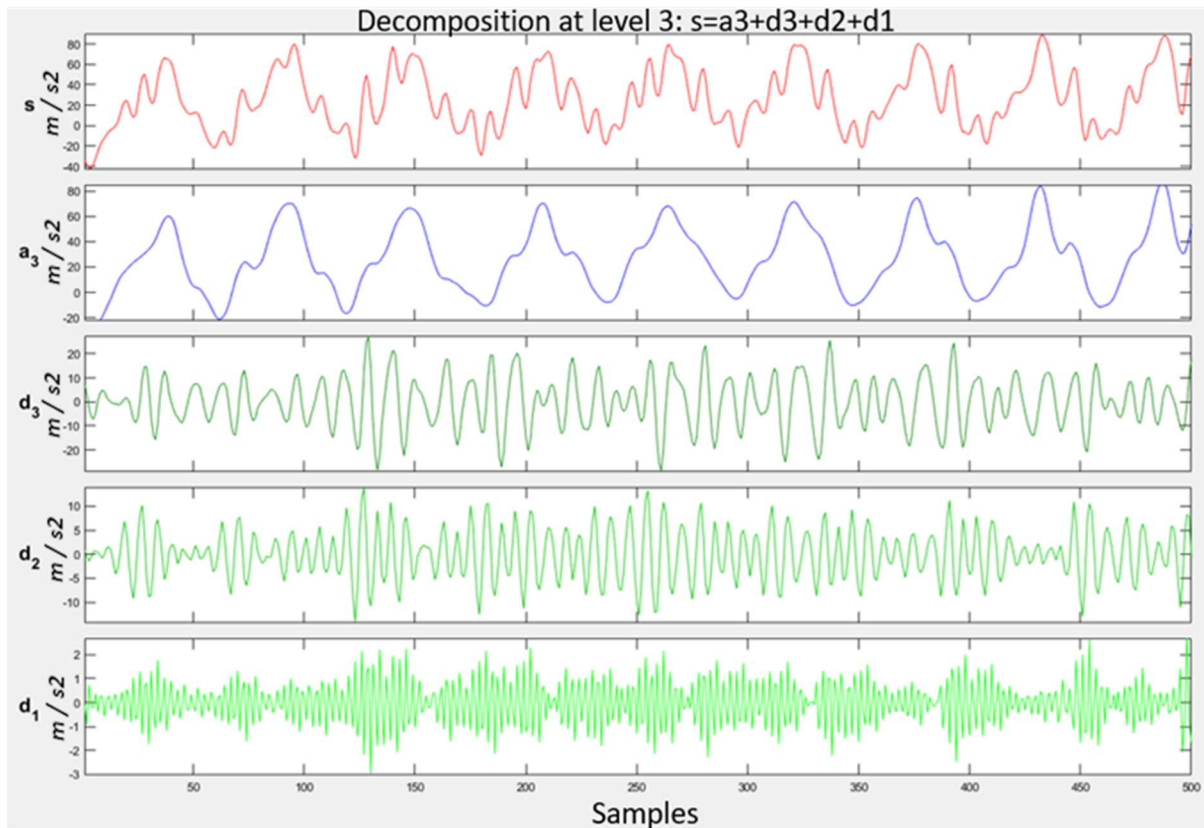


Figure 2-14 - DWT decomposition of a portion of the anteroposterior acceleration at level 3 using a 'db6' mother wavelet. In red, the original signal, in blue the approximation coefficients (which are equal to the denoised signal in the technique used in this work) and in green the detail coefficients.

To allow an easier evaluation, each trial has been segmented by means of the stride segmentation as presented by Falbiard et al. [63] which provides a mid-swing to mid-swing segmentation using the maxima in the mediolateral component of the gyroscope signals, filtered at a stride-frequency dependant cut-off frequency ($0.6 \cdot \text{stride Frequency}$), so that it would automatically adapt to the different speeds.

After the denoising procedure, a template-based method was implemented to estimate the initial and final contact of running cycles coming from trials at different paces. Twenty templates were extracted: 5 mid-swing to mid-swing running cycles for each speed dataset (i.e. at 8 km/h, 10 km/h, 14 km/h and sprints), by annotating the signals with IC and FC with the help of the data acquired with the gold standard. The different combinations of signals for the template construction were to select the best performing one, which consisted of the adoption of acceleration norm and mediolateral angular velocity. The subjects from whom the strides templates were taken (i.e. training set) were not considered in the evaluation of the performance of the method.

For each segmented stride, an algorithm based on the dynamic time warping was developed. This choice was made to ensure that the algorithm would be speed adapting, since the dynamic time warping is a technique which highly relies on the similarity between two signals, which can also be of different lengths: as long as it has the templates of the morphology in exam, it should not incur in any problem. This comes from the idea that, by

covering as many morphologies as possible, the algorithm would be able to detect the running temporal events of different subjects running at different speeds. The dynamic time warping takes the two signals and deforms them so that the distance computed between them would be the least.

The distance measure was chosen empirically, by comparing the performances of the algorithm with all the different types of distances available: squared, absolute and Euclidean. The distance chosen did not affect significantly the performances of the method, but the Euclidean distance, defined as in (2.11), reported slightly better results (~1.3% decrease in the RMSE values).

$$d_{mn}(X, Y) = \sqrt{(x_m - y_n)^2} \quad (2.11)$$

where X and Y are both signals, it returns the distance between the m^{th} sample of X and the n^{th} sample of Y , d_{mn} is a $M \times N$ matrix. After computing the distances between the current stride and all the templates, the algorithm assigns the most similar template to each stride, that is the one that returned the shortest distance. Within the matrix, the algorithm finds a continuous path, called *warping path*, that corresponds to the minimum distance. The identification of the warping path results in two deformation vectors, defined as in (2.12), one for each signal, that indicates how the samples of each signal should be rearranged to maximise the similarity between the two signals.

$$y_1(x_1) \rightarrow Y_1(x_{1_{\text{warped}}}); y_2(x_2) \rightarrow Y_2(x_{2_{\text{warped}}}) \quad (2.12)$$

where y_1 and y_2 are the two signals, x_1 and x_2 are the original way the samples are sorted, Y_1 and Y_2 are the warped signals and lastly $x_{1_{\text{warped}}}$ and $x_{2_{\text{warped}}}$ are the two deformation vectors, as in Figure 2-15.

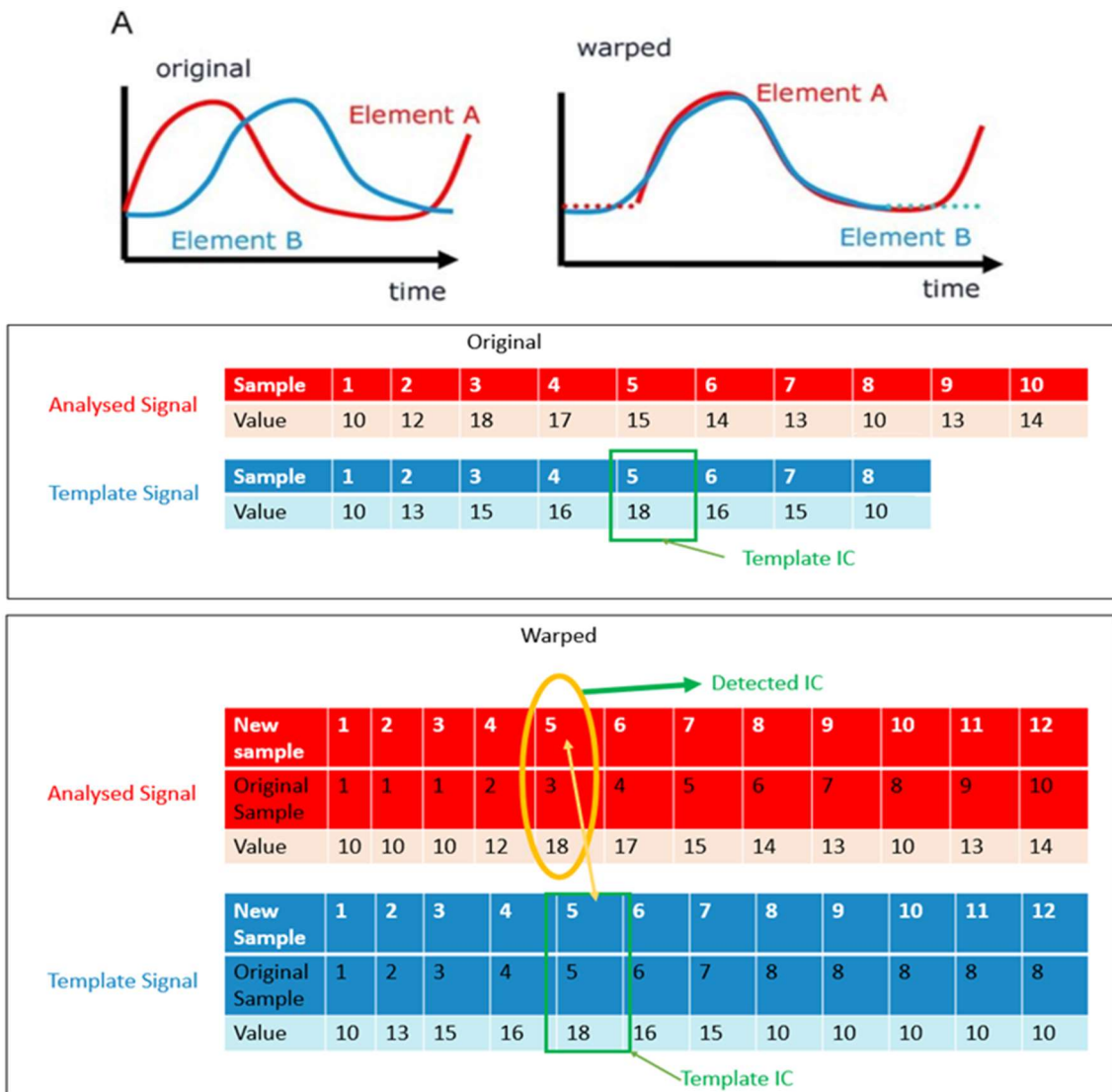


Figure 2-15 – Description of the method for the identification of the events. The way the two signals are deformed is shown graphically at the top of the image, while at the bottom a sample-wise representation is shown. To deform the signal, some sample will be repeated, as defined by the deformation vector, indicated by the figure as ‘Original Sample’, so the positioning of the events will not match exactly what is in the template sample-wise, but the value of the signal in that instance will still be the same. When the two signals are both warped, they are ‘equal’, which means that finding the event on the template signal when is warped is the same of finding the event on the new signal, as it will happen on the same sample.

Once the template is identified, the algorithm takes note of the IC as it was in the template, and it translates it so that it could transfer onto the stride in exam. This is possible because the dynamic time warping algorithm returns the distances between the signal as well as the way they should be deformed to obtain the highest similarity. In order to find the exact location of the IC on the analysed signal, the algorithm takes note on where the IC is on the template sample-wise (Figure 2-16). After the deformation, it investigates the deformation vector to find the new position of the template IC. Since after the deformation the signals are ideally equal, what happens on the n^{th} sample for the template, happens for the same sample on the newly analysed signal. Therefore, the IC is detected on the warped analysed signal. (Figure 2-17) Finally, the information is translated to the non-warped analysed signal by

taking into consideration its deformation vector (Figure 2-18), as described in (2.13). The same is then performed for the final contact.

$$Y(IC_{warped}) \rightarrow y(IC) \quad (2.13)$$

where the value of the signal in $Y(IC_{warped})$ equals the value in $y(IC)$.

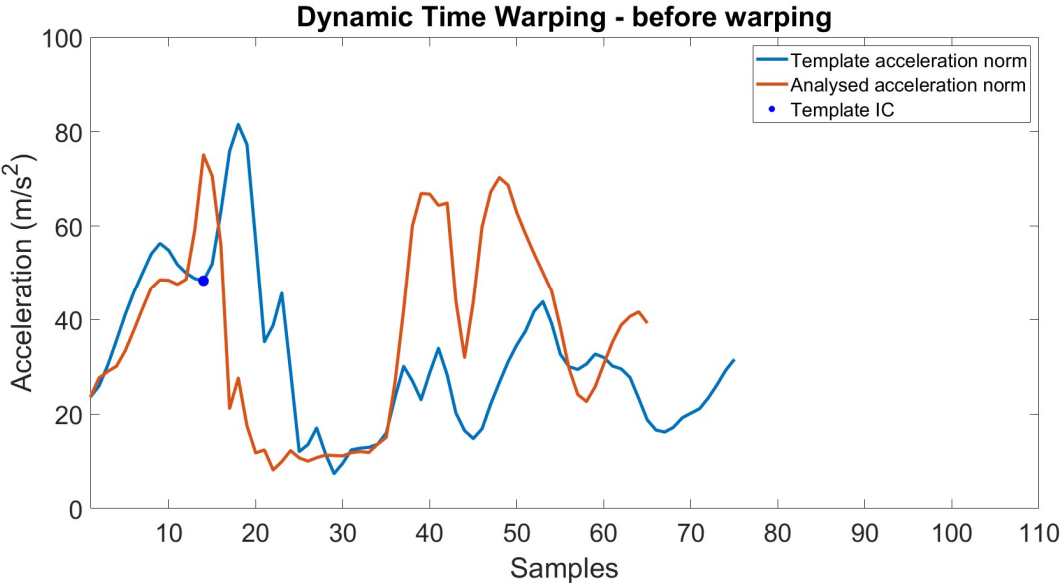


Figure 2-16 – First step, non warped signals. The signal is matched with the template with the highest similarity.

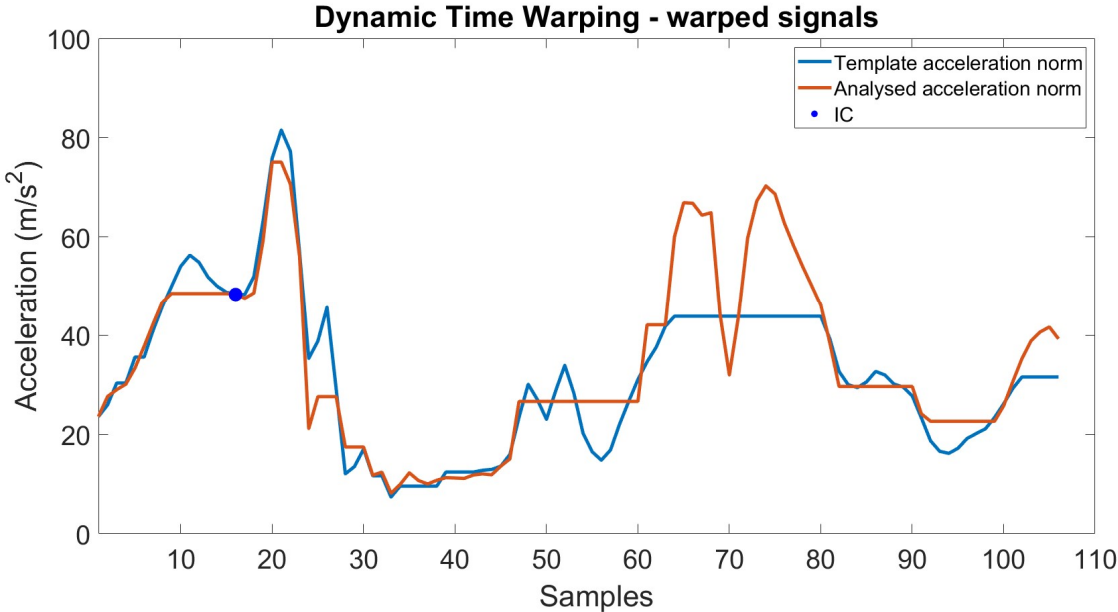


Figure 2-17 – Second step, signals warping. The signals are deformed to obtain the highest similarity. The IC is translated by the deformation. The algorithm takes note of the new IC sample, and translates the information on the analysed signal.

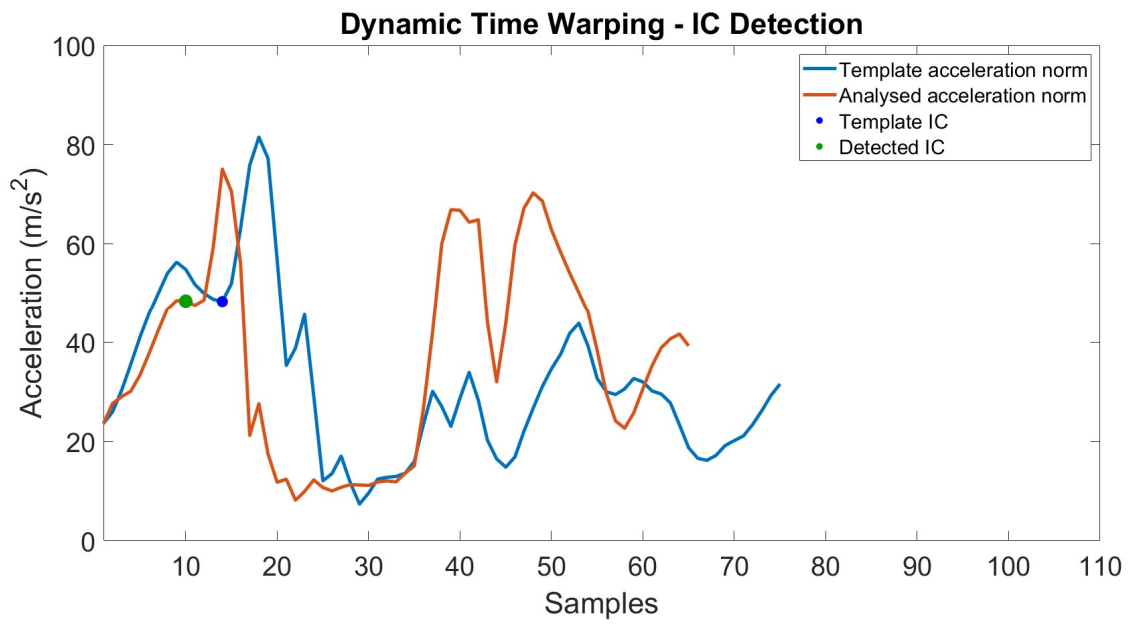


Figure 2-18 – Step three, the information is reported on the original non-warped signals. The event is detected.

Chapter 3

Results

The comparison between the nine different methods from the literature [61-64, 66-70] lead to the production of a set of descriptive statistics by exploiting the available gold standard data, e.g. pressure insoles or stereophotogrammetry system.

The errors on the events have been computed in terms of root mean square error (RMSE) defined as follows:

$$RMSE (s) = \sqrt{\frac{\sum_{i=1}^N (GE_{MIMU_i} - GE_{GS_i})^2}{N}} \quad (3.1)$$

where N is the number of observations, GE_{MIMU} represents the temporal events identified via the methods based on the inertial signals and GE_{GS} represents the temporal events identified by the gold standard.

Additionally, the percentage of missed events, that is the percentage of events that the method failed to detect, was computed as in (3.2). The percentage of extra events, that is the number of events detected by the methods but not detected by the gold standard, computed as in (3.3), was not reported as it remained under a 2% threshold with all the analysed methods.

$$Missed\ events\ (\%) = \frac{\#\ missed\ events}{\#\ true\ events} * 100 \quad (3.2)$$

$$Extra\ events\ (\%) = \frac{\#\ extra\ events}{\#\ true\ events} * 100 \quad (3.3)$$

The errors on the durations, i.e. stride duration, stance duration and swing duration, have been computed in terms of mean absolute percentage error (MAPE) by using the formula in (3.4):

$$MAPE\ (\%) = \frac{\sum_{i=1}^N \left| \frac{D_{MIMU_i} - D_{GS_i}}{D_{GS_i}} \right|}{N} * 100 \quad (3.4)$$

where N is the number of observations, D_{GS} is the duration obtained from the gold standard, and D_{MIMU} is the one computed from the inertial data.

For the novel method, sensitivity has been computed as in (3.5) by considering the number of missed events for each dataset compared to the total number of strides analysed.

$$Specificity (\%) = \frac{\# \text{ strides}}{\# \text{ strides} + \# \text{ missed events}} * 100 \quad (3.5)$$

In this chapter, the above-mentioned results are shown, highlighting which method for the estimation of running events is the most suitable for each analysed dataset. Furthermore, a method was selected as the best trade-off method across all the tested running paces.

Lastly, the performances of the novel template-based method presented in this work were computed and compared to the results obtained via the best trade-off method. The comparison was carried out through Student's t-tests on grand mean values of running cycle, stance and swing durations.

3.1 Results of methods from the literature

In this section, the results of the nine methods from the state of the art described in Chapter 2 are presented. In Table 3.1 the number of total running cycles analysed for each speed is reported.

	8 km/h	10 km/h	14 km/h	Sprints
Running cycles (#)	19014	17337	22991	2091

Table 3.1 – Summary of the number of total running cycles analysed for each speed

3.1.1 Comparison of methods performances at 8 km/h

The first dataset to be analysed is the one composed by trials at 8 km/h. In this dataset, both outdoor and indoor conditions are included. The results, that were obtained by comparing the temporal events computed to the ones acquired thanks to the gold standard, are shown in Table 3.2. RMSE ranging from 0.013 s to 0.025 s are reported on the detection of the IC, from 0.022 to 0.090 s on the detection of the FC, and a percentage of missed events that ranges from 0% to 3.6%. This leads to MAPEs ranging from 1.1% to 2.5% on the Running cycle, from 5.9% to 24.9% on the stance duration and from 4.7% to 20.1% on the swing duration.

The best method for the identification of the ICs, based on the RMSE, is the one proposed by Schmidt et al. [62]. Even if this method was proposed by the authors for higher speeds, the different sampling frequency and sensor positioning adopted for the data acquisition made the signals morphology at 8 km/h in this application suitable for the GE definitions by Schmidt et al. This method enabled an RMSE of 0.013 s and a 3.1% of missed events. As for FCs, the method by Blauburger et al. [61] was identified as the most suitable for 8 km/h, reporting an RMSE of 0.022 s and a 0.7% of missed events. In terms of general performance, the two methods are comparable as they return similar errors. Overall, the method proposed by Blauburger et al. [55] is suggested for running analysis at 8 km/h sampled at 100 Hz as it

reported the least amount of missed events on both ICs and FCs and a MAPE of 1.4%, 17% and 13.4% on the stride, stance and swing durations respectively.

A visual representation of the performances of the nine different methods on 8 km/h is shown in Figure 3-1, where a running cycle between two consecutive mid-swing instants is shown.

8 km/h											
Method	IC		RMSE (s)	FC		Stride Duration		Stance Duration		Swing Duration	
	RMS E (s)	Missed events (%)		Missed events (%)	Mean \pm std (s)	MAPE (%)	Mean \pm std (s)	MAPE (%)	Mean \pm std (s)	MAPE (%)	
Blauberger et al	0.016	0.1	0.022	0.7	0.486 \pm 0.019	1.4	0.179 \pm 0.058	17	0.307 \pm 0.054	13.4	
Schmidt et al	0.013	3.1	0.025	0.1	0.486 \pm 0.176	1.5	0.130 \pm 0.014	24.9	0.356 \pm 0.015	20.1	
Falbiard et al	0.022	0.3	0.036	0.3	0.486 \pm 0.011	0.8	0.155 \pm 0.009	17.7	0.221 \pm 0.011	14.3	
Bailey et al	0.016	3.6	0.029	0.3	0.486 \pm 0.020	2	0.195 \pm 0.024	5.9	0.292 \pm 0.024	4.7	
Reenalda et al	0.024	0.3	0.064	0.3	0.486 \pm 0.024	2	0.144 \pm 0.023	21.1	0.342 \pm 0.030	16.9	
Mo et al	0.023	0	0.066	0.1	0.486 \pm 0.027	2.5	0.165 \pm 0.035	17	0.321 \pm 0.035	14	
Chew et al	0.017	0	0.090	0.3	0.486 \pm 0.014	1.1	0.193 \pm 0.013	7.9	0.293 \pm 0.020	7	
Benson et al	0.023	0.1	0.040	0.3	0.487 \pm 0.019	1.8	0.188 \pm 0.030	6.6	0.298 \pm 0.031	5.4	
Yang et al	0.025	0.3	0.049	13.9	0.486 \pm 0.014	1.4	0.166 \pm 0.033	17.2	0.320 \pm 0.037	13.5	

Table 3.2 - RMSE and missed events for IC and FC, MAPE for stride, swing and stance duration obtained via each of the tested method over the 8 km/h dataset

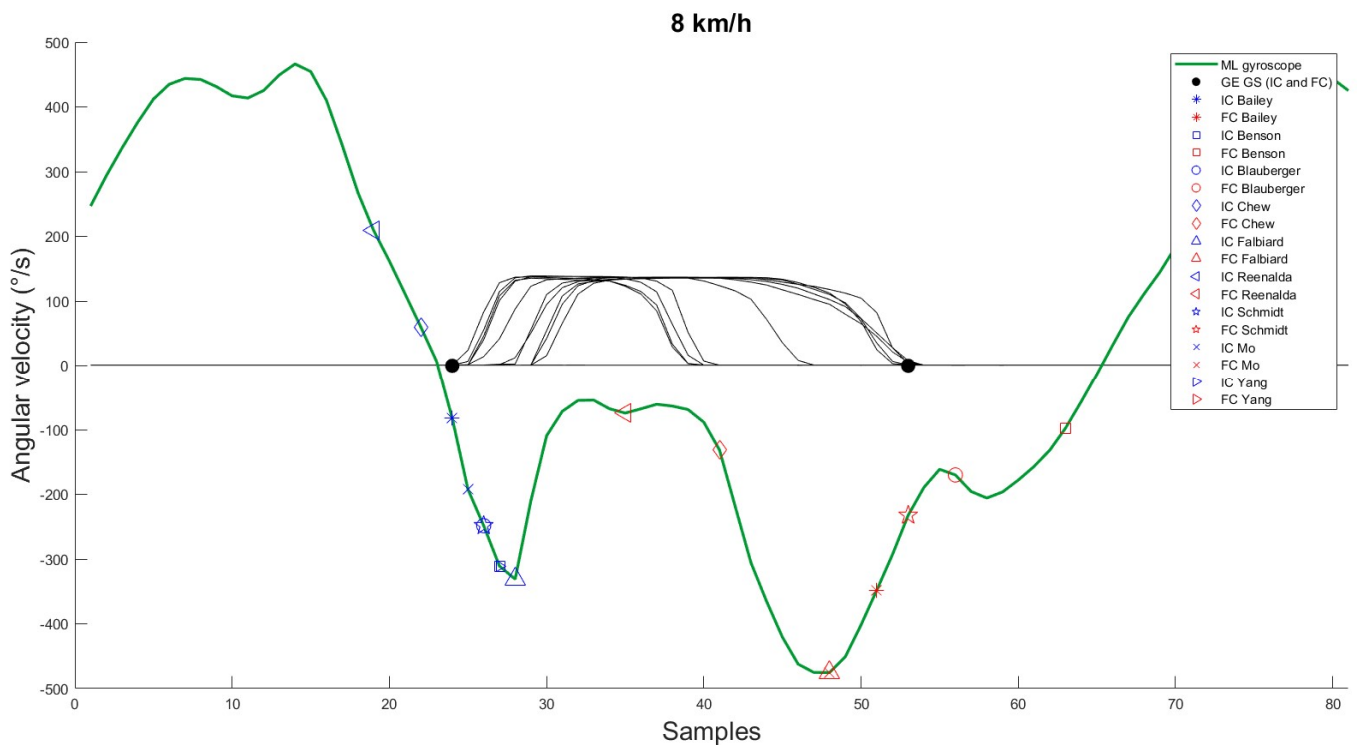


Figure 3-1 – Example image of a mid-swing to mid-swing cycle with the events detected via each of the different methods over the medio-lateral projection of the angular velocity at 8 km/h. The two different colors of the points differentiate ICs, in blue, and FCs, in red. Each method is associated to a different symbol, as stated in the legend. The two black filled points are the actual events, detected via the gold standard. The black lines show the signal acquired via the pressure insoles.

3.1.2 Comparison over 10 km/h

The remaining trials of the first dataset, e.g., the ones at 10 km/h, were then analysed separately in respect to the 8 km/h, so that any possible difference dictated by the slightly higher speed could be underlined.

Table 3.3 shows the results obtained with the methods from the literature. RMSE ranging from 0.014 s to 0.025 s are reported on the detection of the IC, from 0.021 to 0.087 s on the detection of the FC, and a percentage of missed events that ranges from 0% to 4.6%. This leads to MAPEs ranging from 1.1% to 2.6% on the Running cycle, from 6% to 24.1% on the stance duration and from 4.5% to 18.5% on the swing duration.

For this set of data, the best performance in both terms of IC and FC detection is achieved by Schmidt et al. [62] with a RMSE of 0.014 s and a 2.1% of missed events on the IC and a RMSE of 0.022 s and a 0.1% of missed events on the FC. This method also provided a low MAPE on the durations, which adds up to 1.2% for the stride duration, 7.6% for the stance duration and 6.3% for the swing duration.

By means of example, in Figure 3-2 a mid-swing to mid-swing running cycle with the annotations of the detections of all the methods is shown.

10 km/h										
Method	IC		FC		Stride Duration		Stance Duration		Swing Duration	
	RMSE (s)	Missed events (%)	RMSE (s)	Missed events (%)	Mean±std (s)	MAPE (%)	Mean±std (s)	MAPE (%)	Mean±std (s)	MAPE (%)
Blauberger et al	0.016	0.1	0.021	0.5	0.485±0.019	1.5	0.169±0.051	16.8	0.316±0.054	12.4
Schmidt et al	0.014	2.1	0.022	0.1	0.485±0.015	1.2	0.190±0.011	7.6	0.295±0.019	6.3
Falbiard et al	0.022	0.3	0.038	0.3	0.485±0.011	0.9	0.148±0.008	18.2	0.338±0.012	13.9
Bailey et al	0.017	4.6	0.027	0.4	0.485±0.021	2	0.192±0.022	6	0.293±0.024	4.5
Reenalda et al	0.025	0.3	0.061	0.3	0.485±0.025	2.2	0.140±0.023	21	0.345±0.031	16
Mo et al	0.024	0	0.063	0.1	0.485±0.027	2.6	0.166±0.035	15.8	0.319±0.035	12.2
Chew et al	0.018	0.3	0.087	0.3	0.485±0.016	1.4	0.129±0.019	24.2	0.356±0.015	18.5
Benson et al	0.024	0	0.036	0.3	0.485±0.020	1.8	0.178±0.28	6.1	0.308±0.031	4.9
Yang et al	0.025	0.3	0.044	15.4	0.485±0.015	1.4	0.162±0.029	17.2	0.321±0.034	12.2

Table 3.3 - RMSE and missed events for IC and FC, MAPE for tride, swing and stance duration obtained via each of the tested method over the 10 km/h dataset

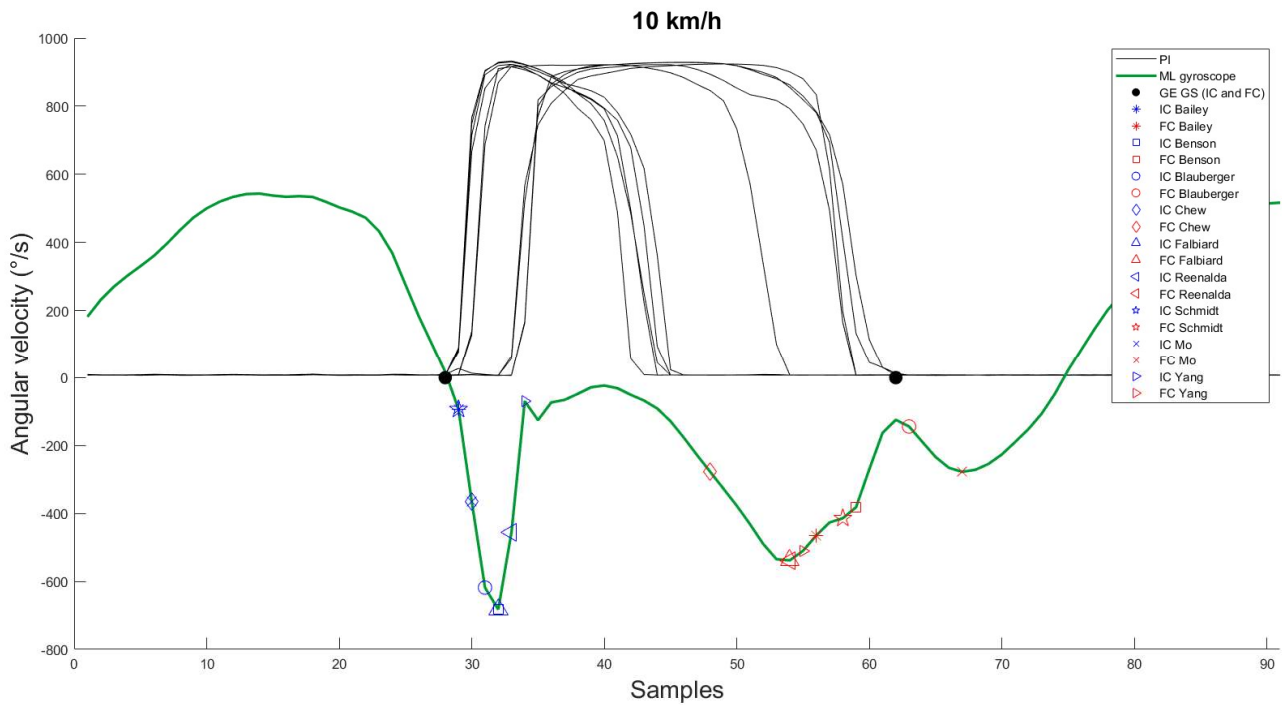


Figure 3-2 - Example image of a mid-swing to mid-swing period with the events detected via each of the different methods over the medio-lateral projection of the angular velocity at 10 km/h. The two different colors of the points differentiate ICs, in blue, and FCs, in red. Each method is associated to a different symbol, as stated in the legend. The two black filled points are the actual events, detected via the gold standard. The black lines show the signal acquired via the pressure insoles.

3.1.3 Comparison over 14 km/h

The results of the nine methods over the 14 km/h trials is reported in Table 3.4. RMSE ranging from 0.026 s to 0.054 s are reported on the detection of the IC, from 0.020 to 0.066 s on the detection of the FC, and a percentage of missed events that ranges from 0% to 9%. This leads to MAPEs ranging from 1% to 2.5% on the running cycle, from 12.8% to 25.7% on the stance duration and from 4.5% to 12.6% on the swing duration.

Overall, the best method for the detection of the ICs for this speed is Benson et al. [69] which reported an RMSE of 0.026 s and a 0.04% of missed events, while Falbiard et al. [63] was the best performing on the detection of FCs, with an RMSE of 0.020 s and a 1.2% of missed events.

All-embracing, the choice for the most fitting method for this dataset falls on Benson et al. that also resulted in a MAPE of 1.3% on the stride duration, 13.3% on the stance duration and 4.7% on the swing duration.

An example mid-swing to mid-swing cycle is reported in Figure 3-3, where the events identified by each method are shown against the vertical displacement of the foot.

14 km/h

Method	IC		FC		Stride Duration		Stance Duration		Swing Duration	
	RMSE (s)	Missed events (%)	RMSE (s)	Missed events (%)	Mean±std (s)	MAPE (%)	Mean±std (s)	MAPE (%)	Mean±std (s)	MAPE (%)
Blauberger et al	0.040	0.9	0.059	1.7	0.689±0.015	1.2	0.234±0.019	17.3	0.455±0.023	8.2
Schmidt et al	0.041	1.8	0.031	0.8	0.690±0.021	1.3	0.208±0.013	14.5	0.483±0.020	7.1
Falbiard et al	0.048	1.3	0.020	1.2	0.069±0.010	1	0.188±0.008	17.3	0.501±0.012	8.9
Bailey et al	0.035	4.6	0.066	1.2	0.689±0.020	2.1	0.263±0.023	12.8	0.426±0.025	4.5
Reenalda et al	0.055	1.3	0.024	1.4	0.689±0.018	1.1	0.185±0.013	23.4	0.503±0.021	11.9
Mo et al	0.032	0.5	0.056	0.7	0.689±0.021	1.8	0.116±0.091	21.8	0.439±0.086	10.6
Chew et al	0.027	0.5	0.057	0.6	0.689±0.027	2.5	0.197±0.019	19.3	0.491±0.019	9.7
Benson et al	0.026	0	0.038	0.8	0.689±0.013	1.5	0.267±0.026	13.3	0.422±0.027	4.7
Yang et al	0.054	1.2	0.052	9	0.689±0.015	1.4	0.193±0.032	25.7	0.596±0.035	12.6

Table 3.4 - RMSE and missed events for IC and FC, MAPE for tride, swing and stance duration obtained via each of the tested method over the 14 km/h dataset

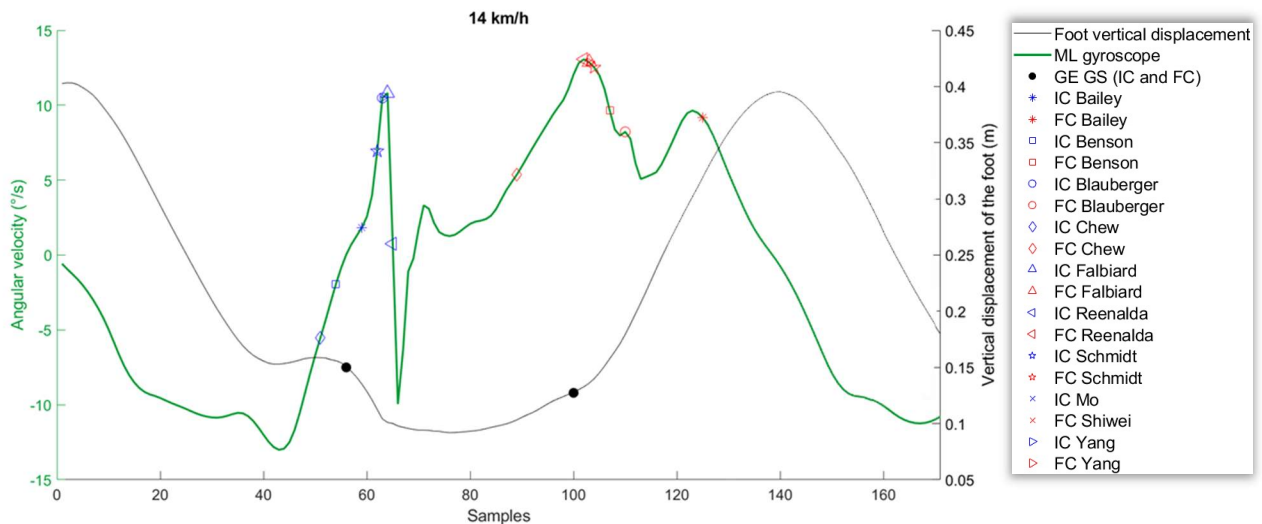


Figure 3-3- Example image of a mid-swing to mid-swing period with the events detected via each of the different methods over the medio-lateral projection of the angular velocity at 14 km/h. The two different colors of the points differentiate ICs, in blue, and FCs, in red. Each method is associated to a different symbol, as stated in the legend. The two black filled points are the actual events, detected via the gold standard. The black line shows the vertical displacement of the foot. The vertical displacement presents a offset equal to ~10 cm due to the treadmill height.

3.1.4 Comparison over sprinters

The data acquired on sprinters (20-32 km/h) were analysed using all the nine different methods from the literature described in Table 2.1. The data thus obtained, that is the identification of ICs and FCs for each method, was then compared to the gold standard data, acquired from pressure insoles for this specific dataset.

For the final results, 11 trials were discarded due to the deterioration of the pressure insoles while running because of the high impact with the ground. This problem arose at the very beginning of the data acquisition, thus was further investigated (see Appendix 1) to cover the sensorised insoles and reduce the likelihood of any damage during the trials. RMSEs computed for each running event, reported in Table 3.5, illustrate the accuracy of each algorithm. RMSE ranging from 0.022 s to 0.083 s are reported on the detection of the IC, from 0.046 to 0.094 s on the detection of the FC, and a percentage of missed events that ranges from 0.9% to 16.7%. This leads to MAPEs ranging from 2.1% to 13.3% on the running cycle, from 20% to 35.5% on the stance duration and from 12.2% to 28.8% on the swing duration.

Starting from the IC, the best performing method is Falbiard et al. [63] with an RMSE of 0.022 s for the IC, even though it reported a 4.9% of missed events. Speaking of FC, on the other hand, the best performing method is the one proposed by Yang et al. [70] with an RMSE of 0.044 s with a 7.3% of missed events. Grouping IC and FC results, the best method on this dataset is the one proposed by Falbiard et al. [16] with a RMSE of 0.022 s on the detection of the IC (e.g., the second best RMSE on the IC) and 0.047 s on the detection of the FC (e.g., the best RMSE on the FC). This method reported a MAPE of 2.1%, 31.1%, 20% on stride, stance and swing duration respectively. A single mid-swing to mid-swing period has been visually represented to give a hint of the performances of each method at higher speed in Figure 3-4.

Sprint										
Method	IC		FC		Stride Duration		Stance Duration		Swing Duration	
	RMSE (s)	Missed events (%)	RMSE (s)	Missed events (%)	Mean \pm std (s)	MAPE (%)	Mean \pm std (s)	MAPE (%)	Mean \pm std (s)	MAPE (%)
Blauberger et al	0.035	1.9	0.056	3.3	0.560 \pm 0.062	5.7	0.200 \pm 0.048	25.1	0.358 \pm 0.052	15.3
Schmidt et al	0.038	16.7	0.046	2.1	0.558 \pm 0.038	3.1	0.133 \pm 0.029	28.5	0.423 \pm 0.029	17.8
Falbiard et al	0.022	4.9	0.047	5.1	0.558 \pm 0.035	2.1	0.129 \pm 0.031	31.1	0.429 \pm 0.026	20
Bailey et al	0.052	6.5	0.059	8	0.556 \pm 0.068	6.9	0.201 \pm 0.060	22.1	0.362 \pm 0.053	12.4
Reenalda et al	0.048	0.9	0.065	3.4	0.558 \pm 0.056	5.1	0.158 \pm 0.036	23.8	0.400 \pm 0.046	15.9
Mo et al	0.082	1.2	0.086	4.5	0.554 \pm 0.110	13.3	0.116 \pm 0.091	51.5	0.439 \pm 0.086	28.8
Chew et al	0.047	3.8	0.094	6.8	0.560 \pm 0.052	5.4	0.175 \pm 0.038	20	0.383 \pm 0.039	12.2
Benson et al	0.083	14	0.083	16.2	0.599 \pm 0.050	8.7	0.214 \pm 0.052	35.6	0.377 \pm 0.081	22.3
Yang et al	0.038	4.7	0.044	7.3	0.559 \pm 0.048	4.4	0.165 \pm 0.041	23.2	0.394 \pm 0.048	15.7

Table 3.5 – RMSE and missed events for IC and FC, MAPE for stride, swing and stance duration obtained via each of the tested method over the sprinters dataset (20-32 km/h)

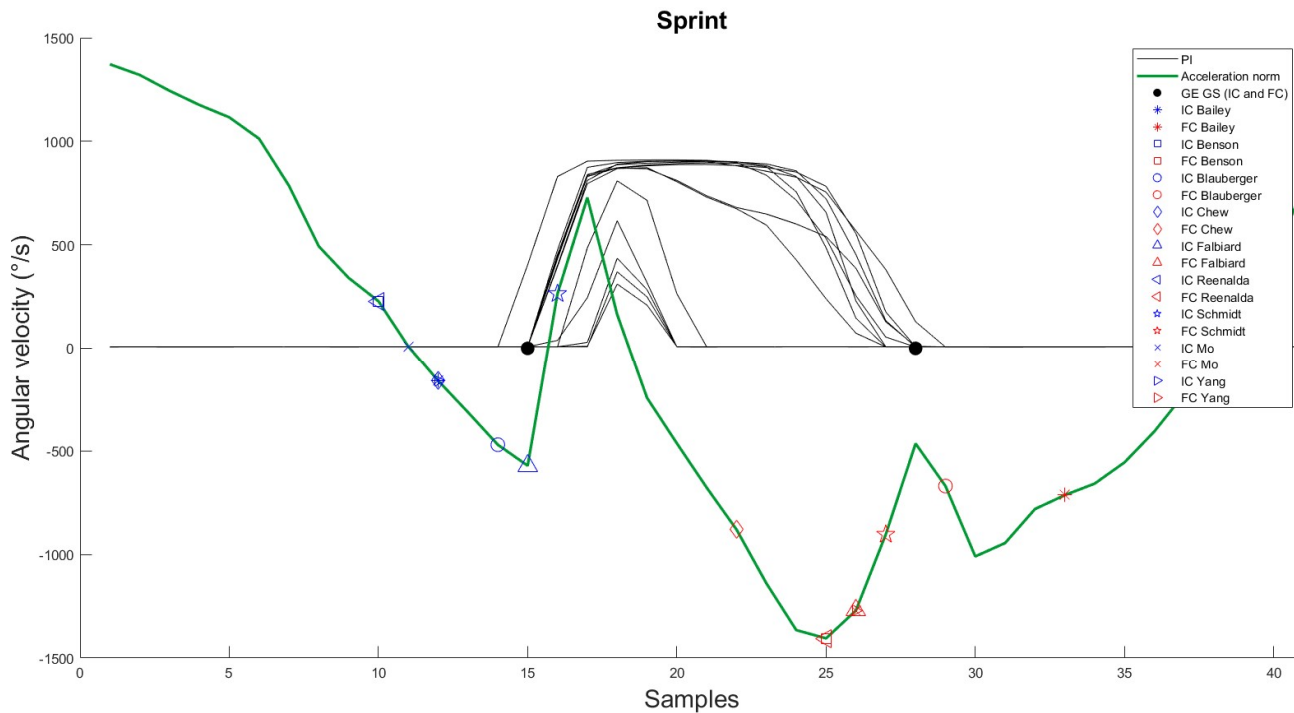


Figure 3-4 –Example image of a mid-swing to mid-swing segment with the events detected via each of the different methods over the medio-lateral projection of the angular velocity of a sprinter. The two different colors of the points differentiate ICs, in blue, and FCs, in red. Each method is associated to a different symbol, as stated in the legend. The two black filled points are the actual events, detected via the gold standard. The black lines show the signal acquired via the pressure insoles.

3.1.5 Choice of the best trade-off method

After analysing the performances of each method on the entirety of the data acquired, a further choice was made to identify the method that provided acceptable performance on all four datasets. The choice was made by considering the RMSE, by looking for a method which resulted in a RMSE lower than 0.030 s for both the IC and the FC, and a MAPE lower than 5% for the running cycle, 20% for the stance duration and 15% for the swing duration for all the speeds considered, while maintaining a percentage of missed events below 4%.

By following this criterion, the trade-off method can be identified as the one proposed by Blauberger et al. [61] that majorly met the criterion utilise, whose results on all datasets are summarized in Table 3.2.

Dataset	IC		FC		Stride Duration		Stance Duration		Swing Duration	
	RMSE (s)	Missed events (%)	RMSE (s)	Missed events (%)	Mean±std (s)	MAPE (%)	Mean±std (s)	MAPE (%)	Mean±std (s)	MAPE (%)
8 km/h	0.016	0.1	0.022	0.7	0.486±0.018	1.5	0.179±0.058	17	0.307±0.060	13.5
10 km/h	0.016	0.1	0.021	0.5	0.485±0.019	1.5	0.169±0.051	16.8	0.316±0.054	12.4
14 km/h	0.040	0.9	0.059	0.5	0.689±0.015	1.5	0.234±0.019	16.8	0.455±0.023	12.4
Sprint	0.035	1.9	0.056	3.3	0.559±0.062	5.7	0.200±0.048	25.1 2	0.358±0.052	15.3

Table 3.6 – Summary of the results obtained by the best method identified for all the four speed ranges. The results are shown in terms of RMSE and missed events for IC and FC, and in terms of MAPE for the durations (stride, stance and swing)

3.2 Novel method results

After identifying the best method suitable for a wide speed range among the ones proposed in the literature, the new method has been investigated.

First of all, different combinations of signals were tested for the definition of the templates:

- only accelerometer norm both for the identification of IC and FC,
- accelerometer norm for the IC and gyroscope norm for the FC,
- vertical accelerometer for the identification of the IC and mediolateral gyroscope for the identification of the FC,
- accelerometer norm for the IC and mediolateral gyroscope for the FC.

In Table 3.7 the results obtained via the new method with the use of the accelerometer norm are shown. The RMSE for the IC detection is always lower than 0.033 s on the detection of the IC, while it appears to be higher for the detection of the FC, with a maximum RMSE of 0.057 s on the detection of the FC for the sprinter dataset.

Template-based method – IC and FC on acceleration norm				
Dataset	IC		FC	
	RMSE (s)	Missed events (%)	RMSE (s)	Missed events (%)
8 km/h	0.020	0	0.035	0
10 km/h	0.021	0	0.037	0
14 km/h	0.033	0.5	0.032	0.6
Sprint	0.033	0.9	0.057	1.5

Table 3.7 – Table showing the results of the template-based method while using the accelerometer norm for the detection of both IC and FC.

Results from the second set of templates (e.g., adding the gyroscope norm) are shown in Table 3.8. It can be noted that the RMSE for the detection of the IC rose up to 0.053 s, which is higher than the one obtained when using the accelerometer norm alone.

Template-based method – IC on the acceleration norm, FC on the angular rate norm				
Dataset	IC		FC	
	RMSE (s)	Missed events (%)	RMSE (s)	Missed events (%)
8 km/h	0.020	0	0.053	0.1
10 km/h	0.021	0	0.048	0.1
14 km/h	0.033	0.5	0.038	0.6
Sprint	0.033	0.3	0.053	1.3

Table 3.8 – Table showing the results of the template-based method while using the accelerometer norm for the detection of the IC and the gyroscope norm for the detection of the FC

. In Table 3.9 the results concerning the search of the IC on the vertical acceleration and the FC on the mediolateral gyroscope are shown. In this table, it can be noted that the RMSE on the detection of the IC reached 0.034 s, while it resulted to be lower than 0.049 s for the FC.

Template-based method – IC on vertical acceleration and FC on medio-lateral angular rate				
Dataset	IC		FC	
	RMSE (s)	Missed events (%)	RMSE (s)	Missed events (%)
8 km/h	0.024	0	0.026	0
10 km/h	0.021	0	0.024	0
14 km/h	0.034	0.4	0.046	0
Sprint	0.034	1.2	0.049	0.7

Table 3.9 – Table showing the results of the template-based method when using the vertical acceleration for the detection of the IC, and the mediolateral gyroscope for the detection of the FC

By comparing these results in terms of RMSE, we can conclude that the best combination for the detection of both temporal events is the one achieved by the use of the acceleration norm (which performed 20% better than the vertical acceleration norm in terms of RMSE on the 8 km/h dataset – 0.020 s of RMSE using the acceleration norm and 0.024 s using the vertical acceleration) for the detection of the IC, and the mediolateral gyroscope for the detection of the FC, that yields the lower RMSE for all the speeds on the detection of the FC (e.g., 0.049 s using the mediolateral gyroscope, 0.054 s using the gyroscope norm and 0.057 s using the acceleration norm).

All considered, the selected templates, whose results are reported in Table 3.10, enabled a RMSE lower than 0.033 s and a missed events percentage lower than 0.5% for the detection of the IC across the whole speed range, and RMSE lower than 0.049 s and missed events percentage lower than 0.7 s for the detection of the FC.

Moreover, the MAPE results lower than 4% for the stride duration, lower than 26% for the stance duration and lower than 15% for the swing duration.

Selected template-based method – IC on the acceleration norm, FC on the mediolateral angular rate

Dataset	IC		FC		Stride Duration		Stance Duration		Swing Duration	
	RMSE (s)	Missed events (%)	RMSE (s)	Missed events (%)	Mean±std (s)	MAPE (%)	Mean±std (s)	MAPE (%)	Mean±std (s)	MAPE (%)
8 km/h	0.020	0	0.026	0	0.486±0.014	1.2	0.208±0.021	6.9	0.278±0.020	5.5
10 km/h	0.021	0	0.024	0	0.485±0.016	1.3	0.199±0.019	7.1	0.286±0.020	5.4
14 km/h	0.033	0.5	0.046	0.6	0.684±0.033	3.4	0.238±0.030	16.1	0.444±0.030	7.6
Sprint	0.033	0.3	0.049	0.7	0.560±0.041	3.7	0.196±0.045	26	0.362±0.040	14.3

Table 3.10 - Summary of the results obtained by the template method for all the four speed ranges. The results are shown in terms of RMSE and missed events for IC and FC, and in terms of MAPE for the durations (stride, stance and swing).

Finally, the specificity for this method was computed and reported in Table 3.11. The value is equal or higher than 95% on all the speeds considered.

Dataset	Number of total strides	Number of total missed events	Specificity (%)
8 km/h	38028	176	99.5
10 km/h	34674	176	99.5
14 km/h	45982	316	99.3
Sprint	4182	220	95.0

Table 3.11 – Specification used for the computation of the specificity. In the table, the total number of strides analysed and the total number of missed events is shown for each speed, together with the specificity derived from these data.

3.2.1 Sensibility analysis

To test the sensibility of the method to changes made to the denoising method, a preliminary investigation on the denoising parameters has been made by varying the denoising level and the mother wavelet exploited. In particular, the method was

further tested by employing: no filtering method, whose results are reported in Table 3.12, decomposition to level 1 and level 3 using Daubachies 6, in Table 3.13 and Table 3.14 respectively, and Symlets 5, in Table 3.15 and Table 3.16, which was the second best mother wavelet recommended by Ji et al [71] for gait analysis. Variations ranging from 3.6 to 130% on the RMSE of the events (IC and FC) and from 7 to 127% on the MAPE of the durations (running cycle, stance duration and swing duration) with respect to the results obtained via the decomposition to level 2 using Daubachies 6 are observed.

No filtering method employed					
Dataset	IC	FC	Stride Duration	Stance Duration	Swing Duration
	RMSE (s)	RMSE (s)	MAPE (%)	MAPE (%)	MAPE (%)
8 km/h	0.029	0.037	2.6	10.2	7.7
10 km/h	0.029	0.039	2.7	11.1	8.1
14 km/h	0.028	0.049	2.7	14.7	7.1
Sprint	0.034	0.044	3.0	22.8	12.7

Table 3.12 – Results obtained via the template-based method bereft of any filtering

Daubachies 6 – level 1					
Dataset	IC	FC	Stride Duration	Stance Duration	Swing Duration
	RMSE (s)	RMSE (s)	MAPE (%)	MAPE (%)	MAPE (%)
8 km/h	0.031	0.038	2.6	10.6	8.1
10 km/h	0.031	0.036	2.6	10.6	7.7
14 km/h	0.028	0.048	2.4	13.9	6.4
Sprint	0.037	0.044	3.5	21.8	11.8

Table 3.13 - Results obtained via the template-based method by using Deubachies 6 and decomposing to the first level

Daubachies 6 – level 3					
Dataset	IC	FC	Stride Duration	Stance Duration	Swing Duration
	RMSE (s)	RMSE (s)	MAPE (%)	MAPE (%)	MAPE (%)
8 km/h	0.026	0.035	2.0	9.4	6.9
10 km/h	0.030	0.038	2.1	10.8	7.8
14 km/h	0.052	0.028	4.0	26.9	12.5
Sprint	0.043	0.047	3.5	21.7	11.7

Table 3.14- Results obtained via the template-based method by using Deubachies 6 and decomposing to the third level

Symlets 5 – level 1					
Dataset	IC	FC	Stride Duration	Stance Duration	Swing Duration
	RMSE (s)	RMSE (s)	MAPE (%)	MAPE (%)	MAPE (%)
8 km/h	0.033	0.031	2.6	10.7	8.0
10 km/h	0.033	0.025	2.7	9.6	6.8
14 km/h	0.029	0.048	2.3	14.5	6.9
Sprint	0.035	0.044	3.5	20.5	11.4

Table 3.15- Results obtained via the template-based method by using Symlets 5 and decomposing to the first level

Symlets 5 – level 3					
Dataset	IC	FC	Stride Duration	Stance Duration	Swing Duration
	RMSE (s)	RMSE (s)	MAPE (%)	MAPE (%)	MAPE (%)
8 km/h	0.027	0.056	2.0	12.9	10.0
10 km/h	0.029	0.054	2.1	14.3	10.1
14 km/h	0.052	0.045	4.7	33.3	15.8
Sprint	0.040	0.049	4.0	26.8	13.5

Table 3.16 - Results obtained via the template-based method by using Symlets 5 and decomposing to the third level

3.3 Comparison of the novel method with the best trade-off from the literature

In order to highlight the differences between the hereby proposed method and Blauburger et al. (i.e. the best trade-off from the literature) a first a Shapiro-wilk test to check on the distribution of the different population has been carried out. Then, if the populations resulted in a normal distribution, a Student's t-test has been employed, otherwise, a Wilcoxon signed rank test has been performed on the results of both methods, in particular by taking into considerations the stride, stance and swing duration computed via them for each dataset.

A t-test is a statistical test commonly used to evaluate whether there is a difference between two distinct groups, usually employed when the number of samples available is too small to perform other more precise statistical analysis.

To perform the t-test, the first step is to infer the mean of the parameter which one wants to investigate. After computing the grand mean of the parameter, which is the mean across all trials, conditions and subjects composing a population, a hypothesis test has been brought on. The aim for this test was to highlight whether the two methods returned statistically different results in terms of durations, which lead to the formulations of the two hypotheses to test:

– H_0 : null hypothesis, the methods are not different, $\bar{x}_1 - \bar{x}_2 = 0$

– H_1 : alternative hypothesis, the methods retain a statistical difference, $\bar{x}_1 - \bar{x}_2 \neq 0$.

With \bar{x} being the grand means for the parameters of each population and 0 being the expected value for the null hypothesis, x_0 .

Subsequently, the test statistic can be computed as in (3.4):

$$Test\ statistic = \frac{(\bar{x}_1 - \bar{x}_2) - x_0}{\sqrt{\frac{s_1^2}{n_1} + \frac{s_2^2}{n_2}}} \quad (3.4)$$

Where s represents the overall standard deviation of the whole population, and n the size of it. The value thus computed must be compared to a p-value, that indicates the probability for the result of the test to be correct. To each p-value chosen, a certain confidence interval is associated. The most commonly used p-value is 0.05, which is associated to a 95% confidence interval [26]. Each p-value leads to a certain value of significance, that is to be researched in the *t-table* [73] by looking for the p-value wanted and the degrees of freedom ν the population has, that equals to the total number of the least numerous population minus one, as stated in (3.5).

$$\nu = \min(n_1 - 1, n_2 - 1) \quad (3.5)$$

Given the p value and the degrees of freedom, the value of significance can be extrapolated from the t-table by intersecting rows and columns. If the test statistics computed in (3.4) is higher than the value of significance, the null hypothesis is rejected, which means that the methods are statistically different. On the other hand, if the test statistic is lower than the value of significance, the null hypothesis cannot be rejected, so the two methods analysed do not retain a statistic difference.

The t-test has been performed by taking into consideration the stride duration, stance duration and swing duration obtained via the newly proposed method and the method proposed by Blauburger et al. [61] over the four different speeds analysed. It relies on the hypothesis that the distributions of the data on which it is used is normal, hence a check on the distributions of the data has been performed through a Shapiro-Wilk test. As a result, the data coming from the 14 km/h and the sprinters all yielded a normal distribution, on the other hand the results obtained via Blauburger et al. for the stance duration on 8 km/h and the swing duration on 10 km/h didn't have a normal distribution. Moreover, the results computed via the template-based method on the swing duration at 8 km/h and all three the duration on 10 km/h didn't have a normal distribution, which made the t-test unsuitable. Subsequently, for the stance and swing durations at 8 km/h and all the duration at 10 km/h a non-parametric Wilcoxon signed rank test was performed, which does not rely on the normal distribution hypothesis.

Speaking of the results, for the stride durations, they are shown in Table 3.17, in Table 3.18 for the stance duration and lastly Table 3.19 for the swing duration, where it can be noted that the value of the p-value is higher than the chosen p-value (0.05) for all the speeds for which the t-test was employed, leading to the conclusion that the null hypothesis cannot be rejected for all the parameters considered, thus no statistical difference between the two methods was detected. However, the Wilcoxon signed rank test for the remaining data rejected the null hypothesis for the stance and swing duration at 8 km/h and 10 km/h, leading to a statistical difference.

Running cycle duration							
	Blauberger et al		Template-based		Test specifics		
Dataset	Grand mean (s)	Grand Std (s)	Grand mean (s)	Grand Std (s)	Test name	P-value	Differences (s)
8 km/h	0.486	0.035	0.485	0.014	T-test	0.43	<0.001
10 km/h	0.485	0.019	0.485	0.016	Wilcoxon signed rank	0.13	<0.001
14 km/h	0.689	0.015	0.684	0.033	T-test	0.18	0.002
Sprint	0.559	0.062	0.560	0.041	T-test	0.58	0.002

Table 3.17 – statistical test results over the three speeds on the stride duration. The values indicated with a * are the ones lower than the reference p-value, leading to a statistical difference. The differences reported are referred to the means of the parameters for the speeds where a t-test was employed, and for their medians otherwise.

Stance Duration							
	Blauberger et al		Template-based		Test specifics		
Dataset	Grand mean (s)	Grand Std (s)	Grand mean (s)	Grand Std (s)	Test name	P-value	Difference (s)
8 km/h	0.179	0.058	0.208	0.021	Wilcoxon signed rank	<0.01*	0.021
10 km/h	0.169	0.051	0.199	0.019	Wilcoxon signed rank	<0.01*	0.029
14 km/h	0.234	0.019	0.238	0.019	T-test	0.79	0.002
Sprint	0.200	0.048	0.196	0.045	T-test	0.69	0.003

Table 3.18 – statistical tests results over the four speeds on the swing duration. The values indicated with a * are the ones lower than the reference p-value, leading to a statistical difference. The differences reported are referred to the means of the parameters for the speeds where a t-test was employed, and for their medians otherwise.

Swing Duration							
Dataset	Blauberger et al		Template-based		Test specifics		
	Grand mean (s)	Grand Std (s)	Grand mean (s)	Grand Std (s)	Test name	P-value	Differences (s)
8 km/h	0.307	0.060	0.278	0.020	Wilcoxon signed rank	<0.01*	0.030
10 km/h	0.316	0.054	0.286	0.020	Wilcoxon signed rank	<0.01*	0.030
14 km/h	0.455	0.023	0.444	0.030	T-test	0.72	0.003
Sprint	0.358	0.052	0.362	0.040	T-test	0.50	0.004

Table 3.19 – statistical tests results over the four speeds on the swing duration. The values indicated with a * are the ones lower than the reference p-value, leading to a statistical difference. The differences reported are referred to the means of the parameters for the speeds where a t-test was employed, and for their medians otherwise.

Chapter 4

Discussion and conclusions

4.1 Discussion

The analysis of the running parameters during actual training sessions could help in identifying the problems and fix them, before they lead to a subsequential injury, that could quite possibly hurt the athlete and their ability to perform [1] .

The aim of the present work has been to firstly compare and evaluate the performances of nine different methods identified from the literature [60-63], [65-69] for the identification of running events, on three running datasets which differ for running conditions, paces and sampling frequency, and then propose a novel template-based method. The first dataset comprised 11 subjects running at 8 km/h and 10 km/h, equipped with a MIMU attached to the shoelaces and pressure insoles. The second one was composed by 10 recreational runners, equipped with a MIMU and retroreflective markers, running at 14 km/h on a treadmill. Lastly, the higher speeds dataset contained data acquired from 9 elite athletes running at 70%, 85% and 100% of their maximal speed while wearing a MIMU on the shoelaces and pressure insoles.

The inertial-based methods from the literature were proposed to be utilised under specific running condition, either outdoor or indoor. They all had either different sensor positioning, different sampling frequency and/or were developed for different speeds with respect to the datasets analysed in this work. Thus, the implemented methods were adapted to the different positioning and sampling frequency.

It has to be noted that all the methods that were developed for higher velocities (i.e. 30-32 km/h) involved higher sampling frequencies for the data acquisition, as it has been proven that the sprint running investigation led to higher accuracies using at least 300 Hz [74] . Thus, a sub-aim of the present work was to test whether the running analysis at 100-200 Hz would be sufficiently accurate, given that there are some commercially available MIMUs that have a sampling frequency constraint.

The morphology of the signals changes a lot as the speed increases the accuracy of all the methods seemed to deteriorate when shifting from lower to higher speeds, which can be noted by comparing the RMSE reported in Table 3.2, Table 3.3, Table 3.4 and Table 3.5. However, the solutions provided in the literature for the sprint investigation heavily relied on peak detection, which lead to the necessity to set different thresholds for the peak identification. Peaks in sprinters tend to be enhanced, especially the ones in the acceleration signals, on the other hand the height of said peaks changes drastically based on subject and speed, which makes the definition of a threshold more complex. No method for sprint evaluation at 100 Hz has been developed yet.

Regardless of the speed, the detection of the FCs always leads to worse performances than the ones obtained for the ICs (e.g. in Table 3.5 for Falbiard et al. the RMSE on IC was 0.022 s and the one on the FC was of 0.047, for Schmidt et al. 0.038 s vs 0.046 s and so on), underlining the difficulty for each algorithm to identify the final contact event, mainly because it is not linked to abrupt changes in the signals [64], unlike the IC.

On the choice of the best method for the detection of events at 8 km/h, Blauburger et al. [61] was chosen as the best performing. This choice was made by taking into consideration the errors on the events in terms of RMSE, MAPE and missed events. Even though the chosen method was proposed for higher speeds (i.e. 32 km/h), the difference in positioning and sampling frequency made the inertial signals for this speed, shown in Figure 4-1, suitable to be analysed with this algorithm. In fact, in the acceleration norm in Figure 4-1 a great peak can be identified, preceded by a minimum that is aligned with the initial contact identified by the gold standard. Similarly, the norm of the gyroscope presents two maximums with a minimum between them that is aligned with the final contact detected via the gold standard. All of these characteristics can also be found in Figure 4-2.

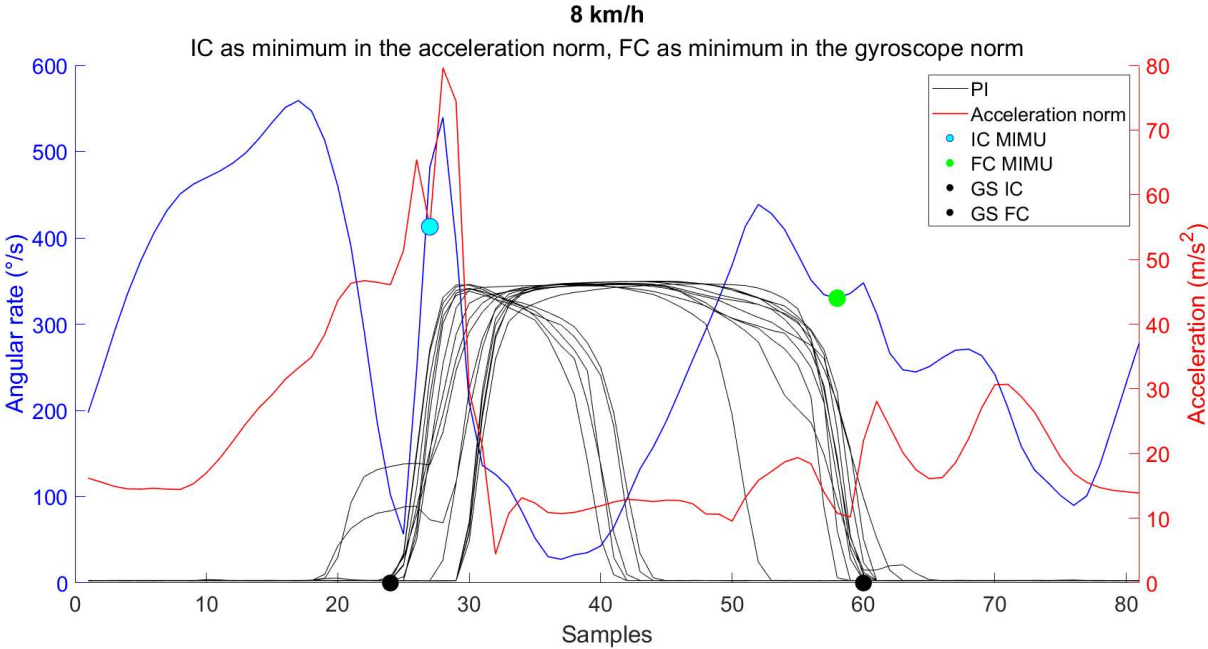


Figure 4-1 – Example of inertial signals acquired during an 8 km/h run. In the picture, the acceleration norm (in red) and the gyroscope norm (in blue) are shown since they are the signals considered by Blauburger et al. for the detection of the events. The black lines represent the pressure insoles signal. The black vertical lines highlight the points in which the events were identified by the method, while the blue and red filled circled indicate the events detected via the gold standard (pressure insoles).

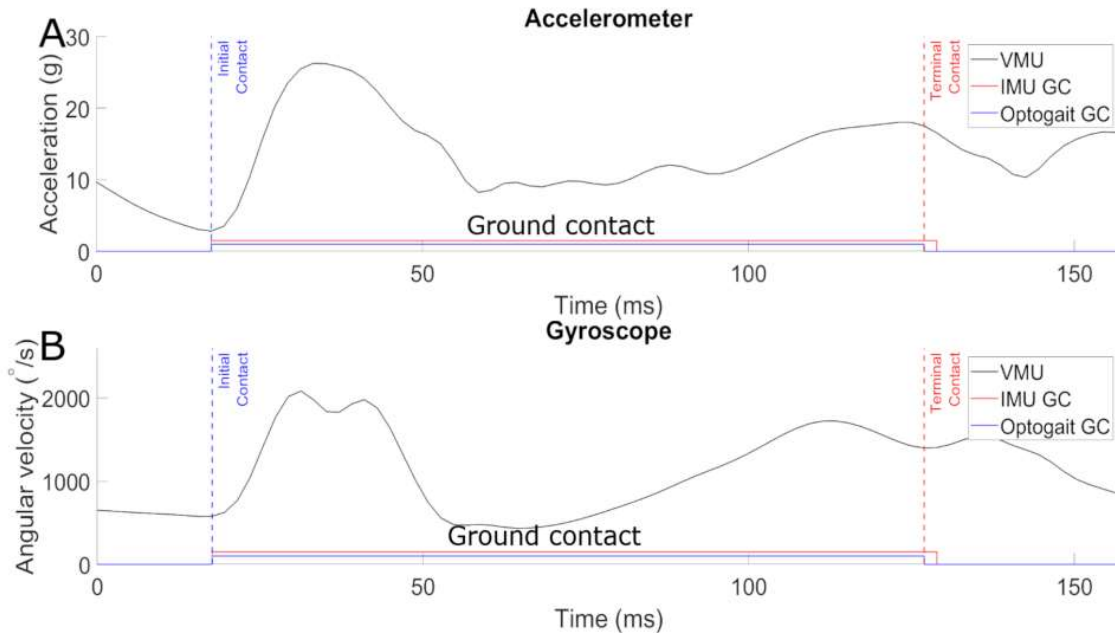


Figure 4-2 – Vector magnitude unit (VMU) of x, y, and z acceleration (A) and angular velocity (B) throughout one single sprint step, that is the norms of the signals, from dataset used in [14]. The blue dashed line marks the initial contact event; the red dashed line the terminal contact. The solid red line indicates the resulting ground contact period for the inertial measurement unit (IMU). The photo-electric-measured (Optogait) ground contact time is represented by the solid blue line.

The same can be said for the choice of Schmidt et al. [62] as the best performing for trials at 10 km/h, but in this case, it resulted in the least amount of errors on the durations. This method was proposed for higher speeds (i.e. 31 km/h), but again changing sensor positioning and the sample frequency the recorded inertial signals at 10 km/h and 100 Hz had a morphology suitable to the running events definitions by Blauburger et al. Figure 4-3 illustrates that in correspondence of the zone in which the vertical accelerometer presents a high peak, the mediolateral gyroscope yields a constant slope, and that is around the time when the IC happens, as it was stated in the reference paper. Additionally, FCs occurred approximately in correspondence of a local maxima in the vertical acceleration.

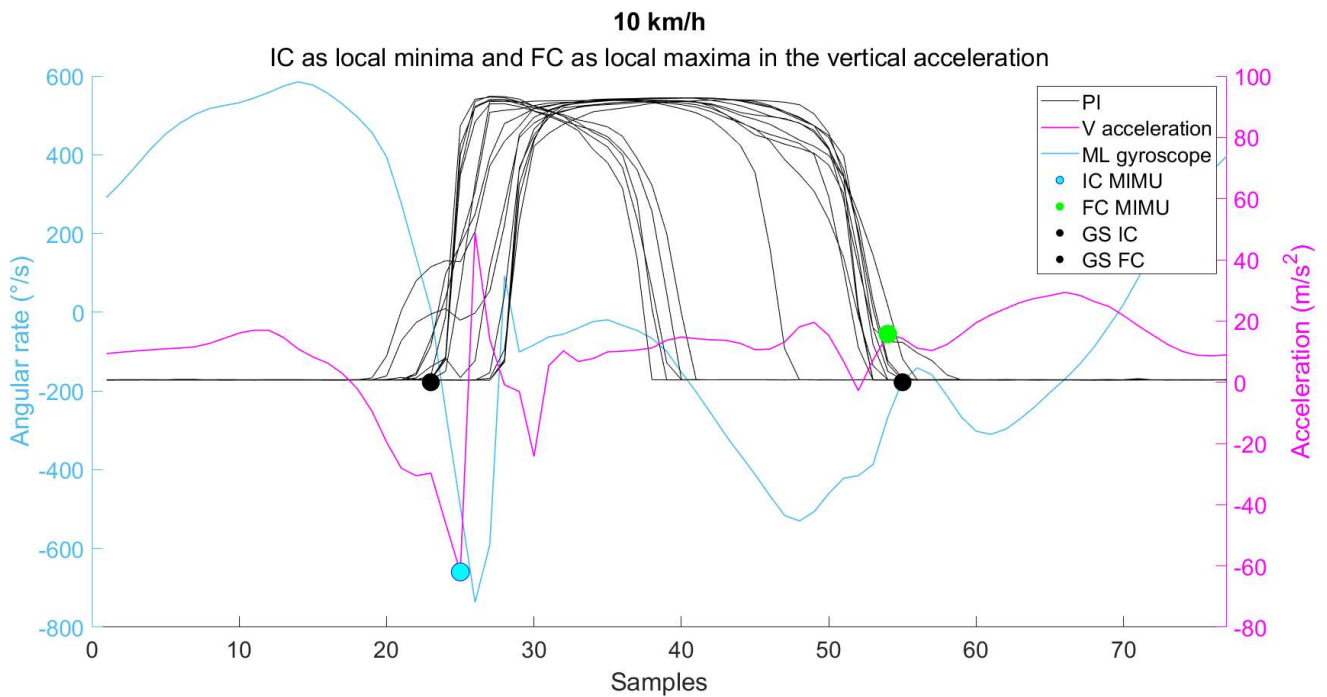


Figure 4-3 – Mid-swing to mid-swing cycle from the 10 km/h trials. In the picture, the vertical acceleration, in pink, and the medio-alteral angular velocity, in light blue, are shown, since these are the signals used in Schmidt et al. [62] for the events identification. The shape of the inertial signals closely resembles the one described in the paper.

At 14 km/h the best performing method of choice has been identified in the one proposed by Benson et al. [69] implemented by the authors for 12 km/h running. When compared to the performances of the second method identified, that is Falbiard et al. [63] it provided a better RMSE on the IC (0.026 s vs 0.048 s) and a slightly worse RMSE on the FC (0.038 s vs 0.020 s), but it provided a better MAPE on the durations (1.3% vs 1% on the running cycle, 14.5% vs 17.3% on the stance duration and 7.1% vs 8.9% on the swing duration), which lead to the choice made.

Finally, for the sprinters, the method deemed to be the best working was the one by Falbiard et al. [63] as it provided the minor RMSE on the IC while also providing a slightly worse RMSE on the FC than Yang et al. [70] which was the best performing in terms of FC on this dataset (0.047 s vs 0.044 s). The chosen method was tested by the authors on a range of speeds (up to 20 km/h). In Figure 4-4 a sprint mid-swing to mid-swing cycle is shown. It can be noted that in correspondence of the events, two local minimums in the angular velocity can be identified, which makes the morphology of the signals compatible to what has been described in the paper, even if the original method was tested on data acquired at 500 Hz.

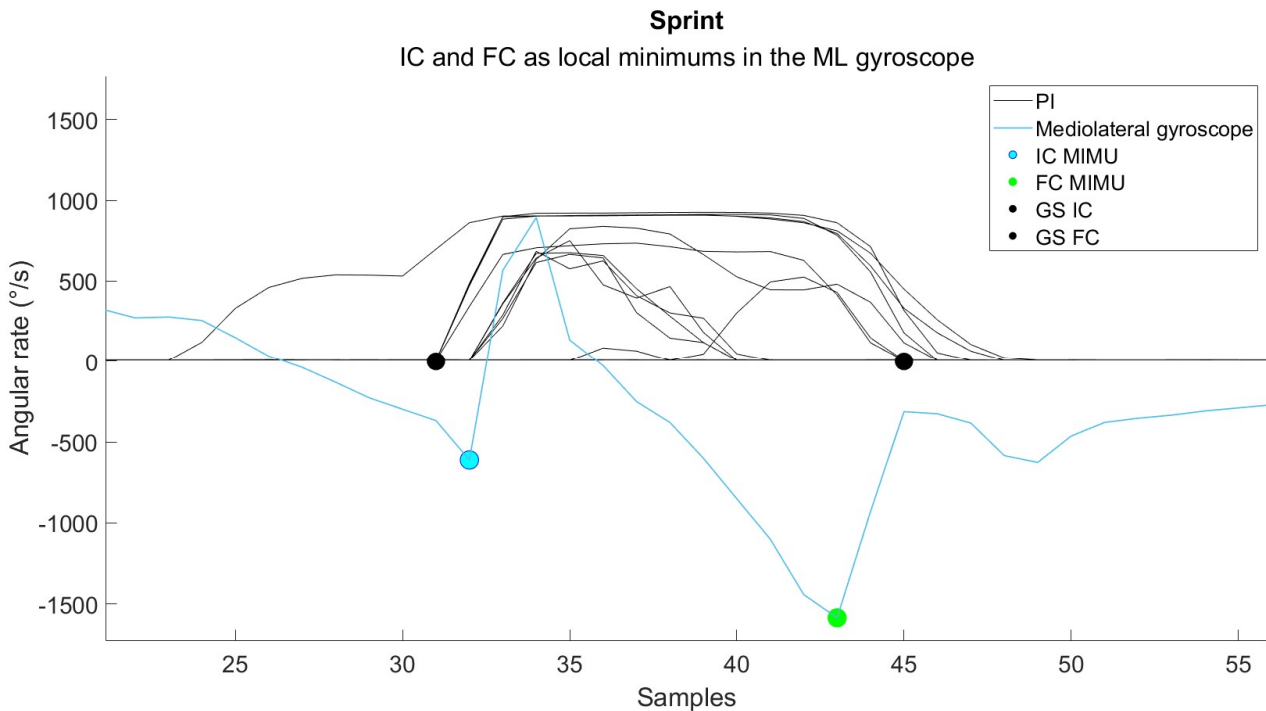


Figure 4-4 – Mid-swing to mid-swing cycle from a sprinter running at 32 km/h . The mediolateral angular velocity has been pictured as it is the inertial signal used in Falbiard et al. [63] for the identification of the events. As shown by the results, the performances in the identification of the FC seem to be worse than the ones on the IC.

Furthermore, the method which enabled the best trade-off performances on the whole speed range has been identified, based on the accuracy it provided via the RMSE. It was the one proposed by Blauburger et al [61] and for which the only parameter to be adapted is the filtering cut-off frequency. In Figure 4-5 a depiction of the performances of this method on all four the speed analysed is provided. Even though its performances were the best trade-off across the nine methods [61-64, 66-70], it still showed high MAPEs for the estimation of the durations (1.2 to 5.7% on the running cycle, 16.8 – 25.2% on the stance duration and 8.2 – 15.3% on the swing duration), hence a new method has been developed to try to improve the estimations.

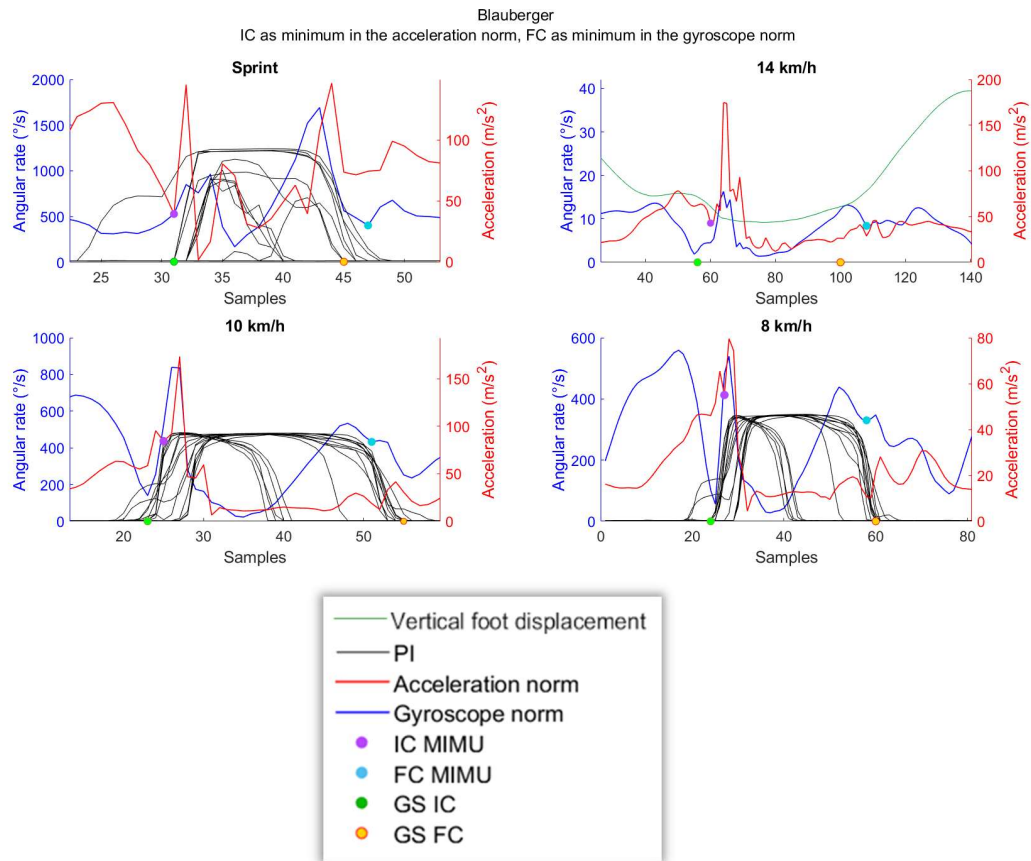


Figure 4-5 – Mid-swing to mid-swing cycles for all the four speeds analysed. The events identified by Blauberger et al. are shown as well as the events detected via the GS. It can be noted that the performance for the method for all four dataset seem to be acceptable based on the distance between the GS and the method-detected event.

Overall, we confirmed that methods for the detection of running events depend on the running pace and the main cause of errors is the highly different morphology of the inertial signals varying speed. Thus, to try to overcome the main limitations of the methods in the literature, the novel proposed method is template based. Twenty templates were constructed, considering 5 running cycle (i.e. mid-swing to mid-swing) of a single subject per dataset. We observed that namely the 30% of the analysed running cycles matched with a template which did not belong to its own population (e.g. a mid-swing to mid-swing cycle from the 8 km/h was used to identify the events of a sprinter or the events coming from a 14 km/h trial).

The proposed method proved to be comparable to the best trade-off from the literature (i.e. Blauberger et al.), which was further confirmed by the results of the statistical analysis lead via t-test and Wilcoxon signed rank tests, which showed no statistical difference between the performances of the two algorithms in terms of durations estimation, except for the stance and swing duration at 8 km/h, where the template based method reported a MAPE of 6.9% and 5.5% on the stance and swing duration respectively, while Blauberger et al. reported a MAPE of 17% on the stance duration and 13.4% on the swing duration, and 10 km/h, where the MAPE for the novel method amounted to 7.1% and 5.4% for the stance and swing duration respectively, while Blauberger et al. yielded a MAPE of 16.8% on the stance duration and 12.4% on the swing duration. The novel method performed better on medium to high velocity (14 km/h with RMSE of 0.033 s vs 0.040 s on the IC detection, 0.046 s vs 0.059 s on the FC estimation, and sprints with RMSEs of 0.033 s vs 0.035 s on the ICs, and 0.049 s vs 0.056 s on the FCs) and slightly worse on lower paces (8 km/h with RMSEs of 0.020 s vs

0.016 s on the ICs and 0.026 s vs 0.022 s for the FCs; 10 km/h with RMSEs of 0.021 vs 0.016 s for the IC detection and 0.024 s vs 0.021 s for the FC detection) than Blauburger et al. Moreover, the results obtained by using the method proposed by Blauburger et al. on the three datasets employed in this work reported higher errors than the ones declared in the original paper. This is probably due to the sampling frequencies adopted in the data acquisitions, which limit the resolution of the results to 1/100 s and 1/200 s for 100 and 200 Hz respectively, while in the original paper they could obtain a 1/500 s resolution.

Finally, a preliminary analysis on the parameters of the denoising methods was performed, extensively reported in Chapter 3. Overall, the variations in terms of both mother wavelet and level of the decomposition lead to an increase in the errors, which ranged from 3.6 to 130% on the RMSE of the events (IC and FC) and from 7 to 127% on the MAPE of the durations (running cycle, stance duration and swing duration). From this, it can be stated that the method is very sensible to the parameters chosen and that a further fine-tuning of the parameters of the denoising method should be performed.

The main drawback of the proposed method is that it needs to know when the true running events occurred for at least a pair of running cycles of a subject to label the templates. On the other hand, it enables to avoid the dependence of the running events detection on thresholds, which frequently needs ad hoc fine-tuning. The only parameters on which the proposed method relies concern the initial denoising (i.e. mother wavelet chosen and level of decomposition). Furthermore, we observed that results did not significantly change between indoor and outdoor acquisitions.

In conclusion, it showed promising results for accurately detecting temporal events on a broad speed range.

4.1 Conclusion

In the present work, the performance of nine methods from the literature for the identification of the instants of initial and final contacts with the ground while running using foot-mounted MIMUs were compared. They were proved to be speed-dependent since the inertial signals morphology highly varies increasing the running speed which is not optimal for the detection of temporal events on a wide speed range, as expected. The best performing method (i.e., the one proposed by Blauburger et al.) on the whole running speed range did not rely on any threshold except for the definition of the cut-off frequency for the filtering of the signals, which was removed in the adaptation phase. Furthermore, an innovative template-based method has been developed. It was based on the matching of each running cycle with the most similar mid-swing to mid-swing template to overcome the limitation of the highly variable signals morphology varying speed and subject. Templates were built with accelerations norms and mediolateral angular velocities and labelled with the events calculated from the available gold standards. Obtained results are in line with the best trade-off from literature (Table 3.10), making it promising for the detection of temporal events on a broad speed range. The main advantage of using the proposed method instead of traditional techniques is that it is automatically speed-adapting.

However, the main drawback is that it is strictly template-dependant, meaning that the number of available templates for a certain speed defines its capability to correctly detect the temporal events for that specific running pace. Furthermore, the datasets used to test its performances contained data acquired at a lower sampling frequency than suggested for running trials, and the number of templates provided to the algorithm may be not sufficient for its optimal functioning.

Future work should concern the increase of the sampling frequency for all the datasets, the inclusion of more templates for each speed on the library which may lead to an improvement in the accuracy of the hereby proposed method and the acquisition of more data at different running speeds than the ones included in the three datasets analysed, to fill the gap between the different speeds (i.e. 10 km/h to 14 km/h and 14 km/h to 20 km/h).

References

- [1] - Taunton JE, Ryan MB, Clement DB, McKenzie DC, Lloyd-Smith DR, Zumbo BD. A retrospective case-control analysis of 2002 running injuries. *Br J Sports Med.* 2002 Apr;36(2):95-101. doi: 10.1136/bjism.36.2.95. PMID: 11916889; PMCID: PMC1724490.
- [2] - S. Chen, J. Lach, B. Lo, G. Yang, Toward pervasive gait analysis with wearable sensors: a systematic review, *IEEE J. Biomed. Health. Inf.* 206 (2016) 1521–1537.
- [3] - Strava, 2020, https://1n4rcn88bk4ziht713dla5ub-wpengine.netdna-ssl.com/wp-content/uploads/2020/12/USA_YIS_2020.pdf
- [4] - T.F. Novacheck, “The biomechanics of running”, *Gait and Posture* 7 (1998) 77–95
- [5] - Gage JR. “An overview of normal walking”, *AAOS Instructional Course Lectures* 1990;39:291–303
- [6] - V. Agostini, G. Balestra, and M. Knaflitz, “Segmentation and classification of gait cycles”, *IEEE Trans. Neural Syst. Rehabil. Eng.*, vol. 22, no. 5, pp. 946–952, 2014
- [7] - S.A. Dugan and K.P. Bhat, “Biomechanics and Analysis of Running Gait”, *Phys Med Rehabil Clin N Am* 16 (2005) 603–621
- [8] - Mathie MJ., Coster ACF., Lovell NH., *Accelerometry: Providing an Integrated, Practical Method for Long-Term, Ambulatory Monitoring of Human Movement* Accelerometry: providing an integrated, practical method for long-term, ambulatory monitoring of human movement. 2004
- [9] - Zrenner M., Küderle A, Roth N., Jensen U., Dümmler B and Eskodier B.M., ‘Does the Position of Foot-Mounted IMU Sensors Influence the Accuracy of Spatio-Temporal Parameters in Endurance Running?’, *Sensors* 2020, 20, 5705; doi:10.3390/s20195705
- [10] - Bergamini E., Picerno P., Piller H., Natta F., Thoreux F. and Camomilla V., “Estimation of temporal parameters during sprint running using a trunk-mounted inertial measurement unit”, *Journal of Biomechanics* 45 (2012) 1123–1126, doi:10.1016/j.jbiomech.2011.12.020
- [11] - Huxham F., Gong J., Baker R., Morris M., Iansek R., Defining spatial parameters for non-linear walking. *Gait and Posture*, 23(2):159–63, 2006.
- [12] - Bertoli M., Cereatti A., Trojaniello D., Estimation of spatio-temporal parameters of gait from magneto-inertial measurement units: multicenter validation

among Parkinson, mildly cognitively impaired and healthy older adults. *Biomedical Engineering OnLine*, 17:58, 2018.

- [13] - Michael W. Whittle, Clinical gait analysis: A review, *Human Movement Science*, Volume 15, Issue 3, 1996, Pages 369-387, ISSN 0167-9457, [https://doi.org/10.1016/0167-9457\(96\)00006-1](https://doi.org/10.1016/0167-9457(96)00006-1).
- [14] - Higginson, Brian K., *Methods of Running Gait Analysis*. *Current Sports Medicine Reports*: May 2009 - Volume 8 - Issue 3 - p 136-141 doi: 10.1249/JSR.0b013e3181a6187a
- [15] - Horsley, B.J., Tofari, P.J., Halson, S.L. et al. Does Site Matter? Impact of Inertial Measurement Unit Placement on the Validity and Reliability of Stride Variables During Running: A Systematic Review and Meta-analysis. *Sports Med* 51, 1449–1489 (2021). <https://doi.org/10.1007/s40279-021-01443-8>
- [16] - A. R. Anwary, H. Yu and M. Vassallo, "Optimal Foot Location for Placing Wearable IMU Sensors and Automatic Feature Extraction for Gait Analysis," in *IEEE Sensors Journal*, vol. 18, no. 6, pp. 2555-2567, 15 March 2018, doi: 10.1109/JSEN.2017.2786587.
- [17] - E. Munoz Diaz, O. Heirich, M. Khider and P. Robertson, "Optimal sampling frequency and bias error modeling for foot-mounted IMUs," *International Conference on Indoor Positioning and Indoor Navigation*, 2013, pp. 1-9, doi: 10.1109/IPIN.2013.6817922.
- [18] - Macadam P, Cronin J, Neville J, Diewald S. Quantification of the validity and reliability of sprint performance metrics computed using inertial sensors: A systematic review. *Gait Posture*. 2019 Sep;73:26-38. doi: 10.1016/j.gaitpost.2019.07.123. Epub 2019 Jul 2. PMID: 31299501.
- [19] - Dot, T.; Quijoux, F.; Oudre, L.; Vienne-Jumeau, A.; Moreau, A.; Vidal, P.-P.; Ricard, D. Non-Linear Template-Based Approach for the Study of Locomotion. *Sensors* 2020, 20, 1939. <https://doi.org/10.3390/s20071939>
- [20] - Oudre, L.; Barrois-Müller, R.; Moreau, T.; Truong, C.; Vienne-Jumeau, A.; Ricard, D.; Vayatis, N.; Vidal, P.-P. Template-Based Step Detection with Inertial Measurement Units. *Sensors* 2018, 18, 4033. <https://doi.org/10.3390/s18114033>.
- [21] - Vienne-Jumeau A, Oudre L, Moreau A, Quijoux F, Vidal PP, Ricard D. Comparing Gait Trials with Greedy Template Matching. *Sensors (Basel)*. 2019 Jul 12;19(14):3089. doi: 10.3390/s19143089. PMID: 31336957; PMCID: PMC6679258.
- [22] - J. Chakraborty, H. S. Dabir and A. Nandy, "Speed Invariant Gait Event Identification using Dynamic Time Warping," 2021 IEEE 18th India Council International Conference (INDICON), 2021, pp. 1-6, doi: 10.1109/INDICON52576.2021.9691550.
- [23] - Aung MS, Thies SB, Kenney LP, Howard D, Selles RW, Findlow AH, Goulermas JY. Automated detection of instantaneous gait events using time frequency analysis and manifold embedding. *IEEE Trans Neural Syst Rehabil Eng*. 2013

Nov;21(6):908-16. doi: 10.1109/TNSRE.2013.2239313. Epub 2013 Jan 11. PMID: 23322764.

- [24] - D. Gouwanda and S. M. N. A. Senanayake, "Application of Hybrid Multi-resolution Wavelet Decomposition Method in Detecting Human Walking Gait Events," 2009 International Conference of Soft Computing and Pattern Recognition, 2009, pp. 580-585, doi: 10.1109/SoCPaR.2009.115.
- [25] - Aminian K, Najafi B, Büla C, Leyvraz PF, Robert P. Spatio-temporal parameters of gait measured by an ambulatory system using miniature gyroscopes. *J Biomech.* 2002 May;35(5):689-99. doi: 10.1016/s0021-9290(02)00008-8. PMID: 11955509.
- [26] - Soangra, R., Lockhart, T. E., & Van de Berge, N. (2011). An approach for identifying gait events using wavelet denoising technique and single wireless IMU. *Proceedings of the Human Factors and Ergonomics Society Annual Meeting*, 55(1), 1990–1994. Doi: <https://doi.org/10.1177/1071181311551415>
- [27] - Ç. P. Dautov and M. S. Özerdem, "Wavelet transform and signal denoising using Wavelet method," 2018 26th Signal Processing and Communications Applications Conference (SIU), 2018, pp. 1-4, doi: 10.1109/SIU.2018.8404418.
- [28] - Ammann, Rahel^{1,2}; Taube, Wolfgang²; Wyss, Thomas¹. Accuracy of PARTwear Inertial Sensor and Optojump Optical Measurement System for Measuring Ground Contact Time During Running. *Journal of Strength and Conditioning Research*: July 2016 - Volume 30 - Issue 7 - p 2057-2063 doi: 10.1519/JSC.0000000000001299
- [29] - Setuain I, Lecumberri P, Ahtiainen JP, Mero AA, Häkkinen K, Izquierdo M. Sprint mechanics evaluation using inertial sensor based technology: a laboratory validation study. *Scand J Med Sci Sports*. 2018;28(2):463–72
- [30] - Alberto Leardini, Lorenzo Chiari, Ugo Della Croce, Aurelio Cappozzo, Human movement analysis using stereophotogrammetry: Part 3. Soft tissue artifact assessment and compensation, *Gait & Posture*, Volume 21, Issue 2, 2005, Pages 212-225, ISSN 0966-6362, doi: <https://doi.org/10.1016/j.gaitpost.2004.05.002>.
- [31] - R. Rossanigo, S. Bertuletti, V. Camomilla, A. Orejel Bustos, C. Agresta, J. Zandler, M. Risatti, A. Sanfelici, A. Cereatti, Estimation of running biomechanical parameters using magneto-inertial sensors: a preliminary investigation, *Gait & Posture*, 97:38-39, DOI: 10.1016/j.gaitpost.2022.09.063
- [32] - Napier C, Willy RW, Hannigan BC, McCann R and Menon C (2021) The Effect of Footwear, Running Speed, and Location on the Validity of Two Commercially Available Inertial Measurement Units During Running. *Front. Sports Act. Living* 3:643385. doi: 10.3389/fspor.2021.643385
- [33] - Mason, R., Pearson, L.T., Barry, G. et al. Wearables for Running Gait Analysis: A Systematic Review. *Sports Med* (2022). <https://doi.org/10.1007/s40279-022-01760-6>

- [34] - E. Dipalma, R. Rossanigo, M. Caruso, R. Nicola, G. Martinez, M. Morrone, M. Meloni, T. Vieira, A. Cereatti, 'Stride detection in running using foot-mounted magneto-inertial sensors: a preliminary investigation for different running paces', Proceedings XXII Congresso SIAMOC 2022, 40, <http://amsacta.unibo.it/7027/>
- [35] - J. Lu, Y. Guo, H. Liu and J. Gao, "Gait Analysis Based on Magnetometer and Inertial Sensors Data Fusion," in IEEE Sensors Journal, vol. 22, no. 18, pp. 18056-18065, 15 Sept.15, 2022, doi: 10.1109/JSEN.2022.3195954
- [36] - Camomilla V, Bergamini E, Fantozzi S, Vannozzi G. Trends Supporting the In-Field Use of Wearable Inertial Sensors for Sport Performance Evaluation: A Systematic Review. Sensors (Basel). 2018 Mar 15;18(3):873. doi: 10.3390/s18030873. PMID: 29543747; PMCID: PMC5877384.
- [37] - Bergamini E, Guillon P, Camomilla V, Pillet H, Skalli W, Cappozzo A. Trunk inclination estimate during the sprint start using an inertial measurement unit: a validation study. J Appl Biomech. 2013 Oct;29(5):622-7. doi: 10.1123/jab.29.5.622. Epub 2012 Nov 21. PMID: 23182857.
- [38] - Nagahara R., Kameda M., Neville J., Morin J.-B. Inertial measurement unit-based hip flexion test as an indicator of sprint performance. J. Sports Sci. 2020;38:53–61. doi: 10.1080/02640414.2019.1680081
- [39] Hettiarachchi C., Kodithuwakku J., Manamperi B., Ifham A., Silva P. A Wearable System to Analyze the Human Arm for Predicting Injuries Due to Throwing; Proceedings of the 2019 41st Annual International Conference of the IEEE Engineering in Medicine and Biology Society (EMBC); Berlin, Germany. 23–27 July 2019; pp. 3297–3301.
- [40] - Rawashdeh S.A., Rafeldt D.A., Uhl T.L. Wearable IMU for Shoulder Injury Prevention in Overhead Sports. Sensors. 2016;16:1847. doi: 10.3390/s16111847
- [41] - Mohammed, Z.; Elfadel, I.M.; Rasras, M. Monolithic Multi Degree of Freedom (MDoF) Capacitive MEMS Accelerometers. Micromachines 2018, 9, 602. <https://doi.org/10.3390/mi9110602>
- [42] - J. Versluis, 'What is Yaw, Pitch and Roll in 3D axis values', 2020, <https://www.versluis.com/2020/09/what-is-yaw-pitch-and-roll-in-3d-axis-values/>
- [43] - Passaro VMN, Cuccovillo A, Vaiani L, Carlo M, Campanella CE. Gyroscope Technology and Applications: A Review in the Industrial Perspective. Sensors (Basel). 2017 Oct 7;17(10):2284. doi: 10.3390/s17102284. PMID: 28991175; PMCID: PMC5677445.
- [44] - N. Yazdi, F. Ayazi and K. Najafi, "Micromachined inertial sensors," in Proceedings of the IEEE, vol. 86, no. 8, pp. 1640-1659, Aug. 1998, doi: 10.1109/5.704269.
- [45] - Aurelio Cappozzo, Ugo Della Croce, Alberto Leardini, Lorenzo Chiari, Human movement analysis using stereophotogrammetry: Part 1: theoretical

background, *Gait & Posture*, Volume 21, Issue 2, 2005, Pages 186-196, ISSN 0966-6362, doi: <https://doi.org/10.1016/j.gaitpost.2004.01.010>.

- [46] - Bobbert MF, Schamhardt HC. Accuracy of determining the point of force application with piezoelectric force plates. *J Biomech.* 1990;23(7):705-10. doi: 10.1016/0021-9290(90)90169-4. PMID: 2384485.
- [47] - Hawkin Dynamics Staff, “So what exactly is a force plate?”, 2018, Hawkin Dynamics, <https://www.hawkindynamics.com/blog/what-is-a-force-plate>
- [48] - E. L. Bontrager, Instrumented Gait Analysis Systems, *Gait Analysis in the Science of Rehabilitation*, Department of Veterans Affairs - Veterans Health Administration, 1998, 11-32.
- [49] - Cengiz, Y., Doç, Y., & Arıöz, U. (2016). Ayrık Dalgacık Dönü , sümü Kullanarak Konu , sma Sinyallerinin Gürültüden Arındırılması için Uygulama An Application for Speech Denoising Using Discrete Wavelet Transform, 1–4
- [50] - A. Graps, “An Introduction to Wavelets,” *IEEE Computational Sciences and Engineering*, vol. 2, no. 2, pp 50-61, 1995.
- [51] - M. Yang, Y. Sang, C. Liu, Z. Wang, “Discussion on the Choice of Decomposition Level for Wavelet Based Hydrological Time Series Modeling”, *MDPI, Water* 2016, 8, 197; doi:10.3390/w8050197
- [52] - B.A. Kerr, L. Beauchamp, V. Fisher, R. Neil, “Footstrike patterns in distance running”. Nigg BM, Kerr BA, editors. *Biomechanical Aspects of Sport Shoes and Playing Surfaces*. Calgary, Canada: University Printing. 1983:135–142.
- [53] - T.L. Nicola and D.J. Jewison, “The Anatomy and Biomechanics of Running”, *Clin Sports Med* 31 (2012) 187–201, doi:10.1016/j.csm.2011.10.001
- [54] - F. Salis, S. Bertuletti, K. Scott, M. Caruso, T. Bonci, E. Buckley, U. Della Croce, C. Mazzà, A. Cereatti, “A wearable multi-sensor system for real world gait analysis”. *Annu Int Conf IEEE Eng Med Biol Soc.* 2021 Nov; 2021:7020-7023. doi: 10.1109/EMBC46164.2021.9630392. PMID: 34892719
- [55] - F. Salis, S. Bertuletti, T. Bonci, U. Della Croce, C. Mazzà, A. Cereatti, A method for gait events detection based on low spatial resolution pressure insoles data, *Journal of Biomechanics*, Volume 127, 2021, 110687, ISSN 0021-9290, doi: <https://doi.org/10.1016/j.jbiomech.2021.110687>.
- [56] - G. Martinez, R. Rossanigo, M. Meloni, M. Morrone, S. Bertuletti, E. Rivolta, E. Urracci, A. Melis, F. Bussu, A. Cereatti, F. Deriu, A. Manca, “A pilot gender-based study on the effects of in-ear music listening on treadmill and overground running biomechanics”, 72nd SIF National Congress, 2022
- [57] -B. Spiriev, “IAAF SCORING TABLES OF ATHLETICS,” 2017
- [58] - R. Nicola, G. L. Cerone, M. Caruso, R. Rossanigo, A. Cereatti and T. Vieira, "On the Detection of High-Quality, High-Density Electromyograms During 80m Sprints: a Case Study," 2022 IEEE International Symposium on Medical

Measurements and Applications (MeMeA), 2022, pp. 1-5, doi: 10.1109/MeMeA54994.2022.9856504

- [59] - R. Ammann, W. Taube, T. Wolfgang, Accuracy of PARTwear Inertial Sensor and Optojump Optical Measurement System for Measuring Ground Contact Time During Running. *Journal of Strength and Conditioning Research*: July 2016 - Volume 30 - Issue 7 - p 2057-2063 doi: 10.1519/JSC.0000000000001299
- [60] - I. Setuain, P. Lecumberri, J. Ahtiainen, A. Mero, K. Häkkinen, M. Izquierdo, Sprint mechanics evaluation using inertial sensor-based technology: A laboratory validation study. *Scandinavian Journal of Medicine and Science in Sports*, 2018, 28(2), 463-472. <https://doi.org/10.1111/sms.12946>
- [61] - Blauburger, P.; Horsch, A.; Lames, M. Detection of Ground Contact Times with Inertial Sensors in Elite 100-m Sprints under Competitive Field Conditions. *Sensors* 2021, 21, 7331. <https://doi.org/10.3390/s212173>
- [62] - M. Schmidt, C. Rheinländer, K.F. Nolte, S. Wille, N. Wehn and T. Jaitner, “IMU- based determination of stance duration during sprinting”, *Procedia Engineering* 147 (2016) 747 – 752, doi: 10.1016/j.proeng.2016.06.330
- [63] - Falbriard M, Meyer F, Mariani B, Millet GP and Aminian K (2018) Accurate Estimation of Running Temporal Parameters Using Foot-Worn Inertial Sensors. *Front. Physiol.* 9:610. doi: 10.3389/fphys.2018.00610
- [64] - Bailey, G. and Harle, R.. Measuring Temporal Parameters of Gait with Foot Mounted IMUs in Steady State Running. In *Proceedings of the 3rd International Congress on Sport Sciences Research and Technology Support (icSPORTS 2015)*, pages 24-33 ISBN: 978-989-758-159-5
- [65] - Rai, A., Chintalapudi, K. K., Padmanabhan, V. N., and Sen, R. (2012). “Zee: Zero-Effort Crowdsourcing for Indoor Localization”. In *Proceedings of the 18th annual international conference on Mobile computing and networking - Mobicom '12*, page 293
- [66] - Reenalda J., Maartens E., Homan L. and Buurke J.H., “Continuous three dimensional analysis of running mechanics during a marathon by means of inertial magnetic measurement units to objectify changes in running mechanics”, *Journal of Biomechanics* 49 (2016) 3362–3367, doi: <http://dx.doi.org/10.1016/j.jbiomech.2016.08.032>
- [67] - Mo S. and Chow D.H.K., “Accuracy of three methods in gait event detection during overground running”, *Gait & Posture* 59 (2018) 93-98, doi: <http://dx.doi.org/10.1016/j.gaitpost.2017.10.009>
- [68] - Chew D., Ngoh K.J., Gouwanda D. and Gopalai A.A., “Estimating running spatial and temporal parameters using an inertial sensor”, *Sports Eng* (2018) 21:115–122, doi: <https://doi.org/10.1007/s12283-017-0255-9>

- [69] - Benson L.C., Clermont C.A., Watari R., Exley T. and Ferber R., “Automated Accelerometer-Based Gait Event Detection During Multiple Running Conditions”, *Sensors* 2019, 19, 1483; doi:10.3390/s19071483
- [70] - Yang, Y.; Wang, L.; Su, S.; Watsford, M.; Wood, L.M.; Duffield, R. Inertial Sensor Estimation of Initial and Terminal Contact during In-Field Running. *Sensors* 2022, 22, 4812. <https://doi.org/10.3390/s22134812>
- [71] Ji et al, ‘Appropriate Mother Wavelets for Continuous Gait Event Detection Based on Time-Frequency Analysis for Hemiplegic and Healthy Individuals’, *Sensors* 2019, 19, 3462; doi:10.3390/s19163462
- [72] - Gordon B. Drummond and Brian D. M. Tom, ‘Statistics, probability, significance, likelihood: words mean what we define them to mean’, *J Physiol* 589.16 (2011) pp 3901–3904, DOI: 10.1113/jphysiol.2011.215103
- [73] - W. W. Piegorsch, ‘Tables of p-values for t- and chi-square reference distributions’, 2002, University of South Carolina Statistics Technical Report No. 194 62Q05-3
- [74] - E. Munoz Diaz, O. Heirich, M. Khider and P. Robertson, "Optimal sampling frequency and bias error modeling for foot-mounted IMUs," *International Conference on Indoor Positioning and Indoor Navigation*, 2013, pp. 1-9, doi: 10.1109/IPIN.2013.6817922.
- [75] - Marmelat V, Duncan A, Meltz S. Effect of sampling frequency on fractal fluctuations during treadmill walking. *PLoS One*. 2019 Nov 7;14(11):e0218908. doi: 10.1371/journal.pone.0218908. PMID: 31697684; PMCID: PMC6837491
- [76] - Prasanth, H.; Caban, M.; Keller, U.; Courtine, G.; Ijspeert, A.; Vallery, H.; von Zitzewitz, J. Wearable Sensor-Based Real-Time Gait Detection: A Systematic Review. *Sensors* 2021, 21, 2727. <https://doi.org/10.3390/s21082727>

Appendix 1

Cover Insole analysis

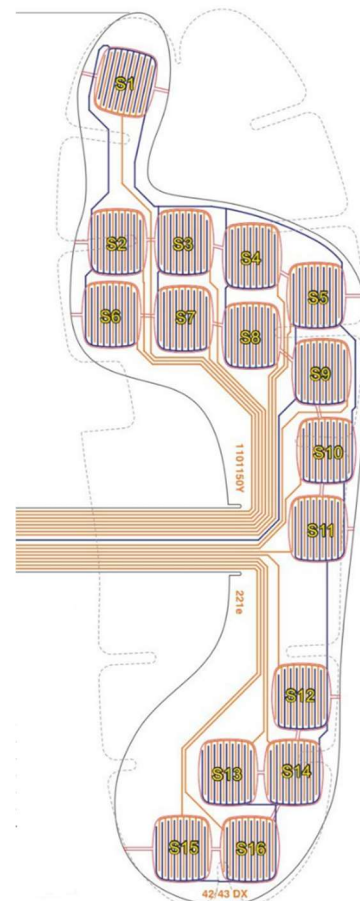
In this section, the analysis brought on to identify the best cover insole for running acquisition is provided. The pressure insoles exploited during the data acquisitions tend to be fragile, so under the high sheer stress to which they are subjected during running, they tend to get damaged, thus not allowing the correct acquisition of the signals. 11 sprinting trials were discarded due to the poor insoles quality, so an analysis on a solution has to be performed.

N.B. For some subjects, it is noted that some sensory units stop functioning after a certain amount of incorrect stimulation.

To discriminate the activation or non-activation of a sensory unit, a threshold of 0.2 was used.

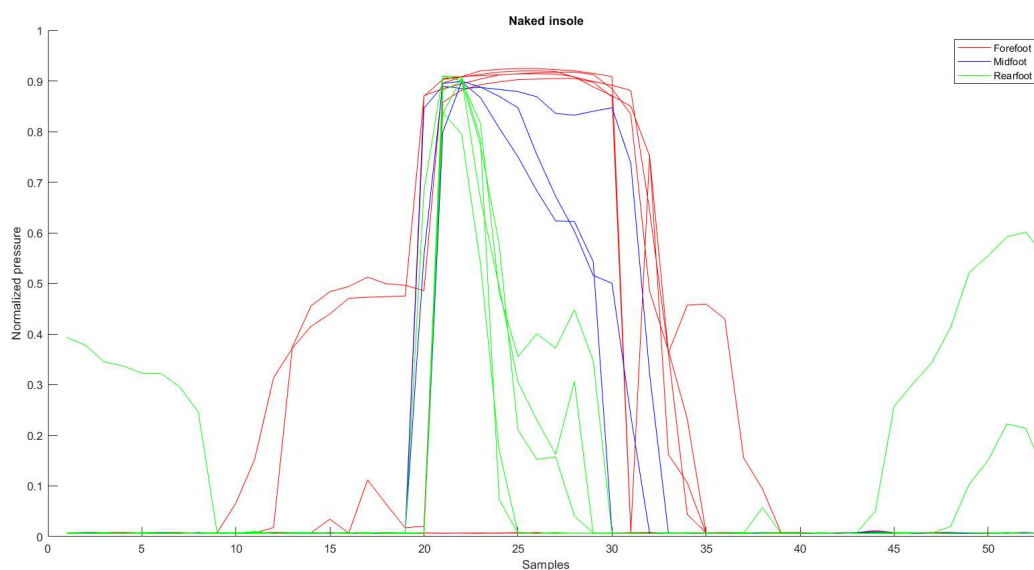
Hereafter the numerical reference for each sensor unit on the sensorised:

- S1 - toe
- S2 – forefoot
- S3 – forefoot
- S4 – forefoot
- S5 - forefoot
- S6 – forefoot
- S7 – forefoot
- S8 – forefoot
- S9 – midfoot
- S10 – midfoot
- S11 – midfoot
- S12 - rearfoot
- S13 – rearfoot
- S14 – rearfoot
- S16 – rearfoot



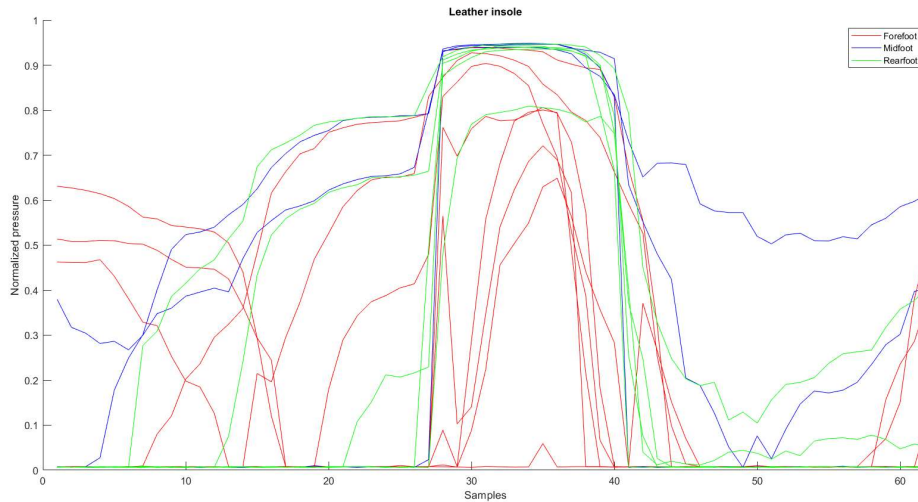
1. Analysis of pressure insoles data quality without any cover insoles

Examples of the acquired signal in the absence of any type of protective insole. Insoles of size 42/43 were used for each subject (41 to 43). At the time of the acquisitions, the insoles had already been used for: 120 minutes, including 14 minutes of actual running time. Three sensors from the forefoot showed no activation, one sensor from the mid-foot showed odd activation, lastly two of the sensors from the rearfoot remained active for the whole time.



2. Analysis of pressure insoles data quality with leather cover insoles

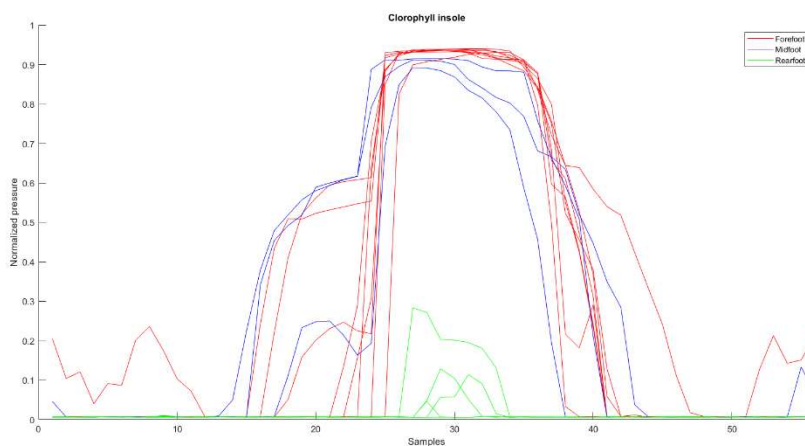
Examples of the signal acquired with the leather insole interposed between the foot and the sensorised insole. Insoles of size 42/43 were used for each subject (41 to 43). At the time of the acquisitions, the insoles had just been replaced. Five sensing units from the forefoot activates when they shouldn't, two sensors from mid-foot and two from the rearfoot show constant activations.



3. Analysis of pressure insoles data quality with Chlorophyll cover insoles

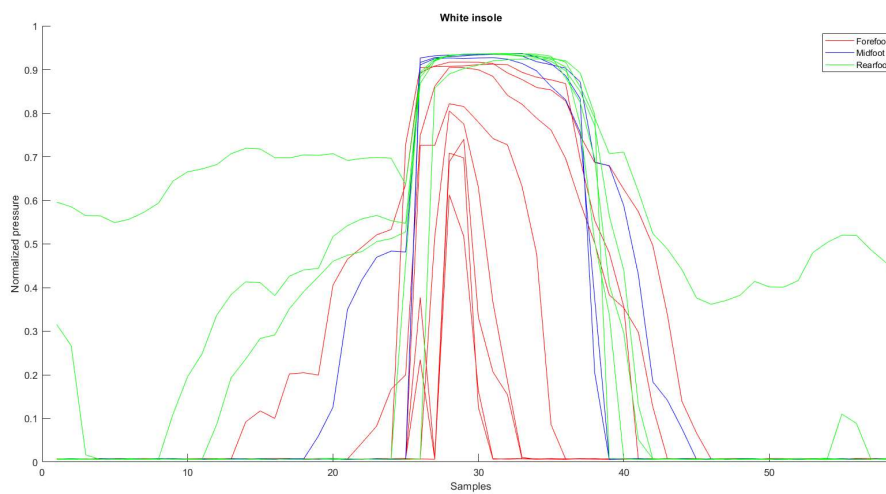
Examples of signals acquired with the chlorophyll insole interposed between the athlete's foot and the sensorised insole. The sensor insole used was size 36/37 for a size 41 subject. At the time of the acquisitions, the insoles had just been replaced. One sensing unit from the forefoot and one from the mid-foot showed constant activation, two from the mid-foot and all the rearfoot sensors returned little to no activation.

N.B. the images in this configuration refer to an acquisition in which slightly lower speeds were achieved compared to the other acquisitions.



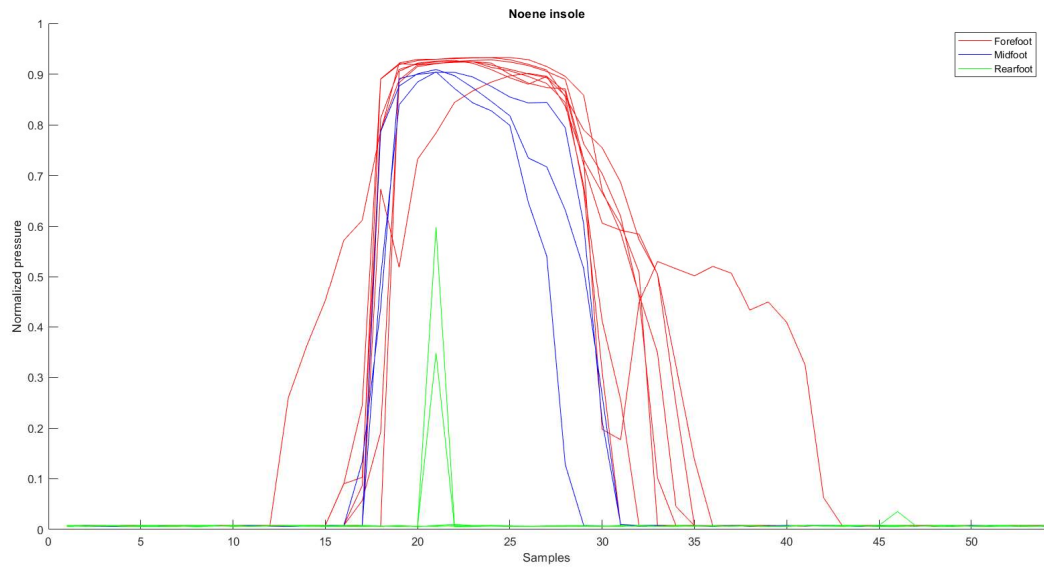
4. Analysis of pressure insoles data quality with cotton cover insoles

Examples of signals acquired using a chlorophyll insole with a layer of cotton in contact with the foot as a protective insole. At the time of the acquisitions, the insoles had just been replaced. Insoles 36/37 were used on subject 41. One sensor from the forefoot shows no activation, while five of them show little activation and three rearfoot sensors show constant activation.



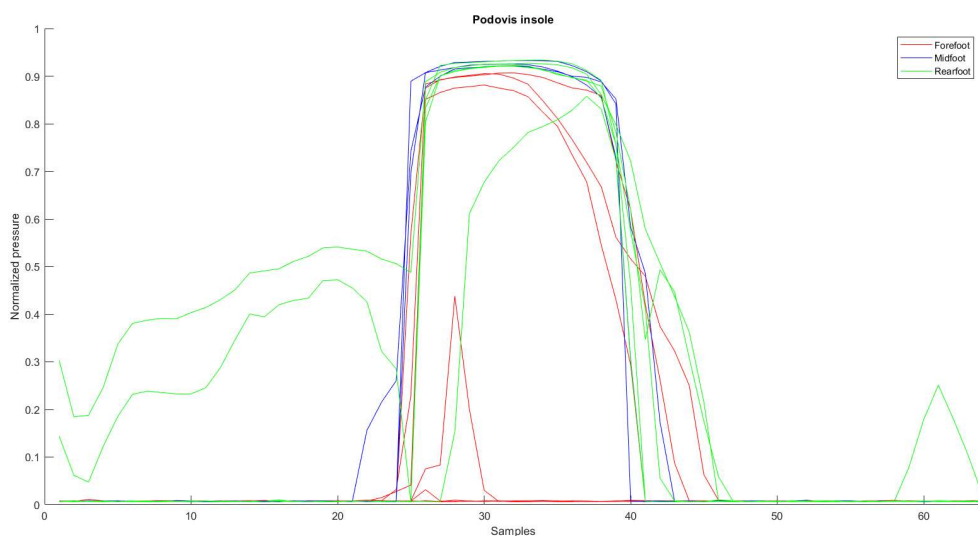
5. Analysis of pressure insoles data quality with Noene Insoles

Examples of the signal acquired with the noene rubber insole interposed between the foot and the sensorised insole. Insoles 36/37 were used for a subject 41. Cost: 26 €/pair. At the time of the acquisitions, the insoles had already been used for: 30 minutes, of which 8 minutes of actual running. All the sensors returned proper activation, additionally the rearfoot sensors were the least active ones.



6. Analysis of pressure insoles data quality with Podovis Insoles

Examples of signals acquired with the insole interposed between the athlete's foot and the sensorised insole. The sensor insole used was size 36/37 for a size 41 subject. Cost: 1.5€/pair. At the time of the acquisitions, the insoles had already been used for: 15 minutes of which 4 minutes of actual running. All the sensors showed proper activation, except two on the rearfoot that showed some activation during the swing phase.



7. Comparison Table

In this section, a table with a brief summary of the sensor units activation is provided. Each color corresponds to a behaviour, specified in the adjacent legend.

	s1	s2	s3	s4	s5	s6	s7	s8	s9	s10	s11	s12	s13	s14	s15	s16
Naked	Not perfect stance activation	Constant swing activation	Not perfect stance activation	Stance activation	Stance activation	Constant swing activation	Not perfect stance activation	Stance activation	Not perfect stance activation	Stance activation	Stance activation	Some swing activation	No activation	Some swing activation	No activation	No activation
Leather	Some swing activation	Stance activation	Stance activation	Stance activation	Always active	Stance activation	Constant swing activation	Constant swing activation	Not perfect stance activation	Some swing activation	Not perfect stance activation	Some swing activation	Constant swing activation	Constant swing activation	Not always active	Constant swing activation
Clorophyll	Not always active	Not always active	Stance activation	Some swing activation	Stance activation	Not always active	Not always active	Not perfect stance activation	Stance activation	Stance activation	Stance activation	Stance activation	Not perfect stance activation	Stance activation	Some swing activation	Stance activation
Clorophyll+paper	Constant swing activation	Constant swing activation	Constant swing activation	Constant swing activation	Constant swing activation	Always active	Almost always active	Always active	Almost always active	Constant swing activation	Stance activation	Not perfect stance activation	Not perfect stance activation	Not perfect stance activation	Not perfect stance activation	Not perfect stance activation
White	Stance activation	Constant swing activation	Stance activation	Stance activation	Stance activation	Almost always active	Constant swing activation	Not perfect stance activation	Stance activation	Stance activation	Not perfect stance activation	Not perfect stance activation	Not perfect stance activation	Not perfect stance activation	Not perfect stance activation	Not always active
Noene	Not always active	Stance activation	Stance activation	Stance activation	Stance activation	Not always active	Stance activation	Stance activation	Stance activation	Stance activation	Stance activation	Stance activation	Stance activation	Some swing activation	Stance activation	Stance activation
Pedovis	Stance activation	Constant swing activation	Stance activation	Stance activation	Stance activation	Constant swing activation	Stance activation	Stance activation	Stance activation	Stance activation	Stance activation	Stance activation	Stance activation	Stance activation	Not always active	Not always active
	Forefoot						Midfoot				Rearfoot					

Table 1 - Comparison of the performances of the sensors with different protection insoles

Sensor activation is often due to the very narrow shoe shape that athletes have to wear during trials. [1]

From this analysis, as detailed in Table 1, the most suitable protection insole for the purpose was Podovis, as it was one of the two best performing (Noene and Podovis), but less expensive and therefore more suitable for use as consumables. It was noted, however, that the quality of the signals varies greatly from athlete to athlete, probably due to the different shoe conformation. To demonstrate this, signals acquired under the same conditions on different subjects are shown below. For each subject, 36/37 insoles were used. The positioning of the sensorised insole inside the shoe does not differ significantly between athletes.

8. References

[1] - Barnett S, Cunningham JL, West S. A comparison of vertical force and temporal parameters produced by an in-shoe pressure measuring system and a force platform. Clin Biomech (Bristol, Avon). 2001 May;16(4):353-7. doi: 10.1016/s0268-0033(01)00026-2. PMID: 11358623.

Appendix 2

Sampling frequency enhancement

The work brought on in this thesis work has highlighted the need to enhance the sampling frequency for the acquisition of running trials. However, the pressure insole, which contains 16 sensing elements, was made with a sampling frequency of 100 Hz. In order to double the MIMU sampling frequency, to 200 Hz, the number of sensing elements must be halved. This section goes into detail into the analysis made to identify which should be the sensing elements to discard to enhance the sampling frequency based on the data acquired at lower and sprinting speeds.

The numerical reference for each sensor unit is the same as in Appendix 1.

1. Analysis protocol

The INDIP multisensory system [1] allows to record inertial and 16-unit pressure insole data at 100 Hz. In the literature, in order to analyse the running and identify contact instants, methods starting from higher sampling frequencies are proposed, such as Schmidt et al [2] using a sampling frequency of 1000 Hz, Reenalda et al [3] 1800 Hz, Benson et al [4] 200Hz and many others.

In order to increase the fs of the INDIP system, the number of sensor units considered must be decreased. For example, to double the fs it is necessary to record the signal of 8 units instead of 16 in order to maintain optimal temporal resolution.

The estimation of contact instants is based on the adaptation to running speeds of the method proposed by Salis et al. [4], which discriminates the rising and falling edges of the pressure signals that define the beginning and end of the support phase, respectively.

The signal acquired by the individual unit is considered to be of poor quality when the insole itself crumples, slips inside the shoe towards the toe, in cases where the signal acquired by that sensor never goes to zero or if it has near-zero values for less than 15% or more than 90% of the total running time.

In order to analyse the performance of the individual sensory units, and thus decrease their number to a sampling frequency of 200 Hz [5], they were evaluated on two different datasets, taking into account the number of times each unit is considered for the identification of running events (initial contacts IC and final contacts FC) and the number of times it is eliminated due to the poor quality of the signal acquired by it.

The data refer to a dataset in which subjects ran at speeds ranging from 20 to 32 km/h (sprinters) and a second dataset in which subjects ran at 8 km/h and 10 km/h (amateurs).

1.1 – Sprinters

The analysis was carried out considering a total of 4 subjects, for 3 of which (0001, 0002, 0003) both feet were taken into account, while for the fourth subject (0007), only the left foot was considered due to problems occurring during the acquisition of data from the right foot. The acquisitions for the three complete subjects were carried out without any type of lining insole, whereas for the subject for whom only the right foot data were available, a Podovis lining insole was used.

Each subject was asked to run on an 80 m long outdoor track at different speeds (70%, 85% and 100% of their maximum speed). A total of 446 steps were taken into account in this analysis.

For each subject, the total number of occurrences of the selection of sensors for contact identification and one to identify the occurrences of the elimination of sensors due to the poor quality of the signal acquired by them was taken into account. The results are summarized in the Table 1.

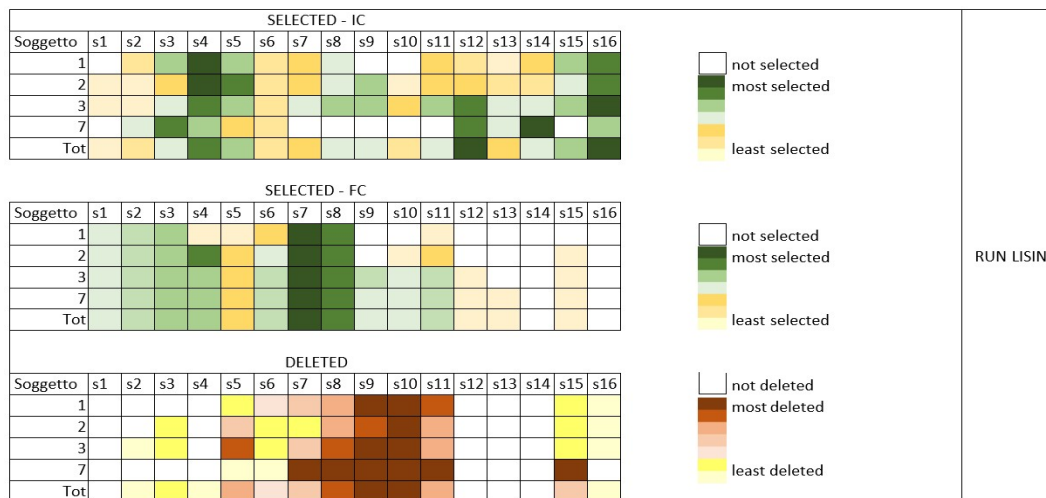


Table 1 - Colour table on sprinters dataset showing selection/elimination occurrences divided by subjects for each individual sensor.

Figure 1 shows the image of the insoles on which the sensory units were coloured according to the colour code used in Table 1, so that the positioning of the sensory units can also be seen at a glance.

Tested professional runners usually impact with the forefoot, followed by a short heel strike. However, overall, due to the slippage of the insole in some cases and the narrow design of the running shoe [4] the quality of the forefoot signals does not always allow for unambiguous discrimination of contacts, so some of the most useful and least rejected sensors for the identification of running events belong to the rearfoot. Furthermore, in order not to damage the insoles, size 36/37 EU insoles were used, although the participants wore greater sized shoes. This leads to partial uncertainty of the relative position of the sensor chosen for the definition of the initial contact in relation to the foot. In fact, the s16 is one of the sensors most frequently chosen for the identification of initial contacts.

In this dataset, it can be seen that the most frequently discarded sensors are located near the forefoot (s5, s8, s9, s10, s11). The instants are most easily identified with the sensors in

the forefoot. In particular, the final contact is most often identified with the help of sensors in the forefoot, as expected.

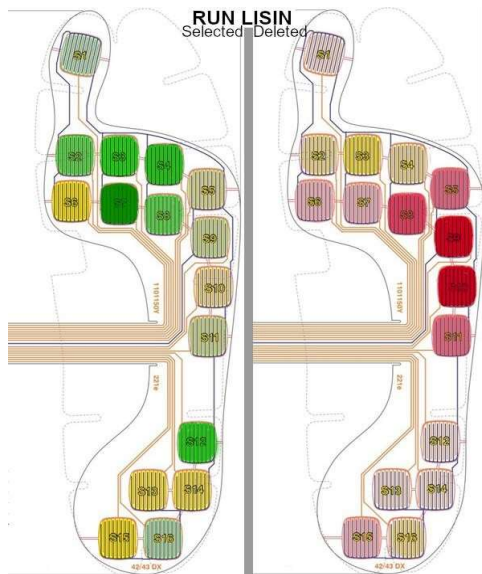


Figure 1 - Representative insole of sensors and their positioning, coloured according to the selection occurrences of the individual sensors. On the left, the selection occurrences for initial and final contact identification, on the right the elimination occurrences.

1.2 – Amateurs

The analysis was repeated on the dataset at 8 and 10 km/h. Each subject was asked to perform four trials on an outdoor and an indoor track. For both, the trials had a total duration of 45 minutes, divided as follows:

- running at 8 km/h for 400 metres;
- running at 8 km/h for 400 metres;
- running at 10 km/h for 400 metres;
- running at 10 km/h for 400 metres.

Of the 11 subjects, 5 were not equipped without protective insoles (subject IDs: 1,2,7,31,38) and the rest of them wore leather protective insole (subject IDs: 22, 25, 29, 30, 32,44). For each subject, data obtained from both feet was considered. In particular, a total of 18166 steps were analysed. The results thus obtained have been summarised in Table 2, where the occurrences of the selection or the elimination of each sensor has been colour coded.

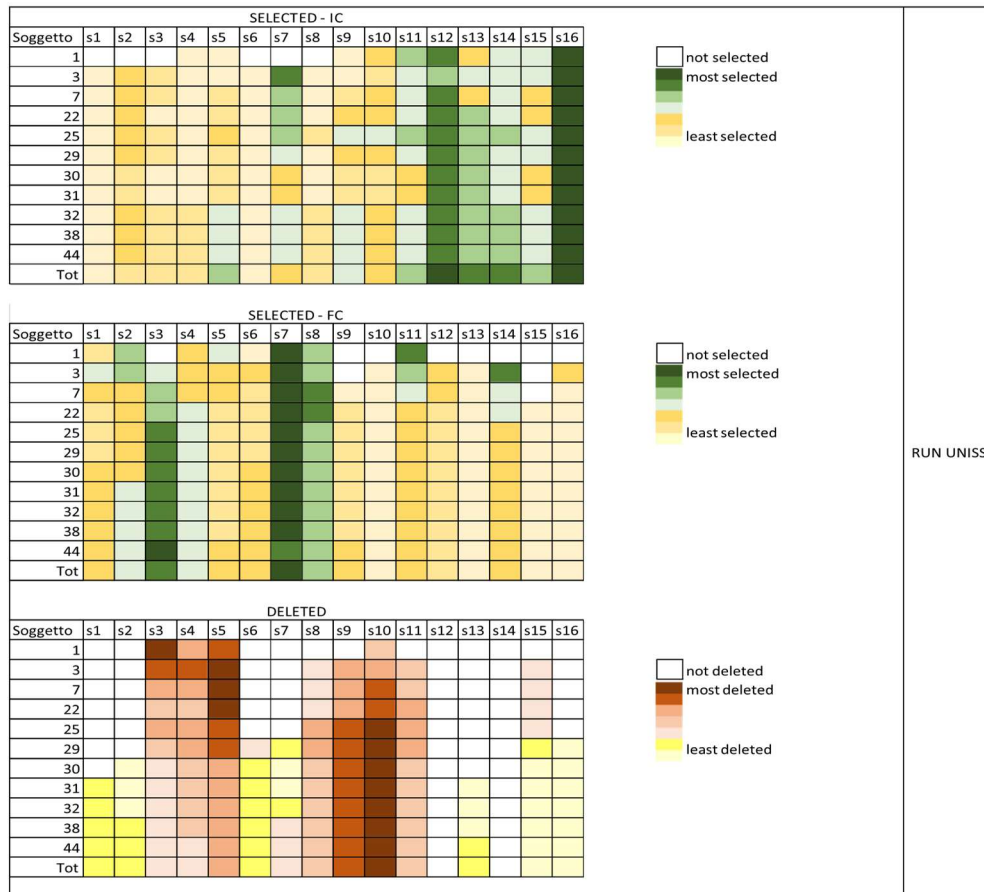
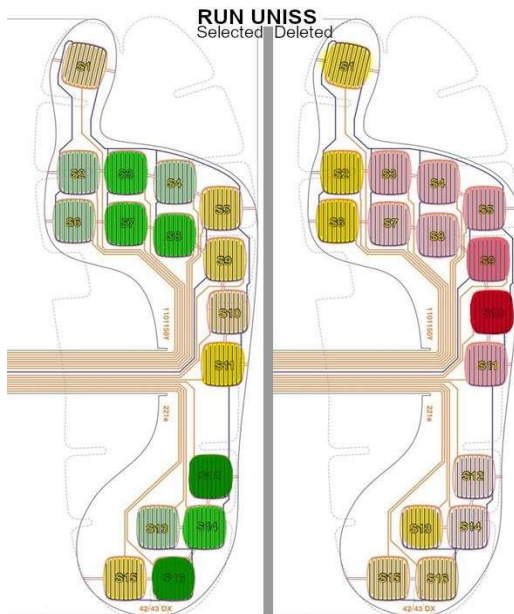


Table 2 - Colour table on amateurs dataset showing selection/elimination occurrences divided by subjects for each individual sensor.



In this dataset, the sensory units with the most reliable and most selected data for the identification of initial and final contacts were divided between the rearfoot and forefoot zones. Since the subjects impact with the heel at the analysed velocities, this is a result in line with what is expected (IC -> rearfoot, FC -> forefoot).

In this dataset, the sensors most frequently chosen for the discrimination of instances are s3, s7, s8, s12, s14 and s16, divided between forefoot and rearfoot. The most frequently discarded sensors are always those in the forefoot and midfoot area, probably due to the sliding of the insole inside the shoe. In Figure 2, a visual representation of the behaviour of the sensors is provided.

Figure 2 - Representative insole of sensors and their positioning, coloured according to the selection occurrences of the individual sensors. On the left, the selection occurrences for the identification of initial and final contacts, on the right the elimination occurrences.

2. Selected pressure sensors

Given the above analysis, the following were considered to be the most reliable sensory units:

- S2
- S3
- S7
- S8
- S10
- S12
- S14
- S16

This result was obtained by jointly evaluating the performance of the 16 sensors on both datasets. Although from the analysis carried out all the most selected sensors for the identification of events turn out to be in the forefoot or rearfoot area, in order to maintain a homogeneous spatial distribution of sensors over the entire foot area, s10 was also included.

Figure 3 - Representative insole of the sensors selected from this survey.



3. References

[1] – Bertuletti et al., Static and Dynamic Accuracy of an Innovative Miniaturized Wearable Platform for Short Range Distance Measurements for Human Movement Applications, *Sensors* 2017, 17, 1492

[2] - Schmidt et al., IMU- based determination of stance duration during sprinting, *Procedia Engineering*, 2016

[3] - Reenalda et al., Continuous three-dimensional analysis of running mechanics during a marathon by means of inertial magnetic measurement units to objectify changes in running mechanics, Elsevier, 2016

[4] - Benson et al., Automated Accelerometer-Based Gait Event Detection During Multiple Running Conditions, *Sensors*, 2019

[5] - Salis et al., A method for gait events detection based on low spatial resolution pressure insoles data, Elsevier, 2021

[6] - West and Barnett, Plantar pressure measurement: which system?, Foot pressure Interest Group, 1999